A SEARCH FOR THE $\delta^-(962)$MESON

by

PASHUPATI NATH UPADHYAY

A Thesis Submitted for the Degree of

DOCTOR OF PHILOSOPHY

of the

UNIVERSITY OF LONDON

-ooOoo-

Department of Physics
Imperial College of Science and Technology
London SW7

June 1971

ABSTRACT

An account is presented of a missing mass counter experiment to study the $\delta^-(962)$ meson produced in the reaction

$$\pi^- p \rightarrow \delta^- p$$

at incident beam momenta close to its production threshold.

The nucleons were detected by a ring of six cylindrical scintillation counters situated downstream of a liquid hydrogen target. Iz = 0 objects were also studied. Both charged and neutral decay particles were detected simultaneously by a decay system surrounding the target. The nucleon time-of-flight in the final state and the incident pion momentum in the initial state were measured to calculate the missing mass.

The apparatus could detect a resonance with good mass resolution and high geometrical collection efficiency close to its production threshold. Well above the threshold, a resonance could only be detected if its production cross-section increased enough to compensate for the decreasing geometrical efficiencies and the poor mass resolution of the apparatus.

A study of the $\eta\pi^-(\eta \rightarrow \gamma\gamma)$ decay mode showed no evidence for an enhancement at a mass of 962 MeV/c^2 in the /t/ region 0.12 - 0.29 (GeV/c)^2. However, a 5.2 standard deviation enhancement of mass 996 MeV/c^2 and Γ=40 MeV/c^2 appeared in $\pi^- \eta \rightarrow \gamma\gamma$ mode in the /t/ region 0.22 to 0.29(GeV/c)^2.

In the decay mode $\pi^{\pm}\delta^0\ \pi^-\eta$(with 0 or 2 charged particles + neutrals$\geq 3\gamma$particles), a neutral enhancement of $\sim$5 standard deviation was observed at mass 956±2 MeV/c^2 with $\Gamma \leq 12$ MeV/c^2.

CONTENTS

CHAPTER 1

INTRODUCTION

1-1 Status of the δ meson

The mass region near 1 GeV/c^2 is not well understood. The existence of several meson states has been explained by the Quark Model[20]. On the basis of this model, Meson Systems are supposed to be made up of a quark q and an antiquark $\bar{q}$.

As quarks are assumed to be fermions, a $q\bar{q}$ system with orbital angular momentum L and total spin S (0 or 1) will have

Parity, $P = (-1)^{L+1}$

Charge Conjugation, $C = (-1)^{L+S}$

G-Parity, $G = (-1)^{L+S+I}$

Where I is the isotopic spin of the $q\bar{q}$ system.

The combination of the orbital angular momentum L with its spin S leads to a sequence of levels denoted by $^{2S+1}L_J$ in Fig 1-1A. Each level contains a nonet of mesons which can be further decomposed into an octet plus a singlet. These states and the candidates for these states are shown in Fig 1-1A. X^o or η' ($I^G J^P = 0^- 0^-$) is the singlet state of the nonet 0^-. The other members of the nonets are also well-established.

Here we discuss the δ meson. In the $q\bar{q}$ system, the δ meson is expected to be a P-state (Fig 1-1A) with its possible quantum numbers $I^G J^P = 1^- 0^+$. Assuming it decays by strong interaction, its expected decay modes would be

$$\delta^- \to \eta \pi^-$$

and $\delta^- \to K \bar{K}$

but $\delta^- \to \pi^- \pi^o$ would be forbidden.

The δ and the X^o mesons, observed in the same mass regions, are believed to be different from each other. This is due to the fact that X^o is seen in abundance in the reaction $K^- P \to \Lambda^o X^o$. But no signal is observed in $K^- n \to \Lambda^o X^-$ at mass of 960 MeV. If $IX^o = 1$, the conservation of I-spin would predict twice the x-section of the former reaction for the latter. $\therefore IX^o \neq 1$. But $I\delta = 1$. The X^o meson is well established but the existence of the δ meson is not confirmed.

A narrow resonance called δ with $\Gamma \leq 5$ MeV at mass 962 MeV was first reported in 1965 by Kienzle et al[1] who observed it in the missing mass study of the $\pi^- P \to X^- P$ at 3.5 GeV/c. Several other groups reported confirming its existence while others claim not to see it.

Oostens et al[7] studying the reaction $pp \to d X^+$ at incident momentum 3.8 GeV/c confirmed the existence of the δ at 960 MeV. However, using the same technique in this reaction at the same beam momentum, no δ was seen by Banner at al[8] and Abolins et al[42]. In the same reaction, some positive evidence for the δ^+ appeared at incident momenta 5.4 GeV/c and 12.3 GeV/c in the data of Anderson et al[21].

TABLE 1-1-A

				SINGLET
	$^1S_0, CJ^P = +0^-$	K	π	η'
	$I^G\ 0^+$	1/2	1⁻	0⁺
$=0$				
	$^3S_1, CJ^P = -1^-$	$K^*(890)$	ρ	φ
	$I^G\ 0^-$	1/2	1⁺	0⁻
	$^1P_1, CJ^P = -1^+$ (?)	$K^*(1320)$	B	(?)
	$I^G\ 0^-$	1/2	1⁺	0⁻
	$^3P_0, CJ^P = +0^+$ $\varepsilon°(700)$	$K^*(1100)$	δ	S(1080)
	$I^G\ 0^+$	1/2	1⁻	0⁺
$=1$				
	$^3P_1, CJ^P = +1^+$ D	$K^*(1240)$	A_1	(?)
	$I^G\ 0^+$	1/2	1⁻	0⁺
	$^3P_2, CJ^P = +2^+$ f^0	$K^*(1420)$	A_2	f'^*
	$I^G\ 0^+$	1/2	1⁻	0⁺

In the reaction $\pi^- P \to \pi^- \pi^0 P$ at a pion momentum 1.7 GeV/c, Allen et al[5] claimed to see at 965 MeV while at incident pion momentum 1.8 GeV/c, Banner et al[2] found no enhancement in this mass region and gave an upper limit of 1% of the ρ cross-section. The claim was also not supported by Jacobs[40], Clear et al[41] and West et al[39]. A two standard deviation enhancement at mass 962 MeV/c^2 was observed by Chung et al[4] in $\pi^- p \to \eta \pi^- p, \eta \to \pi^+ \pi^- \pi^0$

A peak of mass 975 MeV, called πn, was observed by Defoix et al[9] as a decay product of the D^0 (1285 MeV) produced in the reaction $\bar{p}p \to D^0 \pi^+ \pi^-$ They found a branching ratio B,

$$B = \frac{D^0 \to \bar{K} K^0 \pi^+}{D^0 \to \eta \pi \pi} = 0.12 \pm .04$$

Campbell et al[11] studying the reaction $\pi^+ d \to p_s p \pi^+ \pi^- \eta$ at 2.7 GeV/c, reported a mass of 980 ± 10 MeV with width of 40 ± 15 MeV and a branching ratio of B of $0.16 \pm .08$.

Astier et al[10] reported $K \bar{K}$ enhancement due to the presence of a resonance πn (1016) at mass 1016 ± 10 MeV with I = 1. Alternatively, S-wave enhancement in the $K \bar{K}$ system near threshold could be interpreted as the effect of a virtual bound state below the threshold at πn (980)[20]. The possible reaction would be

$$\bar{p} p \to \pi^+ \pi^- D^0$$
$$\hookrightarrow \pi^\pm_n \pi^\mp \quad K^0 K^\pm$$

The D^0 branching ratio, B would be a measure of the relative probability

$\frac{\pi n \to K \bar{K}}{\pi n \to \eta \pi}$; if πn (1016) and π_n (980) are

the manifestations of a single resonance.

The above decay scheme was not proved as the results of Defoix et al and Campbell et al could all be just ω reflection. The decay $D^0 \to \pi^\pm \delta^\mp$ could be observed with the copious production of ω in the multipion final states. Donald et al[44] repeated the experiment of Defoix et al[9] with three times the statistics. They did not find any production of δ on the removal of ω events. But without removing ω events, in 'η' $\pi \pi$ mass plot, X^0 was clear but D^0 was less convincing. In the $\pi_\eta \pi$ mass plot with the double selection of 'η' (in mass region .528 to .568 GeV/c^2) and δ (in mass region 0.955 to 0.995 GeV/c^2), a D^0 claim was not convincing. In the $\eta \pi^-$ plot, they observed a peak at 960 MeV/c^2.

Miller et al[45] in reaction $\pi^+ d \to p_s p \pi^+ \pi^- \eta$ at 2.7 and 3.1 GeV/c observed signal in the $\pi^\pm \pi^0 \eta$ system at D^0 and E^0 masses which were not produced due to ω^0 reflection. But their evidence for $\delta \pi$ decay mode of D^0 was poor.

An enhancement in the $\eta\pi$ mass spectrum was reported by a few groups. In $K^- P \to \Lambda^0 \pi^+ \pi^-$ MM at 5.5 GeV/c Ammar et al[18] reported an enhancement ($t \lesssim 1.5$ (GeV/c)^2) at mass 980 ± 10 MeV and width 80 ± 30 MeV with a selection of MM = M(η) $\pm$ 50 MeV, a figure suggested by the mass reolution.

More than 80% of the genuine missing η passed this missing mass selection; it was verified by the events in which $X^o \to \Pi^+ \Pi^- \eta$ and $\eta \to$ neutrals, a final state for which they got 'clean signal'. Probably $\eta\Pi^-$ sample consisted of 50% genuine η events. J^- determination was prevented by the staistical fluctuation but the probability that its decay distribution was consistent with isotropy was ~10%.

Barnes et al[16] in the same reaction at 3.9 GeV/c, 4.6 GeV/c and 5.0 GeV/c found a resonance of mass 975 ± 15 MeV and width ≤ 50 MeV with 50 MeV mass resolution. The η was selected in the region $0.27 < MM^2 < 0.33$ $(GeV/c)^2$.

At Kiev conference 1970, Oxford UCLA Group reported seeing a peak of mass 995 ± 15 MeV and Γ<40 Mev in Π^- η system in the same reaction at 3.3 GeV/c. Miller et al[14] observed an $\eta\Pi^-$ enhancement at 980 ± 10 MeV in k^-d experiment at 4.5 GeV/c. The measured width 60 ± 30 MeV was larger than 40 MeV, the experimental mass resolution. In the final state $K^-n \to \Lambda\pi^-MM$ they estimated 50% non- η background lying in η region, $0.23 < MM^2 < 0.36$ $(GeV/c)^2$ and η → all neutrals.

Crennel at al[17] in k^-d experiment at 3.9 GeV/c also observed an enhancement at 980 MeV/c^2 in $K^-n \to \Lambda\Pi MM$ with $0.22 < MM^2 < 0.40 (GeV/c)^2$ in η region, η → all neutrals. But no bump was observed for $\eta \to \Pi^+ \Pi^- \Pi^o$. So they suspected that this enhancement could well be explained by $\pi^- \pi^o \pi^o$ events when neutral dipion mass was selected in the η mass region. However, such a kinematical effect, applicable also to the results of Miller et al[14], was ruled out in the experiments of Ammar et al[18] and Barnes et al who did not find an equivalent effect in $K^-P \to \Sigma(1385) + \rho$ π^o $\rho \to \pi^-\pi^o$.

Abolins et al[42] in $pp \to d X^+_2$ at 3.8, 4.5 and 6.3 GeV/c observed an enhancement at 975 ± 6 MeV/c^2 and width 60^{+16}_{-10} MeV/c^2.

Obviously, the study of $\eta\Pi$ system is desirable for the understanding of this complex mass region near 1 GeV/c^2.

1-2 General outline of the experiment

The production and decay of mesons X of I = 0 and I = 1 produced in the interaction

$$\Pi^- p \to X^o n \qquad \text{(i)}$$

and $$\Pi^- p \to X^- p \qquad \text{(ii)}$$

were studied by a missing mass counter experiment. The nucleon time-of-flight in the final state and the incident pion momentum in the initial state were measured to calculate the missing mass.

Both charged and neutral decay particles were detected simultaneously (2-3-4). This enabled us to measure the branching ratios of a resonance for different decay modes. Alternatively, in principle, two resonances closely spaced in mass could be distinguished by their different decay modes.

The apparatus could detect a resonance with good mass resolution and high geometrical collection efficiency close to its production threshold. Although this technique exploited by our group had been successful for investigating ω, η[29] and φ[28], in a way it was a gamble for the search for a resonance near its production threshold where its production cross-section might be low.

Well above threshold, the mass resolution would be worse especially in the case of slow protons from reaction (ii) (§ 2-5) . The production cross-section of a resonance at higher incident pion momentum could also be measured, if compatible with the decreasing geometrical efficiencies and the worse mass resolution of the apparatus.

The experimental results were compared with the predictions of a Monte Carlo simulation.

The performance of the apparatus for detecting η and ω was quite satisfactory.

CHAPTER - 2

THE DESIGN AND PERFORMANCE OF THE APPARATUS

2-1 PRINCIPLE OF MISSING MASS SPECTROSCOPY

Consider the reaction

$$\pi^- \; p \rightarrow X \; N$$

Where X and N are boson and nucleon respectively. The missing mass Mx, of a boson in the laboratory system is given by

$$Mx^2 = (E\pi + Mp - En)^2 - P\pi^2 - Pn^2 + 2P\pi \; Pn \; Cos\theta_n$$

The Variables E, P and M are respectively the energy, the momentum and the mass of the particle denoted by the subscript. θ_n is the angle between the direction of the incident pion and the nucleon N.

To examine the resolution in missing mass we write down the derivatives of Mx^2 $\omega.r.t.$ θ_n, $p\pi$ and pn.

$$\frac{1}{2}\frac{\partial Mx^2}{\partial \theta n} = - P\pi \; Pn \; Sin\theta n$$

$$\frac{1}{2}\frac{\partial Mx^2}{\partial P\pi} = - \beta_\pi (En - Mp) + Pn \; Cos\, \theta n$$

$$\frac{1}{2}\frac{\partial Mx^2}{\partial Pn} = - \beta n \; (E\pi + Mp) + P\pi \; Cos\, \theta n$$

Where $\beta\pi$ and βn are the Velocities of the pion and the nucleon in the laboratory system. The Condition for the missing mass to be independent of θn is $\theta n = o$. The condition for the missing mass to be independent of the nucleon momentum is

$$\frac{\partial Mx^2}{\partial Pn} = o, \quad ie \; \beta n = \frac{P_\pi \; Cos\theta n}{E_\pi + M_p}$$

At $\theta n = o$, this condition becomes

$$\beta n = \frac{p_\pi}{E_\pi + M_p} = \beta_c$$

Where β_c is the velocity of the centre-of-mass of the π-p system in the laboratory. However, at threshold, both conditions $\theta_n = o$ and $\beta_n = \beta_c$ are satisfied and good mass resolution is achieved without an accurate measurement of either θn or Pn.

Near threshold, as nucleons are confined to a narrow forward cone in the laboratory, a high nucleon collection efficiency is obtained. Well above threshold, this condition is not satisfied and nucleon collection efficiency decreases.

The production X-Section σ for any particular missing mass M_X is likely to

be proportional to the centre-of-mass momentum P*, near the reaction threshold.

ie $\sigma = A P^*$

Where A is a constant.

This is because the Lorentz invariant phase-space density factor that enters the expression for σ is proportional to P* and at threshold region P* varies faster than any other factors governing the X-section.

The final state produced near its production threshold is in an S-wave angular momentum state for low P* range. This is because P* is much less than 200MeV/c near threshold and the strong nuclear forces extend over 1 Fermi or less ie the angular momentum (measured in unit of $\hbar$) = P*×R = $200\frac{MeV}{c} \times 1$ Fermi $\lesssim \hbar$.

2-2 THE RESPONSE OF THE APPARATUS

For the fixed values of $\theta_1 n$ and $\theta_2 n$ the shape of the curve relating the C.m. angle θ^* and the centre-of-mass momentum P* has been shown in Fig 2-2A. Where $\theta_1 n$ and $\theta_2 n$ are the limits of the angle, subtended by the neutron counter at the centre of the hydrogen target (Fig 2-2B).

The nucleons with Kinematical co-ordinates θ^* and P* lying in the region B are collected with high geometrical efficiency.

Fig 2-2-C shows the relation between incident pion momentum and the nucleon time-of-flight for a fixed mass and with the angular limits $\theta_1 n$ and $\theta_2 n$. $P_\pi t$ shown by the dashed line is the threshold momentum for Mx and corresponding to the centre-of-mass velocity β_c, the time is t_c. At slightly higher P_π, near the threshold $P_\pi t$, the nucleons within the angular limit are detected efficiently. With an increase in P_π, nucleons gain more energy in the centre-of-mass system and give rise to two peaks in the time-of-flight distribution corresponding to slow and fast nucleons in the laboratory system and backward and forward nucleons in the centre-of-mass system.

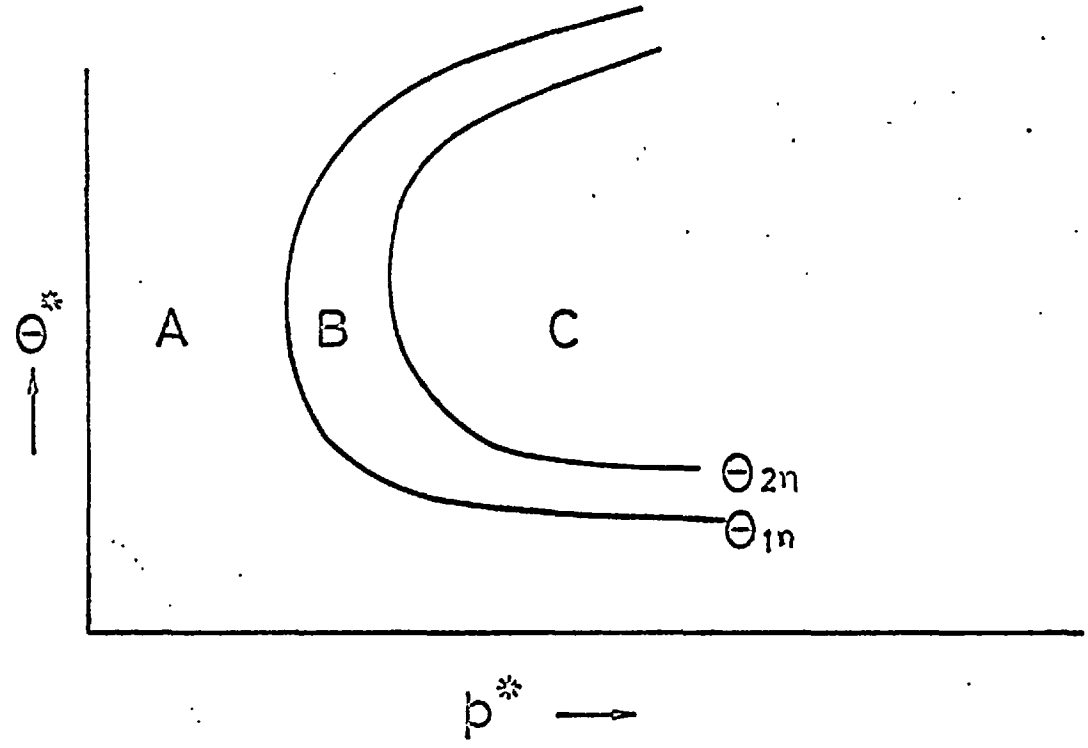

FIG. 2-2-A

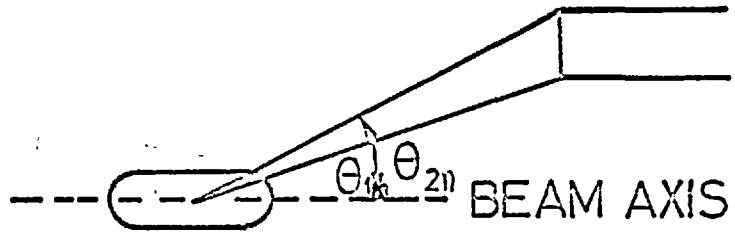

$\theta_{1n} \cong 1.7^\circ$, $\theta_{2n} = 5.0^\circ$ (typically)

FIG. 2-2-B

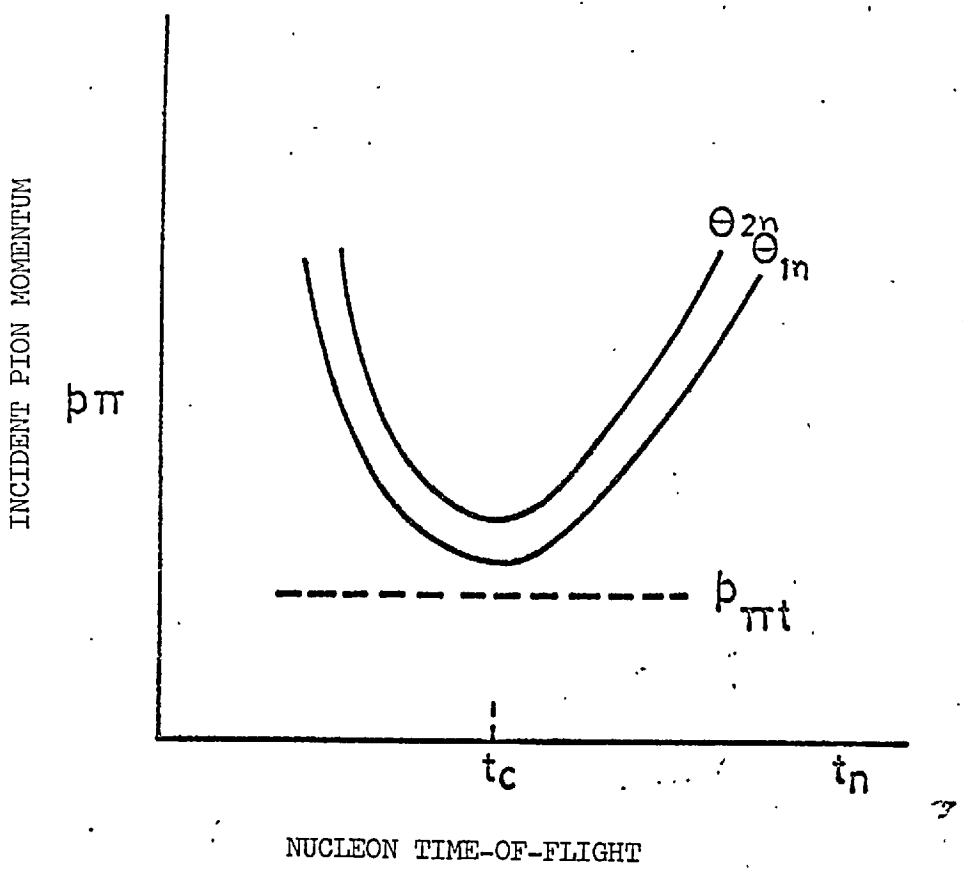
INCIDENT PION MOMENTUM
p_π
θ_{2n}
θ_{1n}
$p_{\pi t}$
t_c
t_n
NUCLEON TIME-OF-FLIGHT

FIG. 2-2-C

YIELD AND THE YIELD CURVE:

For a fixed number of pions, the number of nucleons detected by the apparatus, in a given time-of-flight range called the 'gate' is said to be the 'yield'. The gate around the centre-of-mass region is called the 'c.m. gate'. The curve obtained by plotting the yield in a gate as a function of incident pion momentum is called the 'yield curve'.

An enhancement due to a resonance of small X-section, spread over a few bins of time-of-flight distribution cannot be statistically as significant as it could be in the yield curve. Also, the change in background would be smooth and slow over a small range of incident pion momenta. Therefore, the yield curve is a good method for studying resonances.

Note that the gate can also be expressed in terms of an interval of momentum transfer t as

$$-t = (P_{4n} - P_{4p})^2$$

$$= 2Tn\ Mp - (Mp - Mn)^2$$

$$\simeq 2Tn\ Mp$$

where Tn is the Kinetic energy of the nucleon.

2-3 THE EXPERIMENTAL LAY-OUT:

2-3-1 Beam:

The secondary beam of negative pions, used in this experiment was produced by interaction of protons of energy 7GeV on the Copper target placed in the 5th Octant of Proton Synchrotron, "Nimrod". This π^- beam was transported to the hydrogen target by two stages of a magnet system consisting of quadrupoles (Q_1, Q_2, Q_3 and Q_4) and bending magnets M1 and M2.

In first stage, the image of the internal target was formed at the collimator C1 (Fig 2-3A). The first element of the beam line Q_1, a vertically focussing quadrupole followed by Q_2, a horizontally focussing quadrupole was placed as close to the machine as possible in order to maximise its acceptance. Following this doublet, a bending magnet M1 introduced a deflection of 7.25°. The magnet M1 also selected the particles of desired momentum band in conjunction with the collimator C1, which not only restricted the beam acceptance but also removed some undesired particles coming from other sources.

In the second stage, the dispersion introduced in the first stage was cancelled. The bending magnet M2 deviated the beam by 9.75°. M2 was used to determine the beam momenta with the hodoscope counters G2-10 and H2-7. The image of G was focussed horizontally on the H-counters and vertically at the centre of the hydrogen target by means of the second quadrupole doublet consisting of Q_3, a horizontal focussing and Q_4, a vertical focussing quadrupole.

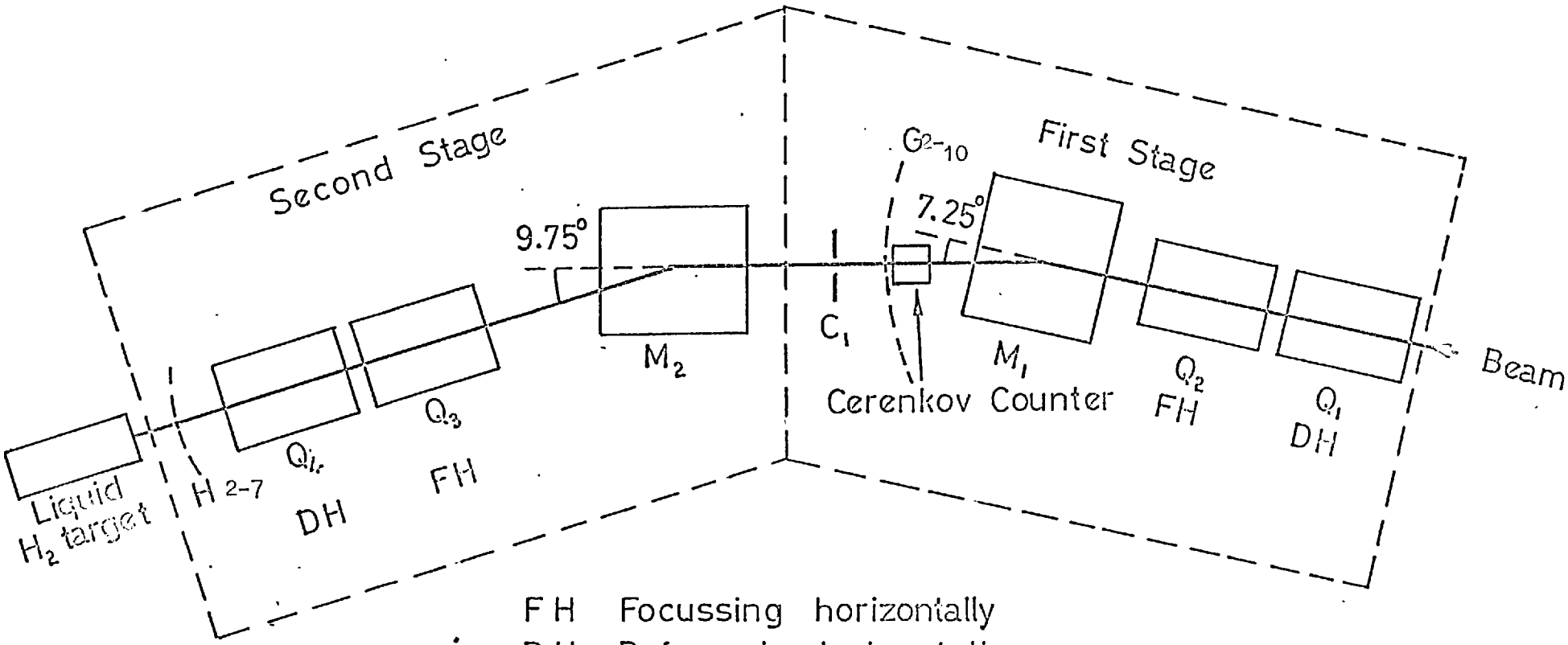

F H Focussing horizontally
D H Defocussing horizontally

BEAM LAYOUT (not to scale)

FIG. 2-3-A

Initially, the required currents for magnets were estimated by using the standard Rutherford Laboratory Computer programmes 'Tramp'[22] and 'Ipso facto'[23]. In order to determine an exact momentum of a particle as accurately as possible, BM2, Q_3 and Q_4 settings were determined by using the standard floating wire technique[24]. The error in the momentum calibration[25] due to errors in tension and wire current was estimated to be 0.14% which corresponded to 2.1 MeV/c in momentum.

The field of M2 was monitored by a standard NMR device using a Varian Associate fluxmeter, a frequency meter with proton and deuteron samples. This gave the NMR frequency for each desired momentum reliable to <.005% in frequency.

Momentum measurement:-

The momentum of particles was defined by M2 and the hodoscope counters. The amount of deflection of charged particles through the bending magnet M2 would depend only upon the momentum of the particles and not upon their emergent angle from G. All the GiHj pairs contributing to the same momentum channels were grouped together and thus five momentum channels or momentum bins were formed separately.

Due to the finite widths of the hodoscope counters, the defined momenta were not unique but were triangular in momentum distribution with full width at half-height of 0.5% ie $\Delta p/p = \pm 0.25\%$.

Setting up of beam

The beam was set at the central momentum channel by adjusting, first of all, M2 current to obtain the resonance pattern produced by the NMR device set at the appropriate frequency. Focussing was achieved by setting the quadrupole currents. In order to get the image of the central momentum channel symmetric about the beam axis at the G and the H counters, the M1 current was adjusted to maximise the beam rate in G_6H_4, the c entral combination of the central momentum channel. Before starting a new run, the symmetry of G-H distributions was also checked.

2-3-2 The target and the interaction defining counters:

The hydrogen target was supplied and maintained by the Rutherford Laboratory. The liquid hydrogen was contained in a 29.6 cms long mylar jacket of 0.01" thickness and of diameter 6.5 cms. The jacket was kept in an evacuated aluminium case with two melinex windows each 0.005" thick. A long pipe, joined to the upstream end of the aluminium case, delivered hydrogen from a reservoir and also acted as a physical support for the target jacket. The effect of the target length on the mass measurement will be discussed in Section 2-5.

Events associated with the non-interacting beam particles were rejected by detecting them either by A0, a counter placed downstream the target or by A01, a counter placed to cover the gap of the neutron counter ring (Fig2-3G).

2-3-3 Nucleon Detection System

A. THE NEUTRON COUNTERS, N_1-6

In order to detect nucleons and measure their time-of-flight, a group

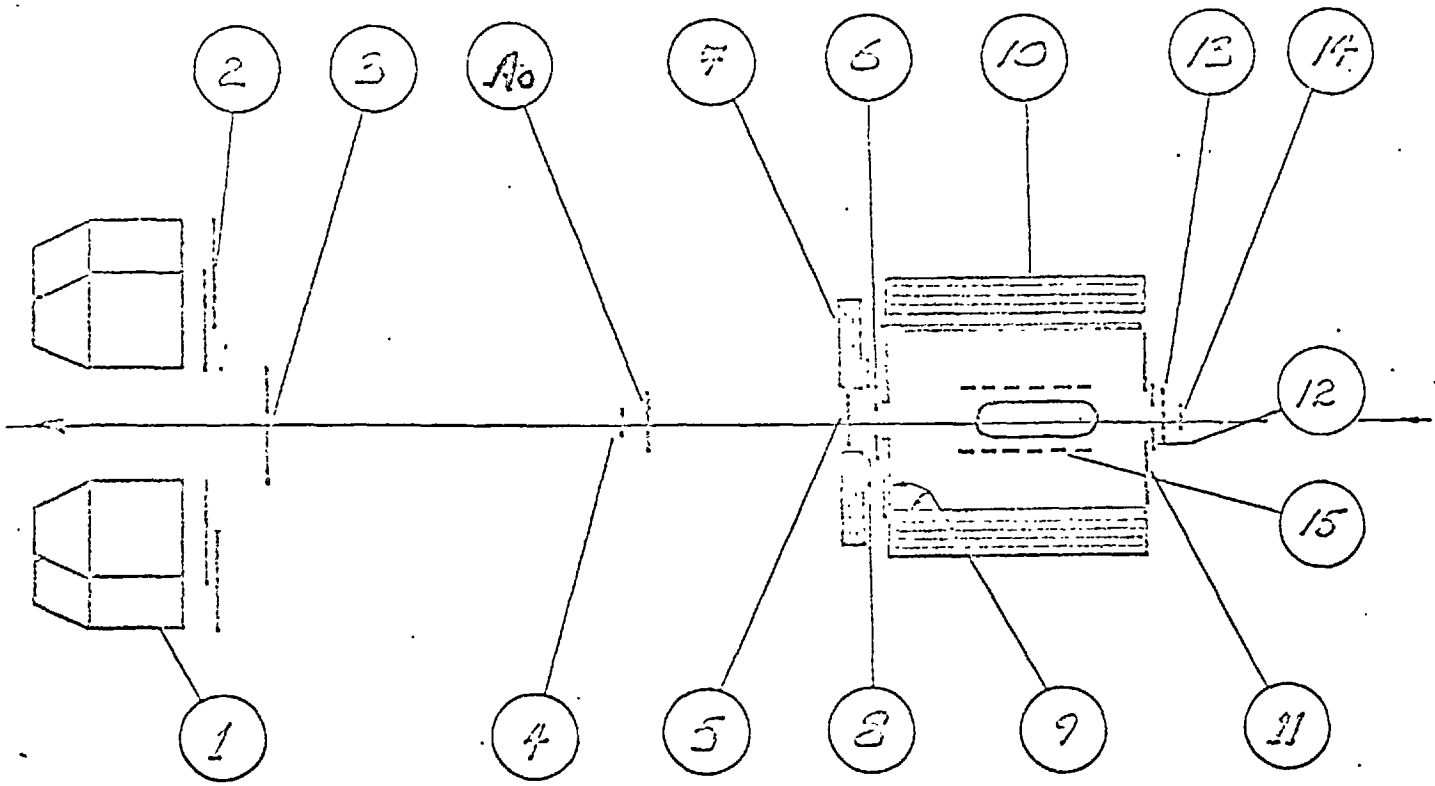

	COUNTER	EFFECTIVE SIZE
1	NEUTRON COUNTER	300 mm ϕ X 300mm LONG
2	PROTON COUNTERS	HEXAGONAL 32 A/F X 9mm THICK
3	VETO A_0 "	CIRCULAR 320 ϕ X 5mm THICK
4	BEAM S_3 "	SQUARE 60mm X 3mm THICK
5	'P' "	CIRCULAR 175mm ϕ X 2mm THICK
6	RING COUNTER R_1 & R_2	210mm O/DIA X 100mm I/DIA 5mm THICK.
7	LID 8 COUNTERS	20 COUNTERS 18° PITCH SANDWICH CONSTRUCTION 6 LAYER 5mm SCINT 4mm LEAD LEAVING 200mm HOLE.
8	POLAR ANGLE L_1 & L_2 COUNTER	400 O/DIA X 200 I/DIA 7·5mm THICK.
9	INNER CHARGED "	19 + 1 SPECIAL 18° PITCH SEGMENT LEAVES 100mm HOLE 10mm THICK 800mm LONG
10	CYLINDER 8 COUNTERS.	19 + 1 SPECIAL 18° PITCH 6 LAYER SANDWICH 5mm SCINT 4mm LEAD X 800 mm LONG.
11	DROOP 1 & 2	580 O/DIA X 160 I/DIA X 10mm THICK.
12	A13 COUNTER	190 SQ WITH 40 HORIZ X 42 HIGH HOLE X 5mm THICK.
13	'H' HODOSCOPE 7 FINGERS	60 HIGH X 7·52mm X 3mm THICK.
14	'S' COUNTER	55mm SQ X 2mm THICK.
15	TARGET COUNTERS TH_1 - TH_6	RING SHAPED AROUND LH_2 TARGET 130 O/DIA X 3mm THICK X 50 WIDE.

Fig 2-39

of six identical neutron counters of plastic scintillator NE 102A, designed for previous experiments[26,27,28] of our group, were used. Each neutron counter consisted of a 58AVP photomultiplier fitted to a 30 cms long conical perspex light guide which was optically coupled to a cylinder of scintillator of 30 cm.long and 30 cm in diameter (Fig 2-3B). The neutron detection efficiency of these counters was measured[29,30,31] to be approximately 25%. Its detection efficiency for the proton was assumed to be 100%.

The counters were arranged in a ring and were kept in a temperature controlled box. The distance between the neutron counter array and the hydrogen target could be varied by changing the position of a trolley containing the neutron counter box.

B. THE PROTON COUNTERS A1-6

.. A 9mm thick hexagonal scintillator (Fig 2-3C) was coupled to a twisted perspex light guide. One of counters A1-6 of this type was placed in front of each of the neutron counters. A neutron would give a pulse only in a neutron counter whereas a proton would give simultaneously a pulse in the corresponding proton counter A.

Uncorrelated N and A events could be classified as neutron or proton. Thus, for example, neutron would be N_i, N_iA_j, N_iN_j; $i \neq j$ and protons would be N_iA_j, $N_iA_jA_k$, $N_iA_jN_k$

$$i = j,\ j \neq k \text{ and } i \neq k$$

C. THE P COUNTER

A genuine proton produced by the pion incident on the hydrogen target would reach the neutron counter through the hole of 10 cms radius in the Lid gamma counters (described later on). A counter "P" with 2 mm thick scintillator of diameter 17 cms was placed downstream of the target so that any charged particle reaching the neutron counter outside the hole could be rejected by requiring a pulse from this counter.

2-3-4 The Decay System

In order to study the charged and the neutral decay modes of the resonances, a decay system was designed which covered the whole of the target except where the beam would enter and leave the target and also the gap caused by the pipe of the hydrogen reservoir connected to the target. See page 13.

The decay system consisted of inner charged counters, gamma counters, 'Droop' counters and 'Ring' counters.

A. The inner charged counters. The charged particles were detected by twenty scintillation counters called the 'Inner Charged Counters' (Fig 2-3-D). At the joint of two pieces of the scintillators, an air light guide was joined (see Fig 2-3-D). Perspex was not used because of the possibility of Cherenkov radiation from fast particles passing through the light-guide.

B. The Gamma Counters. Gamma rays are converted into electron-

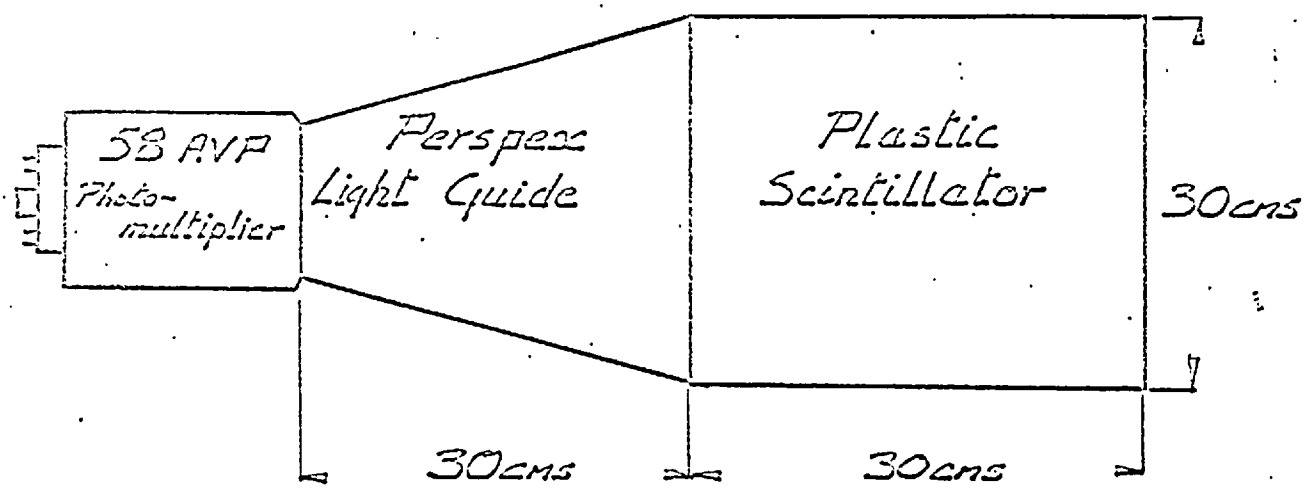

Fig - 2-3B.

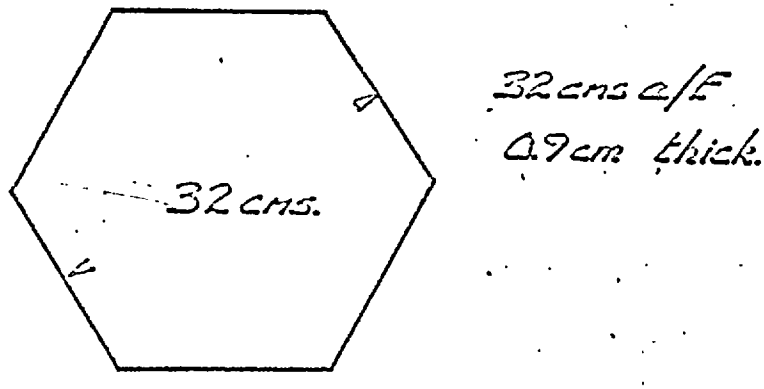

Hexagonal (A1-6) Counter. Fig. 2-3C

Inner Charged Counter

Fig 2-3D.

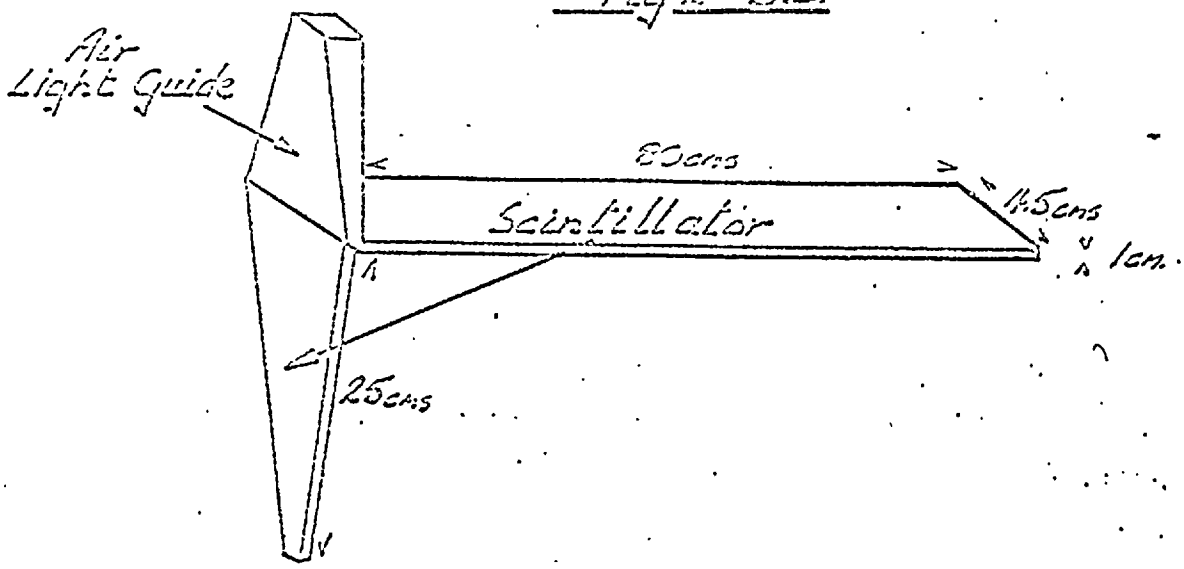

Cylinder Gamma Counter

Fig 2-3E

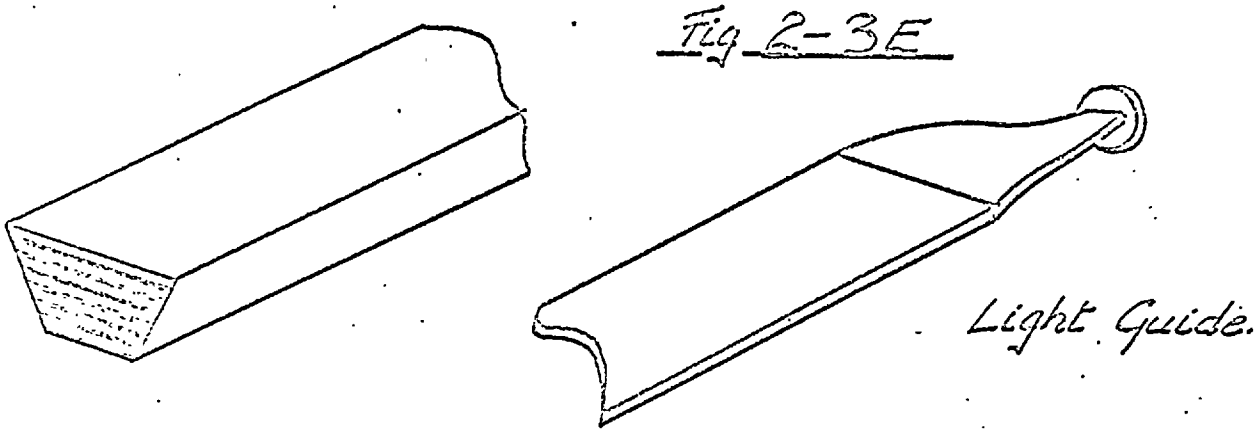

Drop Counter

Fig 2-3F

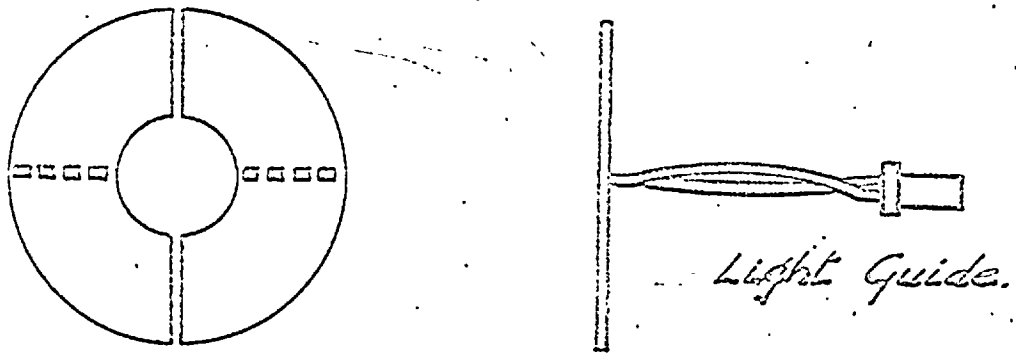

positron pairs which can be detected by scintillators. A gamma counter consisted of six layers of lead each 0.397 cm thick, 80 cms long and six layers of scintillator each connected to a perspex light-guide. Each lead layer except the innermost was sandwiched between the scintillators. The light guides were coupled to a single perspex button to fit on a photomultiplier.

On the sides of the target, the inner charged counters were surrounded by 20 gamma counters called the 'Cylinder gamma counters' (Fig 2-3-E). One of the innercharged counters and its corresponding cylinder gamma counter were made 40 cm long to allow the hydrogen target reservoir pipe to pass through the system.

In the front of the innercharged counters downstream the target, twenty gamma counters called the 'Lid gamma counters' were arranged to form annulus. A hole of 20 cms diameter in the Lid circle was left to allow nucleons to reach the ring of the neutron counter without passing through any decay counter.

Thus, a charged particle would be detected in an inner charged counter and its corresponding gamma counter whereas a gamma would give a signal only from the gamma counter. For convenience, we will call these detected particles 'PI' and 'gamma' or 'γ' respectively and the spare innercharged events as an 'IC'.

C. The Droop Counters. To detect backward going charged particles, the upstream end of the target was covered by two semiannular scintillation counters called the 'Droop Counters' (Fig 2-3-F).

D. The Ring Counter. A pion going forward and missing the gamma counters was detected by an annular 5mms thick scintillation counter placed downstream of the hydrogen target to cover those regions of the innercharged counters which were not covered by the Lid gamma counters. This counter was called the 'Ring counter'. Thus, a pion could be counted once, if the ring counter and a free IC went off.

RESPONSE OF THE DECAY SYSTEM

The efficiency of the gamma counters was determined in a test beam with gammas of known energy.[32,33]

The response of the decay system was also explored by studying not only the well-known decay modes of the known resonances but also two-pion events produced by resonant and non-resonant processes. The response of the system to gamma rays was investigated further by using the decay mode of $\eta \rightarrow 2\gamma$. The total number of events traced in different 'decay channels' for this mode was consistent with the branching ratio (38±2)%. Events with two Coplanar decay particles in the η mass region consisted almost entirely of $\eta \rightarrow \gamma\gamma$ decay. Thus, the probability for a gamma appearing as PI was found to be 14%.by studying Coplanar 'gamma-PI' events. Similarly, to study the behaviour of PI, the Coplanarity between two pions was required for the reliable selection of the event. Probabilities for different processes were measured, for example, the probability for a real pion giving an adjacent IC or an adjacent gamma etc.

An important result obtained from the study of the behaviour of decay particles in the system had shown that a charged particle less than 135MeV/c momentum would fail to reach the gamma counter but with more than 70 MeV/c momentum, it could reach to an innercharged counter.

Using all these figures for the probabilities of different processes in the Monte Carlo programme, 16% of all events produced in the reaction

$$\pi^- \; p \rightarrow \omega \; n$$
$$\omega \rightarrow \pi^+ \pi^- \pi^o$$
$$\pi^o \rightarrow \gamma\gamma$$

were estimated to appear in 2PI 2 gamma mode, which was in good agreement with the experimental results. The different decay modes of the δ^- meson were studied by using similar calculations in the Monte Carlo programme. As the response of our apparatus in $\eta \rightarrow 2\gamma$ was satisfactory, its behaviour in the case of $\delta^- \rightarrow \eta \pi^-$ was also expected to be reliable in the selection of $\pi^- 2\gamma$ due to the $\eta \rightarrow \gamma\gamma$ mode.

2-4 THE MONTE CARLO SIMULATION METHOD

The production and decay of the resonance produced in the π^-p interaction and detected by the apparatus were simulated by 'a computer programme.' A Monte Carlo technique (26) was used in which the following major assumptions were made about the interaction of the particles with the apparatus:

A. The momentum distribution of the pion incident on the target was taken to be triangular with full-width at half-height of 0.5% in momentum as discussed before.

B. The incident pion was allowed to have a small angle to the beam axis and to interact at any position in the target, all positions being equally probable. Allowance was made for the energy lost by the pion in traversing the target before interacting.

C. The neutron counters were supposed to be discs of constant efficiency uniform over their faces, for nucleons of all energies. The plane of the disc was assumed to be passing vertically through the centre of the counter. A nucleon was regarded as detected if its trajectory intersected one of these discs.

D. The nucleon timing error with a gaussian distribution of standard deviation t_1 nsec was added to the true time-of-flight for all events.

E. The assumption regarding the production process for a given width-were i. $\sigma \propto p^*$ up to a certain P^*max

and ii. $Cos\theta^*$ uniformly distributed.

The values of width and 't_1' were specified on the data card. The resonance was also allowed to decay into either two or three particles which were also allowed to decay further. The energies, momenta and directions of these particles were also calculated. Each decay product entering different decay counters was histogrammed separately. Besides calculating the loss of decay particles due to the counter inefficiency and geometrical losses, it also estimated how many events of decay mode would appear in different decay channels' produced due to aberrations of PI's and gammas.

The comparison between the experimental and the Monte Carlo results was a basis for the data analysis.

2-5 THE MASS RESOLUTION AND THE LIMITATIONS OF THE APPARATUS

2-5-1 The Mass Resolution

The mass resolution of an apparatus is an important factor in measurements of the mass and the width of a resonance. If it is greater than the mass difference of closely spaced resonances then the individual structure can not be resolved. Even in the case of a single resonance, it is desirable to have good mass resolution otherwise there would always be a confusion whether it is a single resonance or a combination of unresolved resonances.

The main factors governing the mass resolution ΔM_x of our apparatus are the uncertainties in the measurements of incident pion momentum Δp_π, the nucleon time-of-flight Δtn and the angular acceptance of the neutron counter $\Delta\theta$ so,

$$\Delta M_x = \sqrt{\left(\frac{\partial M}{\partial P\pi} \cdot \Delta P\pi\right)^2 + \left(\frac{\partial M}{\partial tn} \cdot \Delta tn\right)^2 + \left(\frac{\partial M}{\partial \theta} \Delta\theta\right)^2}$$

The uncertainties in these measurements are caused by the length of the hydrogen target, the sizes of the neutron counter and the hodoscope counter, the electronics handling signals from the timing counter S and the neutron counters and the distance between the target and the neutron counter.

However, in the case of the proton time resolution, the situation is different. A proton produced in the π P interaction loses some energy by ionisation in escaping from the target. The amount of energy loss depends upon the velocity of proton as well as the pion interaction point within the target. This affects the proton time-of-flight and in turn, the mass resolution.

With the knowledge of the uncertainty in the interaction point (at present ±15 cms) in the target at a given incident pion momentum, the

mass resolution can be estimated at various time-of-flight regions (Fig 2-5A). High mass resolution is achieved in the centre-of-mass region but it becomes worse in the longer time-of-flight region as the slow particle loses more energy in the target than the fast one. However a wide resonance can be observed in the later region.

2-5-2 The limitations of the apparatus

The accuracy and the sensitivity of the apparatus would be limited more by the systematic errors rather than the statistical fluctuation for example -

i. gain stability:- 1% change in the gain of neutron counter would correspond to 25 picoseconds change in the timing measurement,

ii. Timing stability:- 25psecs change in the width or the position of the gate could change the rate by 0.5% and,

iii. Casual rate: the proper measurement and subtraction of the casual events rate were necessary as it could vary quite significantly. Therefore it was reasonable to collect data with ±1% statistical fluctuation with above mentioned systematic errors.

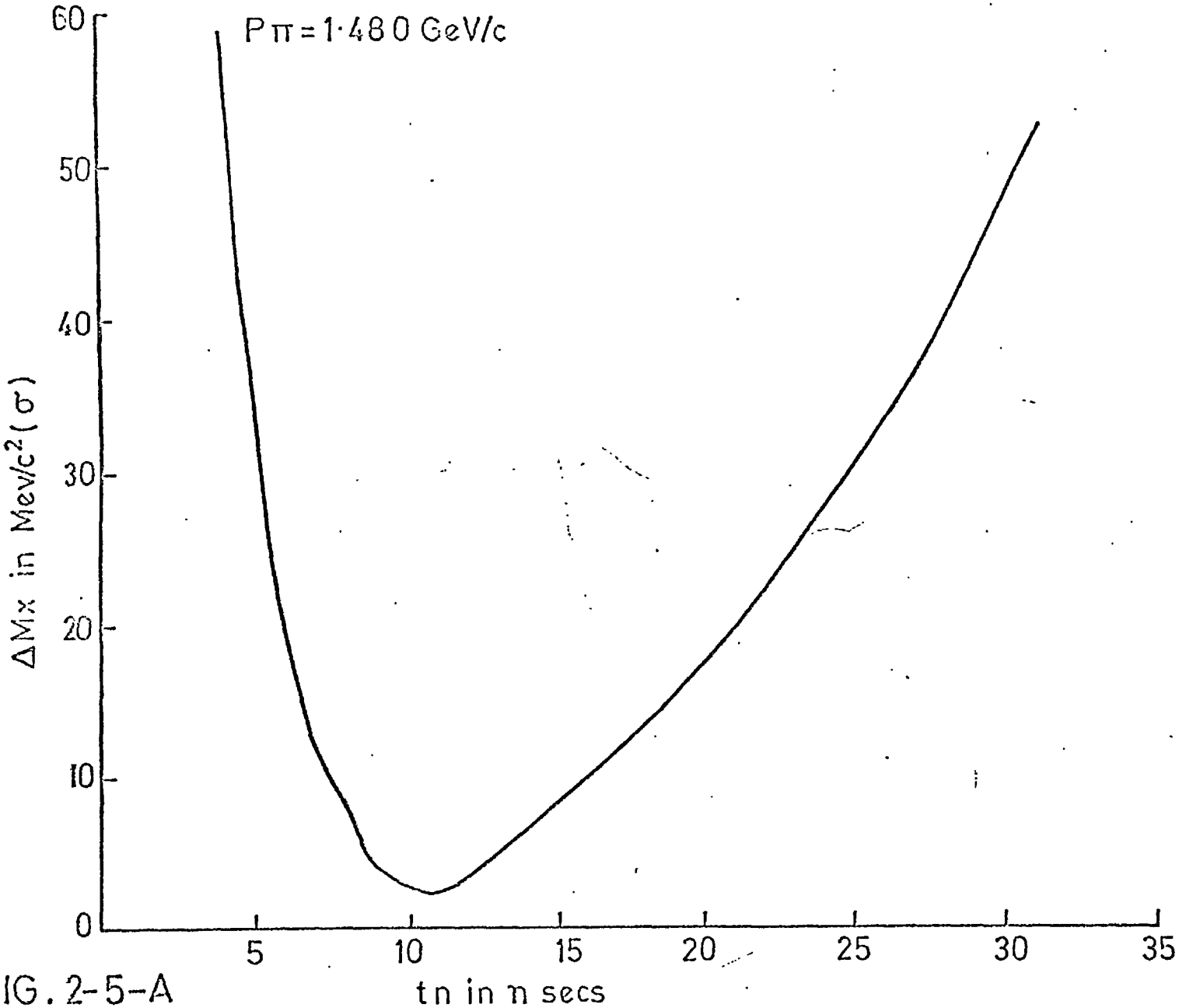

FIG. 2-5-A

Mass resolution (one standard deviation), a function of proton time-of-flight, contributed by (a) time-of-flight resolution of ± .8 nsecs., (b) the error in incident pion momentum measurement ± .25% and (c) the error in determining the point of interaction in hydrogen target = ± 15 cms.

CHAPTER - 3

THE ELECTRONIC SYSTEM

AND

THE ON-LINE PDP-8 COMPUTER

A THE ELECTRONIC SYSTEM

The purposes of the electronic System were four-fold:

(a) to recognise the occurrence of an acceptable signature in the beam-defining Counters followed within a specified time interval by a pulse in the Neutron Counters,

(b) when this occurs, to provide an on-line Computer with the states of all the Counters, the Neutron Counter pulse-height and the time delay after the pulse in the S Counter,

(c) to count the number of beam particles entering the target in each of the five momentum channels,

(d) to monitor the stability of the time-of-flight system and to record certain 'Casual rates' which enabled correction to be made for beam intensity variations.

The electronic system was built using standard "tunnel" and miniature logic systems 34,35. The Cards were available in standard 'AND gate', 'or gate', 'set-reset', 'discriminator', 'level changer' and a few other useful forms. Each photomultiplier pulse was connected to a discriminator to give a standard tunnel pulse.

3-1 BEAM LOGIC

For a 'genuine beam pion' we required a pulse from only a single counter of each hodoscope array, no pulse from the Cerenkov Counter to Veto electrons and a pulse from the timing Counter S.

The determination of the pion momentum relied upon the detection of the pulses from the G and the H combinations of the hodoscope counter. The five momentum channels were formed by grouping their respective Gi Hj Combinations by standard coincidence circuits. This was possible because G and H were conjugate focii in the horizontal plane. These five channels were further combined together to form a '$\Sigma P_{\pi i}$' channel (Fig 3-1A).

The events with two or more particles detected either by the G or by the H Counters were rejected by a circuit called '2G - 2H' Veto. This was to avoid ambiguity in the momentum and reduce casuals (§3-4-2).

At the cost of a few percent of the beam, some casuals were also removed by the 'Interference Remover (IR)'. This Circuit was designed to inspect the S pulse and reject an event with two or three particles coming within 30 nsecs of each other. If, however, the second pulse would come within the dead-time of the S counter discriminator, it was not rejected.

BEAM LOGIC BLOCK DIAGRAM

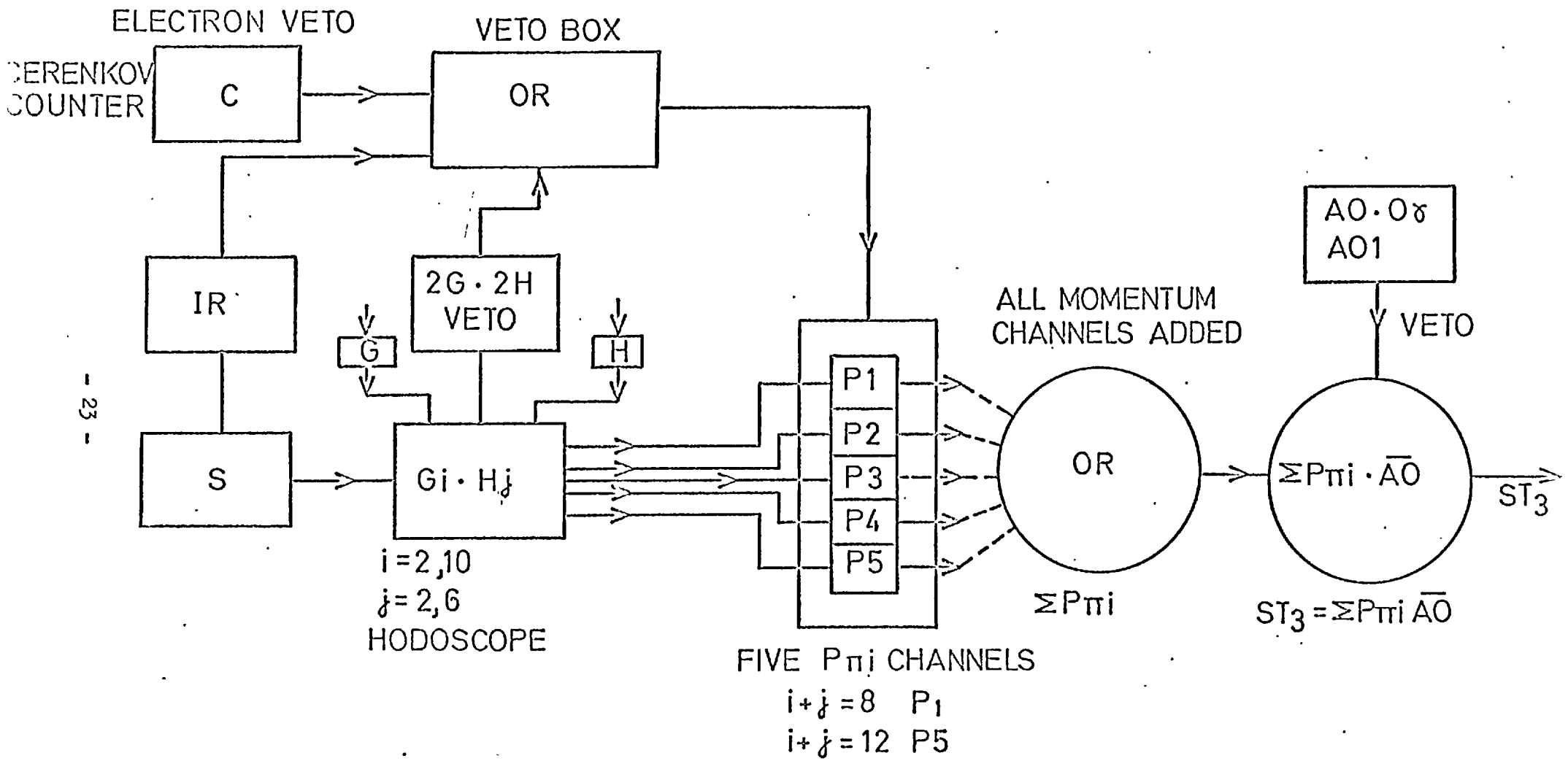

BEAM = S.Hi Gj.$\bar{C}$. $(\overline{2G.2H})$ $(\bar{IR})$

$8 \leq (i+j) \leq 12$

So, a genuine beam particle would satisfy the following conditions -

$$S.\ Hi.Gj.\ \overline{G}\ .\ (\overline{2G.\ 2H})\ .\ \overline{IR}$$

with $8 \leq (i + j) \leq 12$

The total number of pions in the individual and combined momentum channels were scaled during the burst and were transferred to the computer at the end of each burst.

A Signal that a beam particle had interacted in the target was formed by putting counters A0 and A01 in anti-coincidence with $_{\Sigma}P_{\pi}i$ i.e. $_{\Sigma}P_{\pi}i\ .\ \overline{A0}.\ \overline{A01}$. We called this quantity ST3. For convenience, we will write A0 for either or both of the Counters A0 and A01.

3-2 The Neutron Counter timing and the pulse height measurement.

3-2-1 The Neutron Counter timing.

As the neutron rate in a gate would be affected by inaccurate measurement of timing, precautions were taken to minimise the effect.

A major cause of the uncertainty Δt in the timing measurement of the Neutron Counter pulse was the wide range of the amplitude. To reduce Δt, the minimum accepted amplitudes of the pulses were determined by the higher discriminator bias level set in the 'double discriminator method'. The timing of the allowed pulses were determined by the lower bias level. The pulses from the discriminators of a neutron counter were combined (Fig. 3-2A, Part A).

The effect of the pulse height variation on the timing uncertainty was further reduced by applying in later analyses a correction for pulse height to the time-of-flight of the accepted pulses. The correction was estimated empirically by finding what correction was required in the sharp time-of-flight peak in $\pi^- p \rightarrow \eta\, n$

3-2-2 The pulse height measurement

The variation in the gain of the Neutron Counter would cause a change in the pulse height distribution and a variation in the nucleon detection efficiency. A 1% change in the gain of the Neutron Counter would cause 25 psecs change in timing which would change the Neutron rate by 0.5% in a centre-of-mass gate. A 10% change in the detection efficiency would correspond to 1% change in the pulse height.

The amplitudes of Neutron Counter pulses were digitized. The pulse height distribution was calibrated by using fast pions or protons. Fast pions lose about 60 MeV energy ($\sim$ 2 MeV/cm) passing through the Scintillator of the Neutron Counter and produce a corresponding peak in the pulse height distribution. Hence, the Neutron Counter gain was checked by comparing the position of the pion peak with its previous recorded value.

3-3 The trigger logic

The formation of an ST3 ($_{\Sigma}P_{\Pi}i.\ \overline{A0}$) pulse signified the interaction in the hydrogen target of a selected pion of a certain momentum measured by the

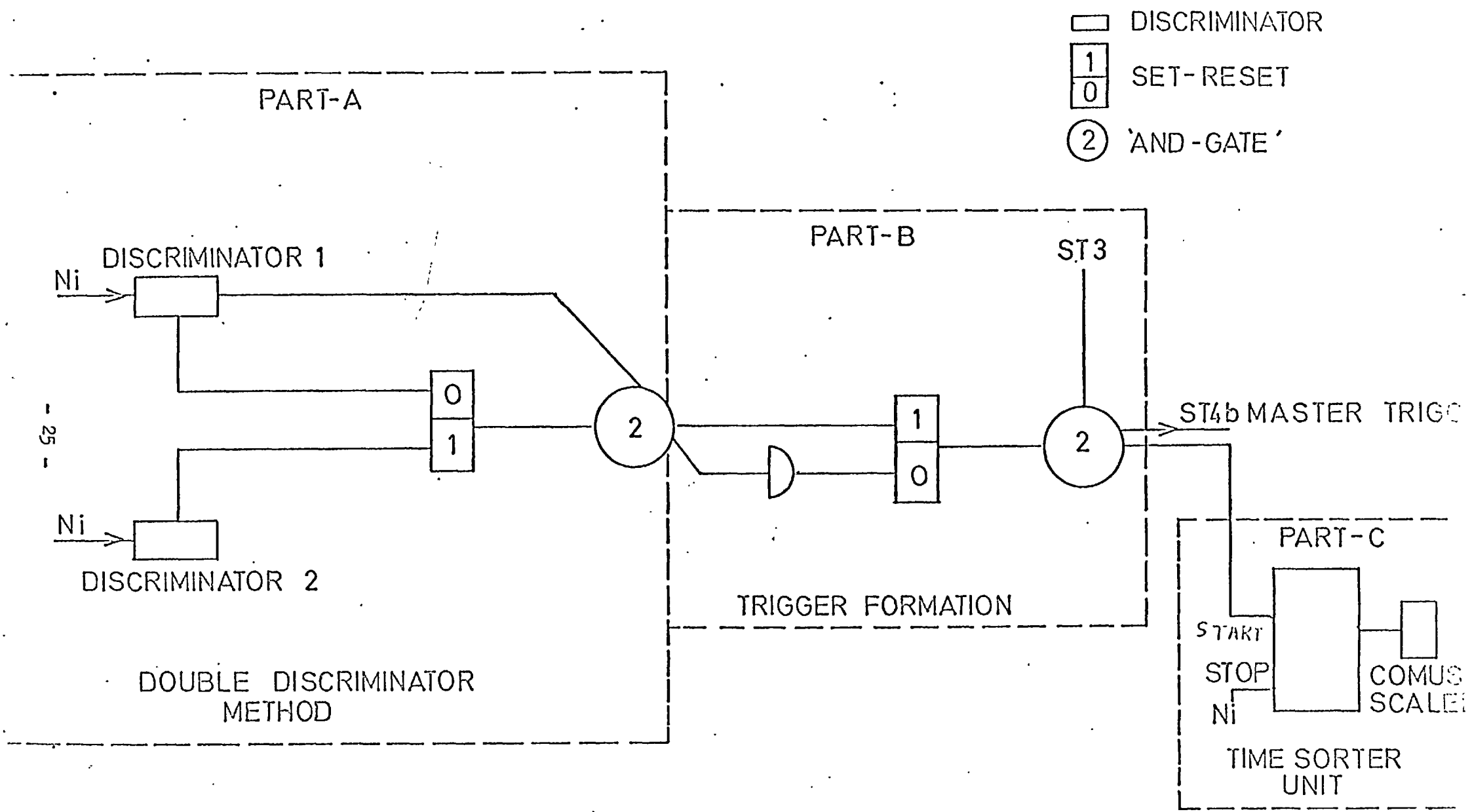
DISCRIMINATOR
1
0
SET-RESET
2
'AND-GATE'
PART-A
PART-B
ST3
DISCRIMINATOR 1
Ni
0
1
2
1
0
2
ST4b MASTER TRIG
Ni
DISCRIMINATOR 2
PART-C
TRIGGER FORMATION
START
STOP
Ni
COMUS
SCALE
TIME SORTER
UNIT
DOUBLE DISCRIMINATOR
METHOD

FIG 3-2-A

hodoscope counters. This, together with the detection of a nucleon within a specified range of time-of-flight (3 to 45 NSec after the reference (§ 3-4-1) peak) constituted a genuine event. With the occurrence of a genuine event, a master trigger, ST4b was formed (Fig 3-2A, part B).

The nucleon time-of flight was measured by the time difference between the pulses from the timing reference counter S and any one of the Neutron Counters. This time-difference was digitized by a 'time-Sorter'. The number obtained was fed to a binary scaler in the 'Comus System'. This system consisted of binary scalers and 12-bit storage registers. Each counter was connected to a bit of a Comus register to store the state in coincidence with the master trigger.

3-4 MONITORS

The monitors were:

3-4-1 Fast Peak

3-4-2 The Casual Monitor

3-4-3 The Occupancy Monitor

3-4-1 Fast Peak

The time-of-flight distribution of the beam scattered into the Neutron Counter was called the 'fast-peak', which was almost entirely due to charged particles of $\beta \simeq 1$. The fast-peak was used as a timing reference for the time-of-flight distribution. It also gave a measure of the timing resolution. The mean position of the fast-peak was determined with $\pm$ 20 psecs uncertainty in time. Thus, a shift in the position of the peak implied accordingly a shift (by the same amount) in the positions of the gates under consideration by the same fraction of a channel.

3-4-2 The Casual Monitor

A casual event could produce random pulses in one or in a group of counters to satisfy the conditions for coincidences and Vetos of the electronic circuits. In our experiment, for example, a casual event in the counter A0 would result in the loss of an event (§ 3-4-3). On the other hand, casual events satisfying the trigger conditions would affect the time-of-flight spectrum as well as the measured nucleon rates in the gates.

Certain types of casuals were discarded by the beam logic, viz a) casual events detected at counter S within 30 nsecs of beam particle during the operative time of the IR, and b) casual events where two counters in either array of the hodoscope fired(rejected by 2G 2H.Veto).

Two other classes of casuals could be defined in analysis and rejected a) events with a neutron signature but with an associated P-counter pulse and b) events with a proton signature but without an associated P-counter pulse.

The rates of various other classes of casuals were measured. One class was found important. When an interacting beam particle failed to produce a detected nucleon, a trigger was formed by an accidental coincidence in the neutron counter. This class of casual was monitored throughout each run by combining the interacting beam pulse ST3 with the delayed neutron counter pulse.

The neutron rate in a gate was corrected assuming a flat distribution of the casuals throughout the nucleon time-of-flight spectrum. This assumption would be unjustified if the casual time-of-flight distribution had structure in some region of the spectrum; which might be produced a) by the events which scattered from the wall or the roof or the floor of the experimental hall or b) by the various Veto or coincidence requirements. As these classes of events could not be measured properly by the casual monitor, it would be difficult to correct the data for each run. At the cost of some signal, the casual background was reduced by discarding certain classes of such events either appearing in some decay modes or associated with some counters (§ 5-2).

3-4-3 The Occupancy Monitor

The absence of a pulse from the counter A0 was required in the trigger formation to reject non-interacting beam particles. The effects due to the presence of an extra count in the A0 counter was estimated and a suitable correction was applied to the affected rates.

The ST3 circuit ($\Sigma P\pi i \cdot \overline{A0}$) was designed so that the dead-time of the A0 discriminator was shorter than the resolving time of the Veto circuit. This was to remove any dead-time effect of the A0 discriminator caused by a casual pulse in A0 counter, in presence of a non-interacting beam particle.

A genuine event could be lost if an accidental pulse in A0, not caused by a particle passing through the beam counter, produced a Veto. The lost fraction of the events was called the "occupancy". To take into account this loss, the occupancy of the A0 counter was estimated by measuring $A0.\overline{S}$ rate by the 'occupancy monitor'. Its logic was formed by combining the beam pulse with the delayed $A0.\overline{S}$ pulse. As some of the beam particle would be rejected if some classes of casuals associated with the A0 counter come within the operative time of the IR or 2G 2H Veto and also pass through the S-Counter and hodoscope counters, $\overline{S}$ was required to exclude these particles. Corrections were applied to the ST3, the neutron and proton rates in a gate to work out their true rates.

B. THE ON-LINE PDP-8 COMPUTER

The raw data in blocks of up to 64 events was written on the 7-track magnetic tapes by an on-line PDP-8 Computer. With the trigger formation, information from the Comus Scalers was fed to the PDP-8 via a suitable interface. The PDP-8 with 4 K words storage was equipped with a magnetic tape deck, a teletype, a CRT display and a disc of 32K storage(36)(Fig 3-5A).

Each block was labelled by the block number, the run number and the number of the block within the burst. The states of all the counters were written on the tape by setting a bit to 1, if a counter triggered, otherwise zero. The time-of-flight information was also recorded. Some scalers which counted throughout the burst were read in at the end of each burst.

Each event was analysed by an on-line analysis program. The analysed summary of various monitors, scalers and decay information was contained on a block of memory on the disc. This summary was updated with the results from each burst.

At the end of each run, the computer printed a 'run summary' which contained the nucleon time-of-flight distributions, pulse height distribution, the yields of nucleons and the selected decay modes in a specified gate, the scaler information, the monitor rates and the number of times each counter fired. At the beginning of each run, the 7-track tape was indexed with the run numbers, the momenta, the tape number and the magnet current values.

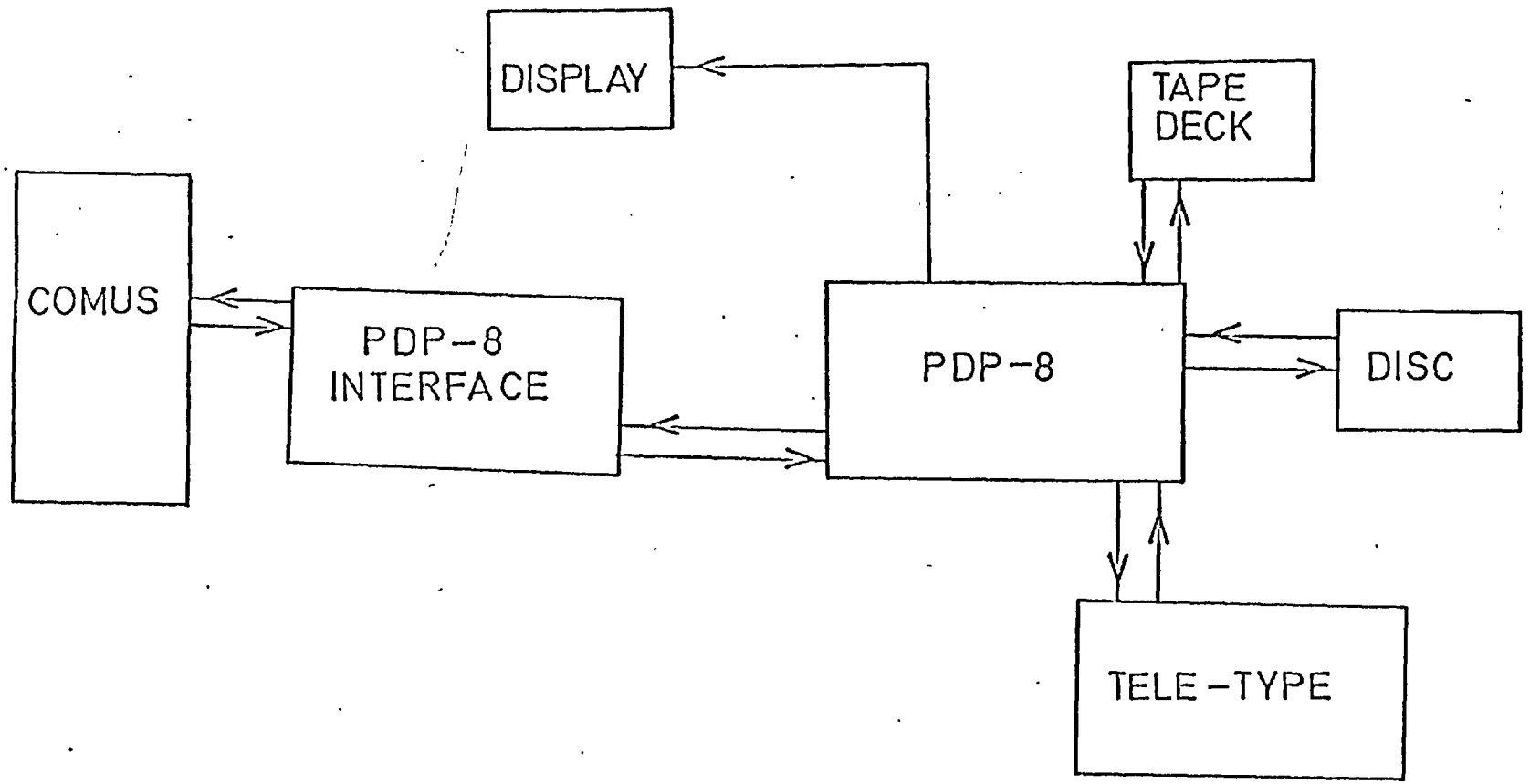

FIG : 3-5-A

The facility was also available for off-line analysis of data. A run summary or print out of single events with desired selection of the decay modes could be obtained.

CHAPTER 4

PRELIMINARY DATA ACQUISITION

AND

GENERAL METHOD OF ANALYSIS

4.1 PRELIMINARY DATA ACQUISITION

The aim of the first set of data-taking runs was to scan the mass region from 0.5 GeV/c^2 to 2.0 GeV/c^2 in order to study the resonances very close to their respective production thresholds. The distance of the neutron counters from the target was chosen to be 5MS to collect nucleons with a reasonable rate (24) and to obtain good mass resolution (24). The data was taken in February 1969; scanning from higher to lower momenta at intervals of five momentum bins, corresponding to approximately 35 MeV/c steps of incident pion momentum in the X^0 region. Two runs each for 200 million incident pions at each momentum interval allowed the reproducibility of data to be checked to $\pm$ 1% on the neutron yields in a centre-of-mass gate. (§2-5-2)

Eighteen runs in the δ region covering incident pion momenta from 1.38 GeV/c to 1.64 GeV/c were part of the general scan. A few "hydrogen-out" runs were also taken. Three later runs taken in November 1969 were rejected as they were affected by troubles in the temperature stability unit of the electronic rack.

At the end of each run, various rates obtained by the on-line summary out-put were plotted against the pion momentum to check whether any fault developed suddenly during the data-taking and also to see the general trend of their variations with change in the pion momentum; for example, the casual rates, the ST3 rate, the occupancy rate, and the corrected nucleon rates as well as some interesting decay modes rates in the centre-of-mass gate.

At the beginning of each run, after setting the beam at a desired momentum (§2-4-1), different monitors and the counter rates were also checked on the C.R.T. display.

4.2 GENERAL METHOD OF ANALYSIS

The full data analysis was carried out on the Rutherford Laboratory 360 Computer which read information from 9 track magnetic tapes duplicated from the 7 track data tapes.[37] All this information was read by a Fortran program.

The fortran program checked an event and classified it according to its decay signature. The time-of-flight distribution and the yield in a gate were also obtained. A subroutine examined all the inner-charged and the gamma counters and the event was classified as "PI", "IC" or "gamma" accordingly (§2-3-4). The PI class was enriched by including the PI detected by either the droop counter alone or the ring counter with an extra IC counter. In the case of more than one IC associated with the ring, it was optional to count either as many PI's as IC's or just one PI, so that this could be decided later on depending upon the decay mode of interest. A facility was also provided either to ignore the state of the ring counter or to discard all events in which the ring counter fired. Two classes of gammas were γ and γ_2. In the former class, a signal from one gamma counter was required while in the latter case, signals from the adjacent gamma counters were required. The separation between two particles could be worked out.

All the qualified events of different classes at each momentum bin, were histogrammed in time-of-flight bins and their yields in a gate were also calculated. The events of all the bursts of a run were analysed one by one and the end of burst scalers of each burst were accumulated.

At the end of the analysis of the run, the time-of-flight histograms along with other information were printed. The yield in the gate was corrected for the casuals, the occupancy of the AO Counter and the fast-peak position (§3-4) and was called the "corrected yield". The corrected yields were normalised to 100 $m\pi$, for convenience, and printed (100 $m\pi = 10^{8}$ pions or, 100 million pions).

4.3 BACKGROUND

All events except the Signal from a resonance under consideration were said to be "background". The background could arise due to two sources (i) physical and (ii) instrumental.

(i) Physical Sources of background.

a) Phase-space: the background produced from the interaction of the pions on the target not via any resonance.

b) Other boson resonances decaying with same decay signature could also produce background for the resonance under consideration.

c) Baryon resonances can participate both as reaction products along with bosons and as an "Intermediate State" in the S-Channel.

(ii) Instrumental Sources of background.

a) Background from other decay mode: In our system, background in a decay mode could be contributed by some channels of other decay modes (See for example §6.3.1).

b) The non-hydrogen events: produced by the interaction of the beam particle with either the material in the mylar end caps of the hydrogen flask or with the proton counter or the ring counter.

c) Casual events: produced by various processes (§3.4.2).

A run below the production threshold of the resonance could be considered to study some of the backgrounds.

4.4 REPRODUCIBILITY

Since changes in the experimental conditions or the development of some faults in the apparatus during the data-taking could result in the non-reproducibility of data, it was desirable to check that various rates were reproducible. Thus, the factors affecting the reproducibility would be the variation in some of the background rates, lack of hydrogen in the target and variation in the time measurement system, etc. Therefore it was necessary to check the reproducibility of data by comparing rates of two runs taken at same momentum.

CHAPTER 5

THE X^o RESULT

5-1 INTRODUCTION

To investigate the production of the X^o meson near threshold, the data was treated in two different ways. Firstly, the total neutron event rate was studied as a function of incident momentum but with an attempt being made to reduce the background by discarding events which, by virtue of their signatures in the decay counters, were recognized as predominantly non-hydrogen or as coming from reactions to which the X^o could not contribute. Some of these events were associated with the P-counter and the ring counter. Secondly, decay signatures were selected corresponding to the known decay modes of the X^o and the yield of such events was plotted as a function of momentum.

In plotting event yield versus momentum, a c.m. gate of PDP-8 channels 42 to 53 corresponding to 6.8 to 13.2 nsec after the fast peak was chosen by maximizing the ratio of predicted signal to noise n, (the statistical fluctuation of the background). The signal was obtained from the montecarlo predictions for a mass of 960 MeV/c^2. Three other gates were also used (see table 5-1A).

GATE POSITIONS		
In nsecs after the fast-peak	PDP-8 channels	$\|t\|$ $(GeV/c)^2$
4.7 to 6.8	38 - 41	1.1 - 0.79
6.8 to 13.2	42 - 53	0.79 - 0.38
13.2 to 18.4	54 - 63	0.38 - 0.25
6.3 to 12.2	41 - 51	0.86 - 0.42

TABLE 5-1A Selected gates (FAST-peak in PDP-8 channel 28.50)

5-2 EVALUATION AND REDUCTION OF THE TOTAL NEUTRON BACKGROUND

The total neutron background was evaluated in a gate of PDP-8 channels 41 to 51 corresponding to another centre-of-mass gate 6.3 nsecs to 12.2 nsecs. A run below the X^o production threshold at incident pion momentum, P_π = 1.408 GeV/c with hydrogen in and a run at P_π = 1.339 GeV/c with hydrogen out were analysed in order to study the background. The non-hydrogen rates were assumed to be equal at both momenta.

Types of events discarded from total neutron rate.

(a) Neutron events with 'P' Counter:

At the cost of 6% signal, the total neutron background in the gate was reduced by 36% by discarding the neutron events associated with the P-Counter.

This was reasonable as a genuine neutron produced in the $\bar{\pi}$ p interaction would not give any signal in the P-counter. This requirement was also suitable for the selected decay mode study, as a forward going charged particle detected by the P counter would give a wrong decay signature.

Description	Number of events per 100 m π	fraction of total	PI, IC, GA 000	010	020	100	110	200	210
H_2 - in	3600	1.0	.026	0.090	.040	.040	0.060	0.106	0.033
H_2 - out	1013	.280	.026	0.040	.007	0.035	0.012	.021	.008
H_2 in events with the Ring Counter	909	.250	.007	0.070	0.030	0.005	0.025	0.005	.005
Percentage of X^o signal predicted by the montecarlo program			.04	.09	.08	.3	.9	3.0	.7

Total = 5.1%

Table 5-2A

Fraction of background and signal appearing in various decay modes. In each case, gate 6.3 to 12.2 nsecs was used. Events associated with the P-counter were rejected and the ring counter was ignored in the definition of PI.

With the requirement of no pulse from the P-counter, we tabulate (see table 5-2A) the observed background, the contribution of the non hydrogen and the ring counter events, and estimate of loss of signal predicted by the montecarlo program (with an assumption of isotropic decay distribution of the X^o meson) in each discarded decay mode. The loss of signal in each case was small.

(b) 000 and 100 (PI, IC, GA): Most of the events with these decay signatures were non-hydrogen events (see table 5-2A).

(c) 010 and 020: 77% of all these events were associated with the ring Counter.

For convenient study of the ring events, a PI going through the ring counter was distinguished from the rest of the PI's and was not included in definition of PI. This convention was maintained throughout the analysis discussed in this chapter. If required, the ring PI event could be added in the desired decay channel.

(d) 200: 10.6% of the total neutron background was reduced at the cost of 3% of the signal (see table 5-2A). Further analysis of this mode revealed that the shape of its yield curve was changing rapidly which could make it difficult to estimate the shape of the X^{o} background.

(e) 210 and 110 (PI, IC, GA)

Two charged particles in the decay system could also be detected in channels 210 and 110, by producing an extra IC as a PI aberration in the former case. In the latter case, however one charged particle would be detected only by one IC counter alone or with the ring counter. Rejection of these two channels reduced the background by 9.3% at the cost of 1.6% of the signal.

(f) more-than-one-neutron-counter event, $\geq$ 2N events: the neutron time-of-flight of such events could be ambiguous.

(g) The non-concurrent N and A events N_i A_j, $i \neq j$.

a) there was a structure in the long time-of-flight region.

b) 44% of such events were casuals.

The last two classes (f) and (g) were rejected to reduce the background by 5.7% and 6% with negligible loss of signal.

Thus, the total neutron background was reduced by $\sim$60% at the cost of 11.1% signal. Events of type (a), (f) and (g) were also rejected for the decay mode analyses.

It is worth pointing out that all the neutron events associated with the ring counter were not rejected as a loss of 8% signal could have occurred.

5-3 RESULTS

With the above selections the corrected neutron yields in the centre-of-mass gate of 6.8 to 13.2 nsecs after the fast-peak at each point, obtained by combining momentum bins in fives, contributed from different runs were found reproducible within the statistical fluctuation.

Thus, the yield curve for 'the selected total neutron events' in the centre-of-mass gate had indicated an enhancement in the X^{o} region (Fig 5-5A). The number of the X^{o} in the peak channel above the background was estimated to be 150 X^{o}/100 mπ . This figure will be used for estimating the number of X^{o} in its different decay modes. For discussion see §5-5.

5-4 THE DECAY MODES OF THE X^{o} MESON

The X^{o} search in its various decay modes (tabulated in table 5-4A) required the estimation of the signal and the observed background in each case. The number of X^{o} produced in each decay mode was calculated by taking into account the branching ratio and the number of the X^{o} estimated from the yield curve 5-5-A i.e. 150 X^{o}/100 mπ.

No significant enhancement was observed in the yield curve of either $\pi^+\pi^-\gamma$ (table 5-4-C) or $\pi+\pi-\gamma\gamma$ (table 5-4-F). However, for $X^o \rightarrow \pi\ \pi\ \eta$ an enhancement in the yield curve of the decay channels $\pi^+\pi^-$ all neutrals $\geq 3\gamma$ and neutrals $> 3\gamma$, added together was observed (see § 5-4-3, § 5-4-4 and § 5-5.) The decay modes are discussed below separately.

5-4-1 $\pi^+\pi^-\gamma$ mode

The signal in this decay mode was expected from

$$X^o \rightarrow \pi^+\pi^-\gamma$$
$$\text{and } X^o \rightarrow \pi^+\pi^-\eta \quad \eta \rightarrow \gamma\gamma \quad 1\gamma \text{ missing.}$$

The estimated number of the X^o to be detected in the decay channel 201 for this decay mode was 17.2 for $150X^o$ per 100 mπ (Table 5-4-B). The observed background in the gate of 6.8 to 13.2 nsecs was $\simeq$ 150 per 100 mπ with the statistical fluctuation of $\pm$ 5.6, estimated for the available data (i.e. 400 mπ pion).

No improvement in the S/B ratio was expected by adding the other channels viz $\bar{\pi}1$ IC 1γ i.e. 1o1. Therefore only 201 was considered.

X^o branching ratio, B.R.		η branching ratio		
MODE	B.R.	MODE	SIGNATURE	B.R.
$X^o \rightarrow \pi^+\pi^-\eta$	44%	$\eta \rightarrow 2\gamma$	$\gamma\ \gamma$	38.2%
$\rightarrow \pi^o\ \pi^o\ \eta$	22%	$\rightarrow \pi^+\pi^-\pi^o$	$2\pi\ 2\gamma$	23.0%
$\rightarrow \pi^+\pi^-\gamma$	30%	$\rightarrow \pi^o\ \pi^o\ \pi^o$	All neutrals	31.4%
$\rightarrow \gamma\gamma$	4.7%	$\rightarrow \pi^+\pi^-\gamma$	$2\pi\ 1\ \gamma$	5.4%

Table 5-4A. The X^o and the η decay modes with branching ratios[46]

The correction factors for the casuals and the occupancy of the A0 counter were small. No significant enhancement was observed in the uncorrected yield curve of channel 201 (Fig. 5-4-D).

So, it was desirable to understand the background in order to improve s/n ratio.

(a) The hydrogen-out background, 10% of the total, was the biggest single background. 80% of non-hydrogen and 20% of the hydrogen-in backgrounds were reduced by discarding the events associated with the droop counter at an estimated cost of 2% of the signal.

Decay Mode	X^o b.r.	Detection efficiency montecarlo prediction	Signal detected	Signal expected for 150 X^o per 100 m π
$\pi^+\pi^-\gamma$	0.300	0.337	0.101	15.2
$\pi^+\pi^-\eta$ $\hookrightarrow\gamma\gamma$	0.168	0.079	0.013	2.0
			Total	17.2

Table 5-4B Signal expected in decay channel (PI, IC, GA) 201.

Description	Background	Noise, n	S, signal expected	s/n
P Counter in Veto	150	$\pm$ 5.6	17.2	3.07
P Counter and 'Droop' Counters in Veto	125	$\pm$ 5.0	17.0	3.40
" " + adjacent γ rejected	90	$\pm$ 4.5	16.5	3.67

Table 5-4-C The s/n ratios for $\pi^+\pi^-\gamma$ mode in decay channel 201 (PI, IC, GA)

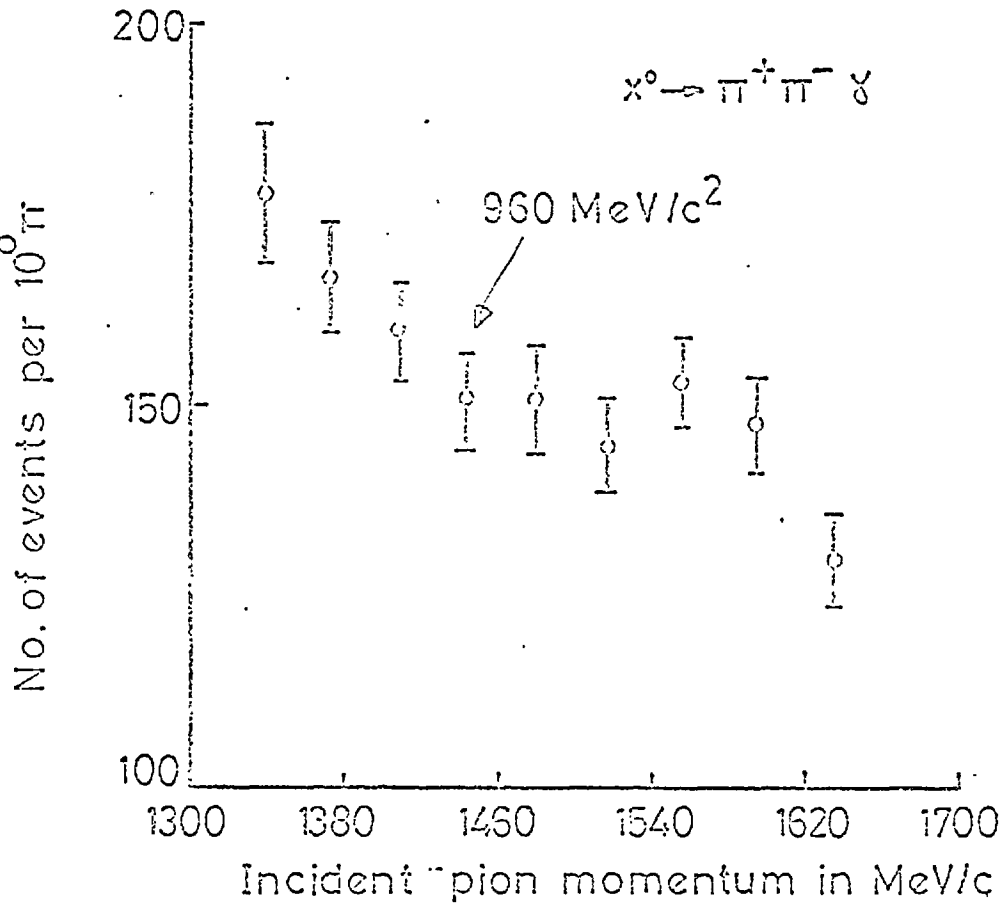

FIG. 5-4-D

Uncorrected neutron yield curve, obtained with momentum bins combined in fives, for $\pi^+\pi^-\gamma$ events in decay channel (PI. IC. GA) 201 in the gate of 6.8 to 13.2 nsec. After the fast peak. The events associated with the P counter were rejected.

(b) The main sources of background in this mode were expected from

$$\pi^- p \rightarrow \pi^+ \pi^- \pi^0 \eta \qquad \text{..... (A)}$$
$$\eta \rightarrow \gamma\gamma \quad (1\gamma \text{ missing})$$

and $\pi^- p \rightarrow \pi^+ \pi^- \eta$ ..... (B)

An extra γ count due to PI aberrations.

The background produced in $\pi^+ \pi^- \gamma$ mode by the former process (A) could not be distinguished from signal. However, in the latter Case (B), 27% background could be reduced at the cost of 3% signal by rejecting events with a gamma adjacent to the PI.

The result in the table 5-4-C is obtained from one run. The noise n, was estimated by considering all the data ($\sim$400 mπ). The s/n ratios for the other two cases were not very different from the first. The ratio could only be improved by acquiring more data. It was decided not to study it further with this poor statistical significance.

5-4-2 $\pi^+ \pi^- \gamma\gamma$ mode

The signal in this decay mode was expected from

$$X^0 \rightarrow \pi^+ \pi^- \eta \rightarrow \gamma\gamma$$

and $X^0 \rightarrow \pi^+ \pi^- \gamma$ giving an extra γ

The estimated number of X^0 events to be detected in decay channel 202 for this decay mode was 7.5 for 150 X^0 events per 100 mπ (table 5-4-F). The observed background in the gate was 131/100 mπ with the statistical fluctuation ± 5 estimated for the data available.

The S/B ratio for channel 202 (PI, IC, GA) was 1.6 times better than that for the combined channels 202 and 112. Therefore, only 202 channel was considered. Again, not more than $\sim$1.5 standard deviation enhancement was expected.

(i) The background in the gate of PDP-8 channels 41 to 51 was considered. At the cost of 1.2% signal, 65% of the hydrogen out events were reduced by rejecting the events with the droop counters. The non-hydrogen events were only 5% of the total.

(ii) The main source of the background would be

$$\bar{\pi} \cdot p \rightarrow \pi^+ \pi^- \pi^0 n$$

The azimuthal separation of $\gamma\gamma$ coming from π^0 would be less than for those coming from η (Fig 5-4-E). According to the montecarlo prediction, by accepting $\gamma\gamma$

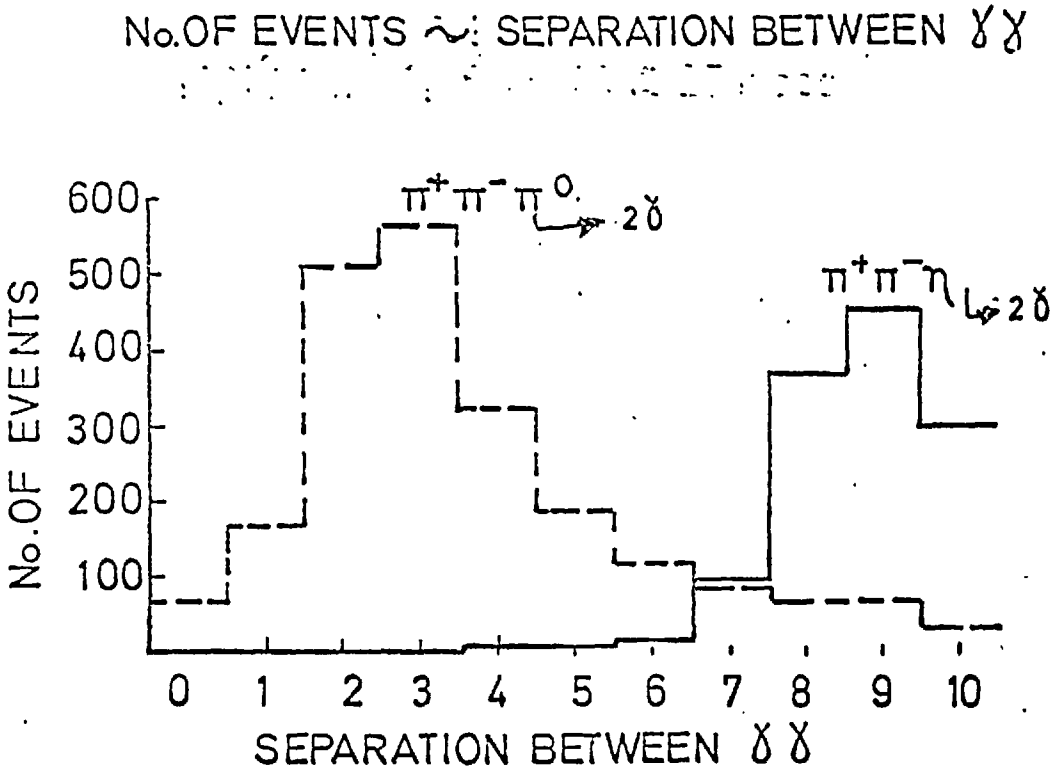

FIG. 5-4- E

MonteCarlo prediction for separation between γγ in the cases of $\pi^+\pi^-\eta$ and $\pi^+\pi^-\pi^0$ events generated at mass 960 MeV/c^2 in gate of 6.3 to 12.2 nsecs at incident pion momentum = 1.450 GeV/c

Mode	B.R.	A Montecarlo predicted detection efficiency	B.R. x A	Signal expected for 150 X^o per 100 mπ
$\pi^+\pi^-\gamma$ a) $\pi^+\pi^-\gamma$ b) $\pi^+\pi^-\gamma_2$	0.300	0.054 .079	0.024	2.4 3.6
$\pi^+\pi^-\gamma\gamma$	0.168	0.156	0.026	3.9
			Total	7.5

Table 5-4-F signal expected in decay channel 202 (PI, IC, GA) for decay mode; $X^o \rightarrow \pi^+\pi^-\eta$, where $\eta \rightarrow \gamma\gamma$. The observed background was 131 ± 5.

events separated by more than six counter bins 89% of $\pi^+\pi^-\pi^0$ could be reduced at the cost of

a) 1.6% of $\pi^+\pi^-$ signal and

b) 2.4 events/100 $m\pi$ of $\pi^+\pi^-\gamma$ signal (see table 5-4-F). In practice, 84% of the observed background was eliminated with this constraint on $\gamma\gamma$ (Fig 5-4G).

Thus, with above constraints (i) and (ii) the background in the gate 6.8 to 13.2 nsecs was 21 $\pm$ 2.5 and the expected signal was $\sim$5.0/100 $m\pi$. Again, we did not expect to see a significant enhancement with these constraints unless the background could be further reduced. No significant enhancement was observed in the uncorrected yield curve (Fig. 5-4-H). This mode was not considered for further analysis.

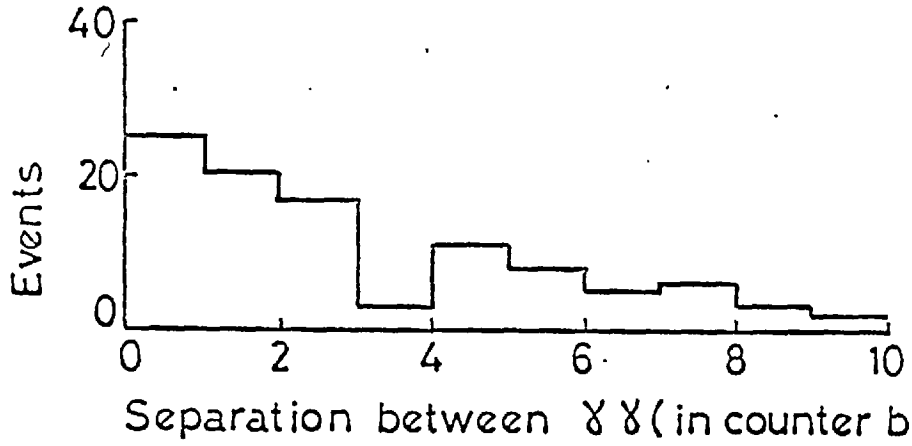

FIG. 5-4-G

Observed separation between two gammas in case of $\pi^+\pi^-\gamma\gamma$ mode at P_π = 1.408 Gev/c in a gate of 6.3 to 12.2 nsecs after the fast-peak.

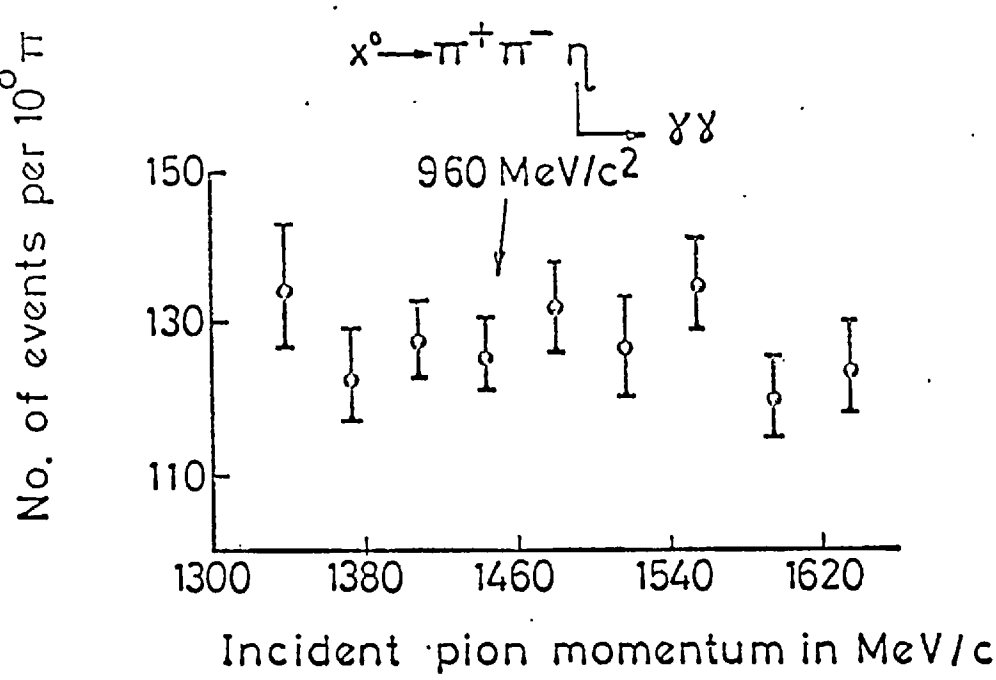

FIG. 5-4-H

Uncorrected neutron yield curve, obtained with momentum bins combined in fives, for $\pi^+\pi^-\gamma\gamma$ events in decay channel (PI, IC, GA) 202 in the gate of 6.8 to 13.2 nsecs after the fast-peak. The events associated with the P-counter were rejected.

5-4-3 $\pi^+ \pi^-$ all neutrals $\geq 3\gamma$ events

The signal in the selection $\pi^+ \pi^-$ all neutrals $\geq 5\gamma$ (table 5-4-I) was expected from

$$X^o \rightarrow \pi^o \pi^o \eta$$

and $$X^o \rightarrow \pi^+ \pi^- \eta$$

Some of the gammas of the final state would either be lost or give an extra count in the decay system. As a result they would appear in decay channels (PI, IC, GA) 203, 204, 205, 206 etc as well as in some other channels viz 21 $\gg 3$ etc. The channels 20 ≥ 3 and 21 $\gg 3$ were therefore considered for this decay mode.

To reduce the non-hydrogen background, the events associated with the droop counters were rejected. The main source of the background was

$$\pi^- p \rightarrow \pi^+ \pi^- (m\,\pi^o)\, n$$

where m = 1, 2, 3.

The uncorrected yield curve for events with decay signature $2^o \geq 3\gamma$ suggested an enhancement (Fig 5-4K). For further discussion see §5-4-4 and §5-5.

TABLE 5-4-I

Decay modes	Signature	X^o b.r.	η b.r.	Events produced for $150 X^o$ per $100 m \pi$
$X^o \rightarrow \pi^o \pi^o \eta_{\hookrightarrow \pi^+ \pi^- \gamma}$	$2\pi 5\gamma$	0.22	0.05	1.6
$X^o \rightarrow \pi^o \pi^o \eta_{\hookrightarrow \pi^+ \pi^- \pi^o}$	$2\pi 6\gamma$	0.22	0.23	7.6
$X^o \rightarrow \pi^+ \pi^- \eta_{\hookrightarrow \pi^o \pi^o \pi^o}$		0.44	0.31	20.4
		Total		29.6

TABLE 5-4-J

Decay modes	Signature	X^o b.r.	η b.r.	Events produced for $150 X^o$ per $100 m \pi$
$X^o \rightarrow \pi^o \pi^o \eta_{\hookrightarrow \gamma\gamma}$	6γ	0.22	0.38	12.5
$X^o \rightarrow \pi^o \pi^o \eta_{\hookrightarrow \pi^o \pi^o \pi^o}$	10γ		0.31	10.2
		Total		22.7

5-4-4 All neutrals $\geq 3\gamma$ events.

The signal in the selection $00 \geq 6\gamma$ (table 5-4-J) was expected from

$$X^o \rightarrow \pi^o \pi^o \eta \quad \eta \rightarrow \text{All neutrals}$$

As some of the gammas of the final state would either be lost or give an extra count in the decay system, all the events with decay signature (PI, IC, GA) $00 \geq 3$ along with its aberrations $10 \geq 3$ and $01 \geq 3$ were added.

The possible source of the background was

$$\pi^- p \rightarrow (m\ \pi^o)\ \eta$$

where m = 1, 2, 3.

As both $2^o \geq 3\gamma$ (§ 5-4-3) and $00 \geq 3$ channels were expected to contain X^o signal, they were treated together for further analysis. The corrected yield curve indicated an enhancement in the X^o mass region (Fig 5-5-F). For discussion see § 5-5.

5-5 Discussion and conclusions

The enhancement observed in the corrected yield curve in the c.m. gate of 6.8 to 13.2 nsecs (Fig 5-5A) was believed to be genuine as

a) No corresponding dip in the yield curve in the c.m. gate either for the events associated with the p-counter (Fig 5-5B) or for the events in the rejected decay modes (Fig 5-5-C) was found.

b) The fact that i)the high points were not contributed by one run and ii) all the points at different momentum bins of a run were not high, ruled out any possibility of these runs being accidentally high (Fig 5-5-E).

The enhancement could be said to be due to a resonance-production as

a) No corresponding enhancement in the same momentum range was observed in the other gate (Fig 5-5-D). This ruled out the possibility of an S-channel effect.

b) No enhancement was observed in the yield curve of the forbidden decay mode $\eta^+ \eta^-$ of the X^o. The enhancement in the selected decay modes of the X^o suggested that it was contribution of the X^o meson (Figs 5-5-F and 5-5-G).

For the yield curve, the incident pion momentum range from 1400 MeV/c to 1532 MeV/c was considered as suggested by the Montecarlo predicted yield curve generated for mass 960 MeV/c^2 with Γ = 4.0 MeV/c^2. The X^o enhancement was expected in the incident momentum range from 1436 to 1480 MeV/c.

The mass, the width and the cross-section of the enhancement was found by comparing the observed yield curve with the Montecarlo yield curves.

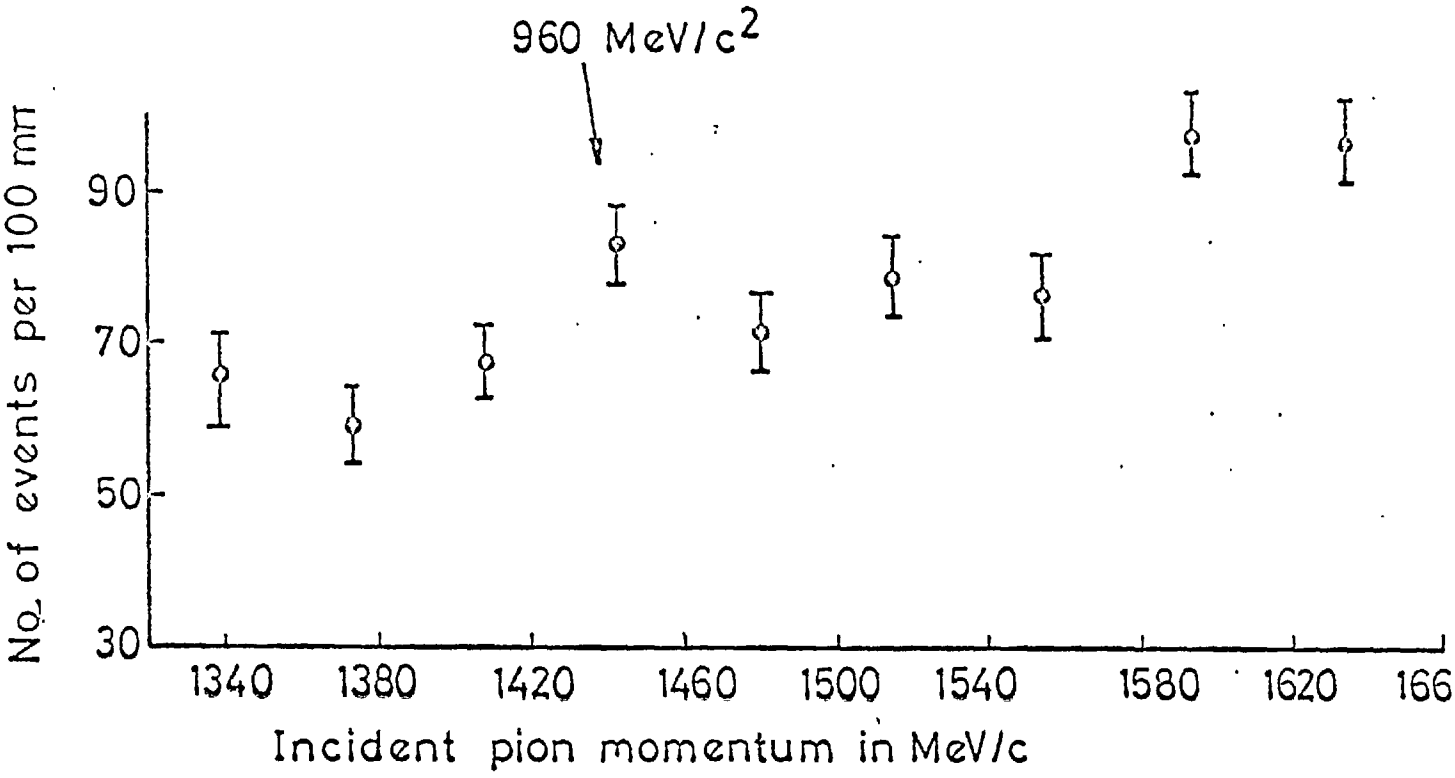

FIG 5-4-K

Uncorrected yield curve, obtained with momentum bins combined in fives, for $x^0 \to \pi\pi\eta$ events in the decay channel 2 0 7 3 8 , in the gate of 6.8 to 13.2 nsecs after the fast peak. The events associated with the p counter were rejected.

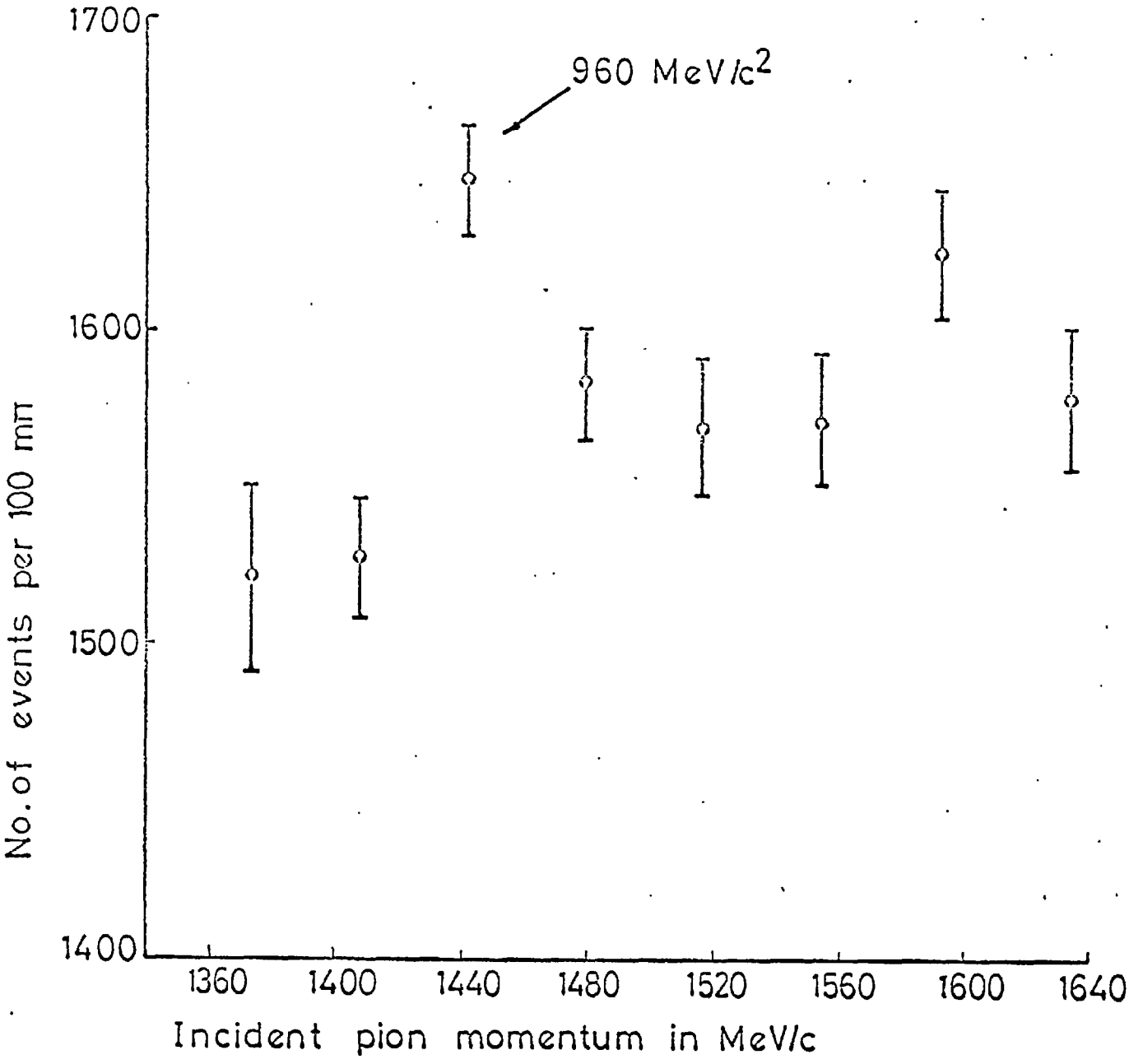

FIG. 5-5-A

The corrected neutron yield curve, obtained with momentum bins combined in fives, in the gate of 6.8 to 13.2 nsecs after the fast peak. Events with decay signatures (PI, IC, GA) $0 \leq 20$, $1 \leq 10$ and $2 \leq 10$ were rejected. Events associated with the P counter were also rejected.

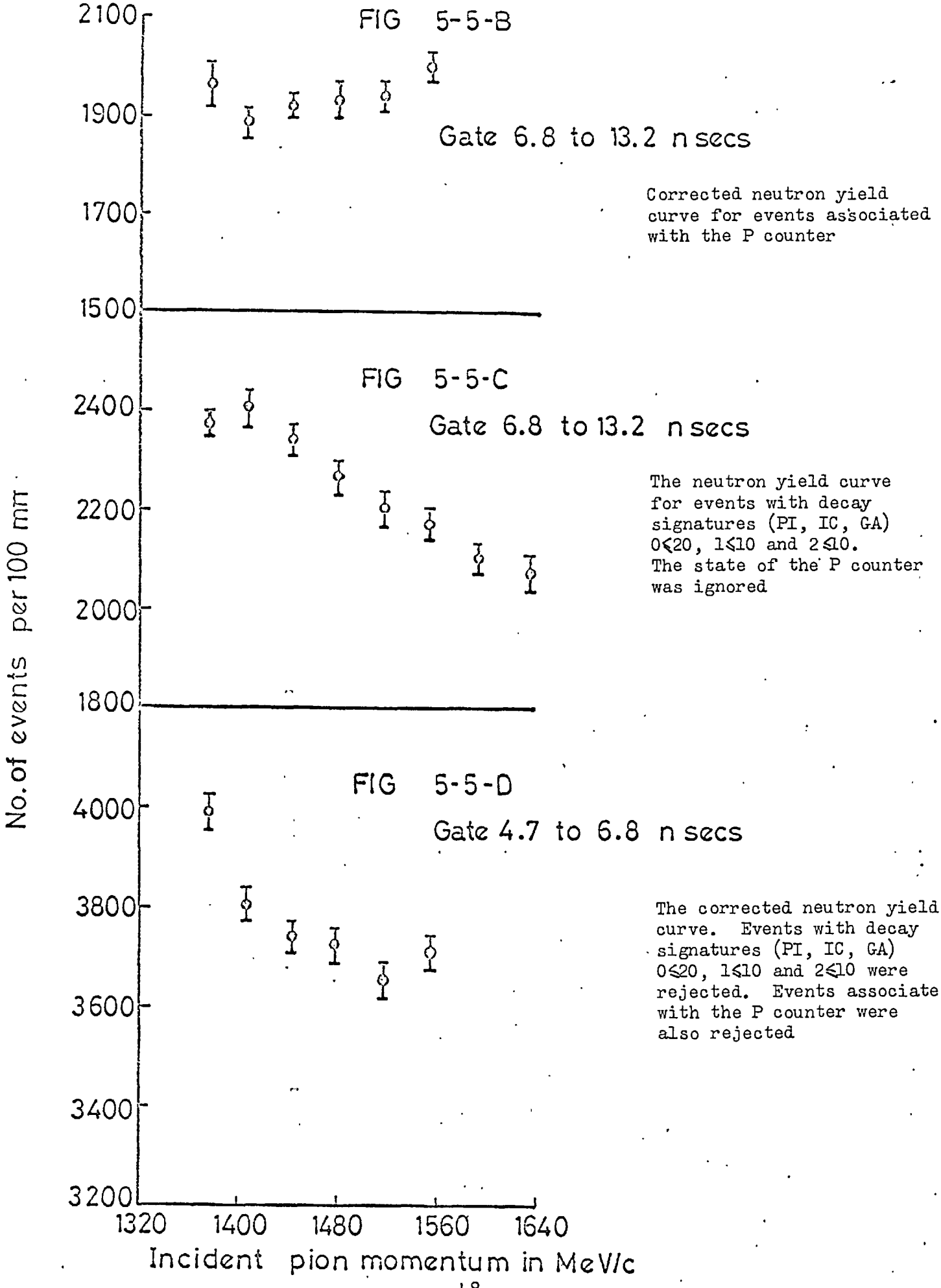
FIG 5-5-B
Gate 6.8 to 13.2 n secs
Corrected neutron yield curve for events associated with the P counter
FIG 5-5-C
Gate 6.8 to 13.2 n secs
The neutron yield curve for events with decay signatures (PI, IC, GA) 0≤20, 1≤10 and 2≤10. The state of the P counter was ignored
FIG 5-5-D
Gate 4.7 to 6.8 n secs
The corrected neutron yield curve. Events with decay signatures (PI, IC, GA) 0≤20, 1≤10 and 2≤10 were rejected. Events associate with the P counter were also rejected
No. of events per 100 mm
2100
1900
1700
1500
2400
2200
2000
1800
4000
3800
3600
3400
3200
1320
1400
1480
1560
1640
Incident pion momentum in MeV/c

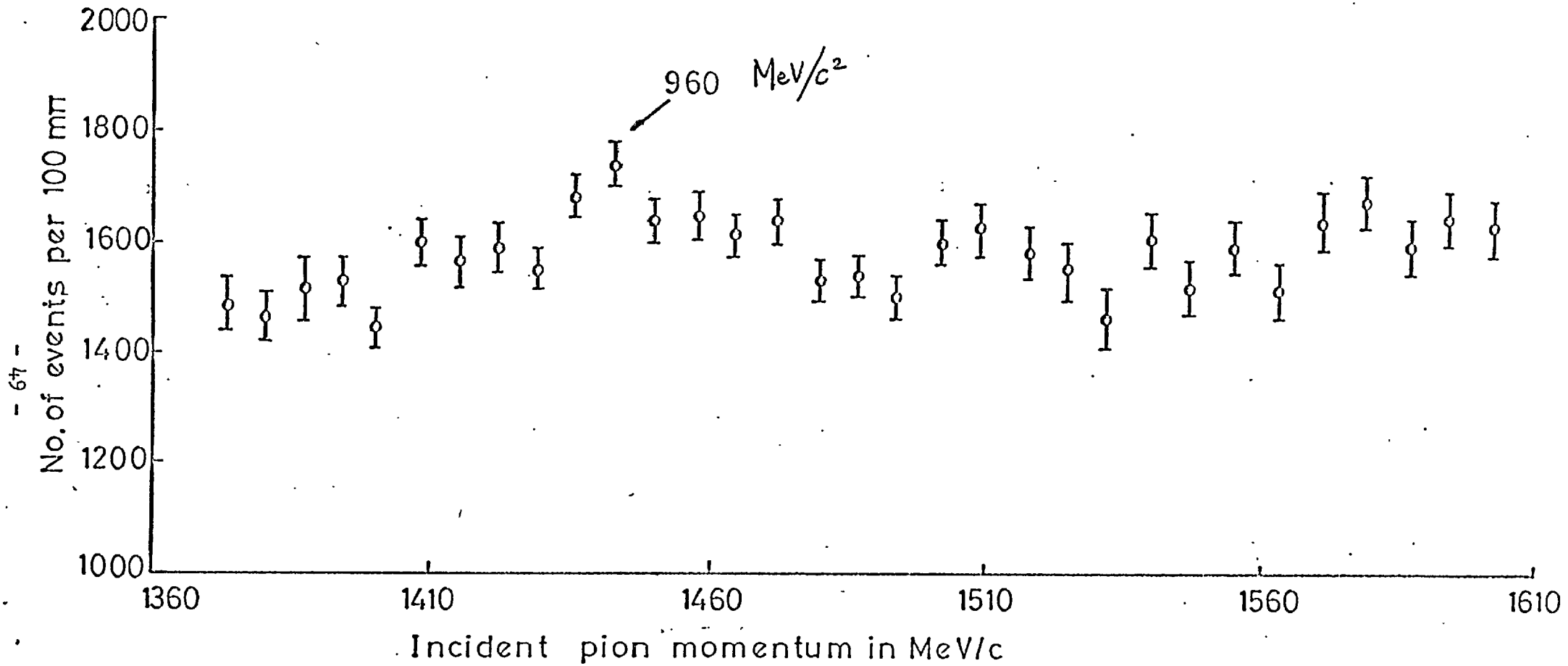

FIG. 5-5-E

The corrected neutron yield curve in the gate of 6.8 to 13.2 nsecs for individual momentum bins. Events with the decay signatures (PI, IC, GA) $0 \leqslant 20$, $1 \leqslant 10$ and $2 \leqslant 10$ were rejected. Events associated with the P counter were also rejected.

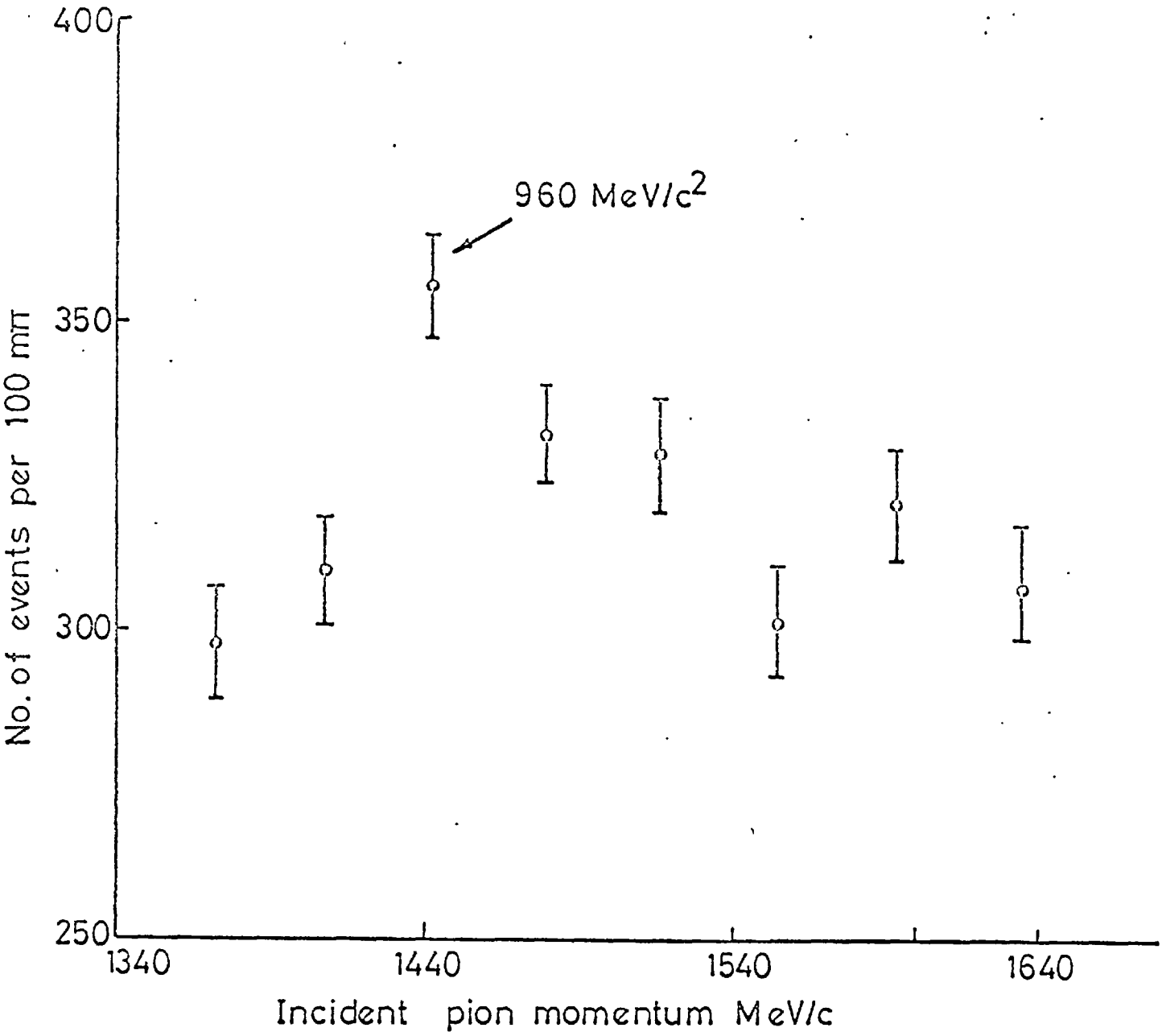

FIG. 5-5-F

The corrected neutron yield curve, obtained with momentum bins combined in fives, for events with the decay signatures (PI, IC, GA) 20⁄3, 00⁄3, 10⁄3, 11⁄3 and 01⁄3 selected in the gate 6.8 to 13.2 nsecs after the fast-peak. Events associated with the P counter were rejected.

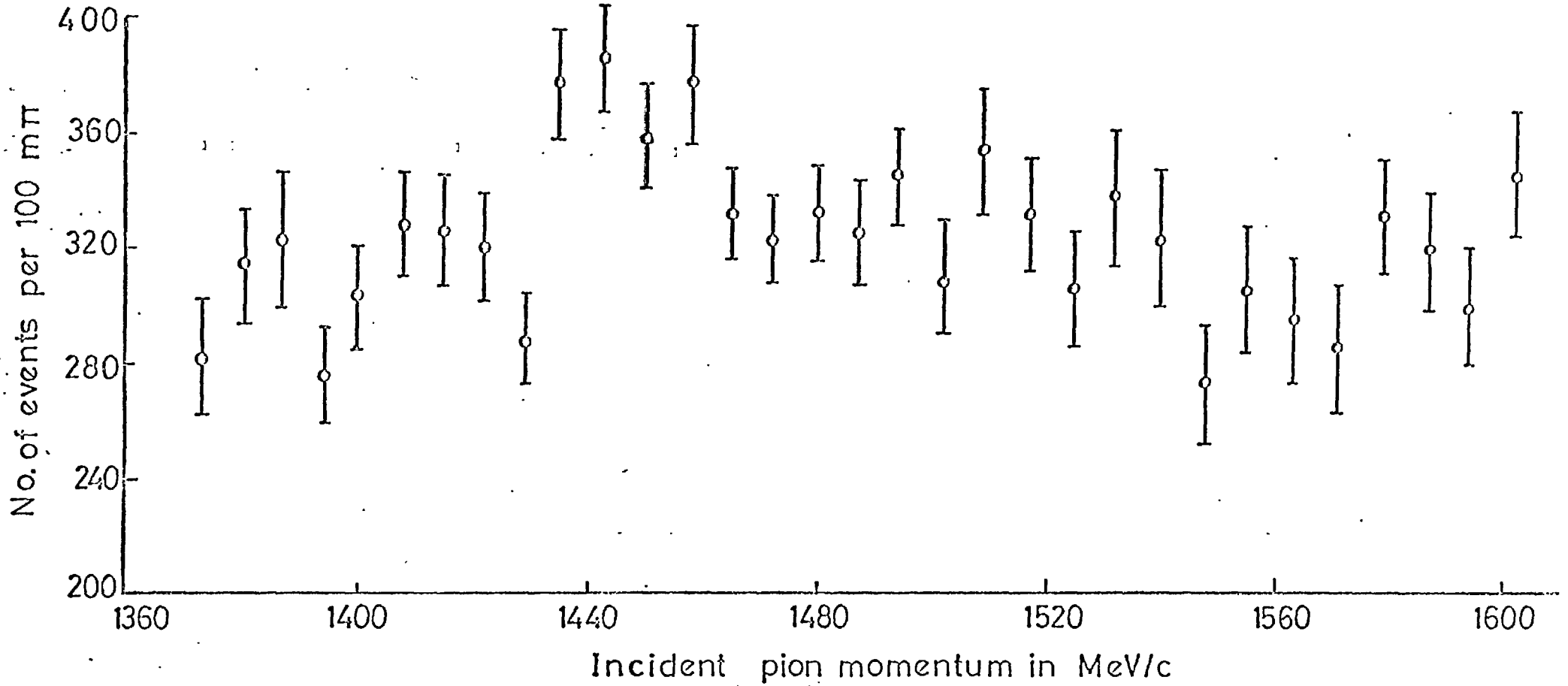

FIG. 5-5- G

The corrected neutron yield curve, obtained with individual momentum bins, for events with the decay signatures (PI, IC, 20⩾3, 00⩾3, 10⩾3, 11⩾3 and 01⩾3 selected in the gate 6.8 to 13.2 nsecs after the fast-peak. Events associated with the P counter were rejected.

The curve-fitting was subjected to a χ^2-test. The quantity χ^2, defined as

$$\chi^2 = \sum_i \frac{(V_{oi} - V_{ti})^2}{\sigma_i^2} \quad , \text{ was minimised.}$$

where V_{oi} = the observed rate at momentum bin i with its standard deviation σ_i.

and V_{ti} = the true value, predicted by the Montecarlo program.

Straight lines through the points of theyield curves for the decay mode and the selected total neutron events were poor fits with CL of $P(\chi^2) \leq 0.1\%$. But straight line fits through the points of non-x^o regions (in the incident pion momentum range 1400 - 1429 MeV/c and 1487-1532 MeV/c) of the yield curve gave fits with CL of $P(\chi^2)$ 42.6% and 7% respectively. Thus, the background shape was consistent with the straight line in both cases. The data were fitted to a straight line plus the Montecarlo predicted yield curve for different masses and widths of the X^o. The values of χ^2 were plotted a) for different values of mass at a constant width and b) for different values of width at the constant mass value.

Mass: At a constant width value of Γ = 4.5 MeV/c^2 the minimum value of χ^2 occurred at the values of mass 956 $\pm$ 3 and 956 $\pm$ 2 MeV/c^2 for the decay and the selected total neutron curve respectively. Figs (5-5-H,I). The quoted errors were obtained for 95% CL and were purely statistical. The correction to the mass value due to uncertainty in the floating wire calibration was small and, therefore, neglected.

13

The world value of the averaged mass of the X^o is quoted to be 957.7 $\pm$ 0.8 MeV/c^2. The values of mass obtained by us and other experiments have been shown in figure 5-5-J.

Width: At the constant mass 956 MeV/c^2, three Montecarlo curves were generated at Γ = 4.5, 6.0 and 12.0 MeV/c^2, which gave χ^2 probability, $P(\chi^2)$ for the fit 23.5%, 17.9% and 8.7% for the decay modes and 9.2%, 9.0% and 3.3% for the selected total neutron rates respectively. So, we quote $\Gamma \leq 12$ MeV/c^2 with 91.3% CL for the selected decay modes and 96.6% CL for the total neutron events. The mass resolution averagedover the gate 6.8 to 13.2 nsecs was estimated to be about $\pm$ 14 MeV/c^2.

Production cross-section near threshold:

Allowing for 25% detection efficiency of the neutron counter and 11.1% losses for the discarded events, we expect 3196 X^o/100 mπ in the yield curve for the selected total neutron events with an assumption of A = 1 in

$$\frac{\sigma^*}{p} = A \ \mu b/(MeV/c)$$

The total number of events in the observed yield curve (Fig 5-5-K) above the fitted background was 1165 $\pm$ 241/100 mπ which corresponded to A = (0.36 $\pm$ .08) μb/(MeV/c). The quoted error includes the statistical error of the points as well as the uncertainty in the background level. This value of A measured near the X^o production threshold is not incompatible with the results of Dufey et al[38] who quoted

σ_{total} for X^o = $(61 \pm 11)\ \mu b$ at P_π = 1.500 GeV/c

and = $(92 \pm 7)\ \mu b$ at P_π = 1.520 GeV/c

which correspond to

A = $(0.40 \pm .07)\ \mu b/(MeV/c)$ at P_π = 1.500 GeV/c

and A = $(0.52 \pm .10)\ \mu b/(MeV/c)$ at P_π = 1.520 GeV/c

The statistical significance of the enhancements given by

$\frac{S', \text{ the total number of events above the fitted backgrounds.}}{\text{error on } S'}$

are (1132/241) =4.7 standard deviation and (435/85) = 5.1 standard deviation for the selected total neutrons and the decay modes respectively. The ratio of the signal to background for the selected total neutron events is 4.02%.

Decay mode: The decay mode is consistent with $X^o \rightarrow \pi\ \pi\ \eta$ mode, but $\delta^o \rightarrow \eta\ \pi^o$ can not be ruled out as the events of this decay mode would also appear in $\pi^+\ \pi^-$ neutrals $\geqslant 3$ and $00 \geqslant 3\gamma$ channels.

Conclusions

We see an enhancement of ~ 5 standard deviation in the $|t|$ region, 0.4 to $0.8\ (GeV/c)^2$, close to the X^o production threshold. Our mass resolution is $\pm$ 14 MeV/c^2. We measure the mass and width to be 956 MeV/c^2 and $\Gamma \leq 12\ MeV/c^2$ respectively. The decay mode is consistent with $X^o \rightarrow \pi\ \pi\ \eta$ mode.

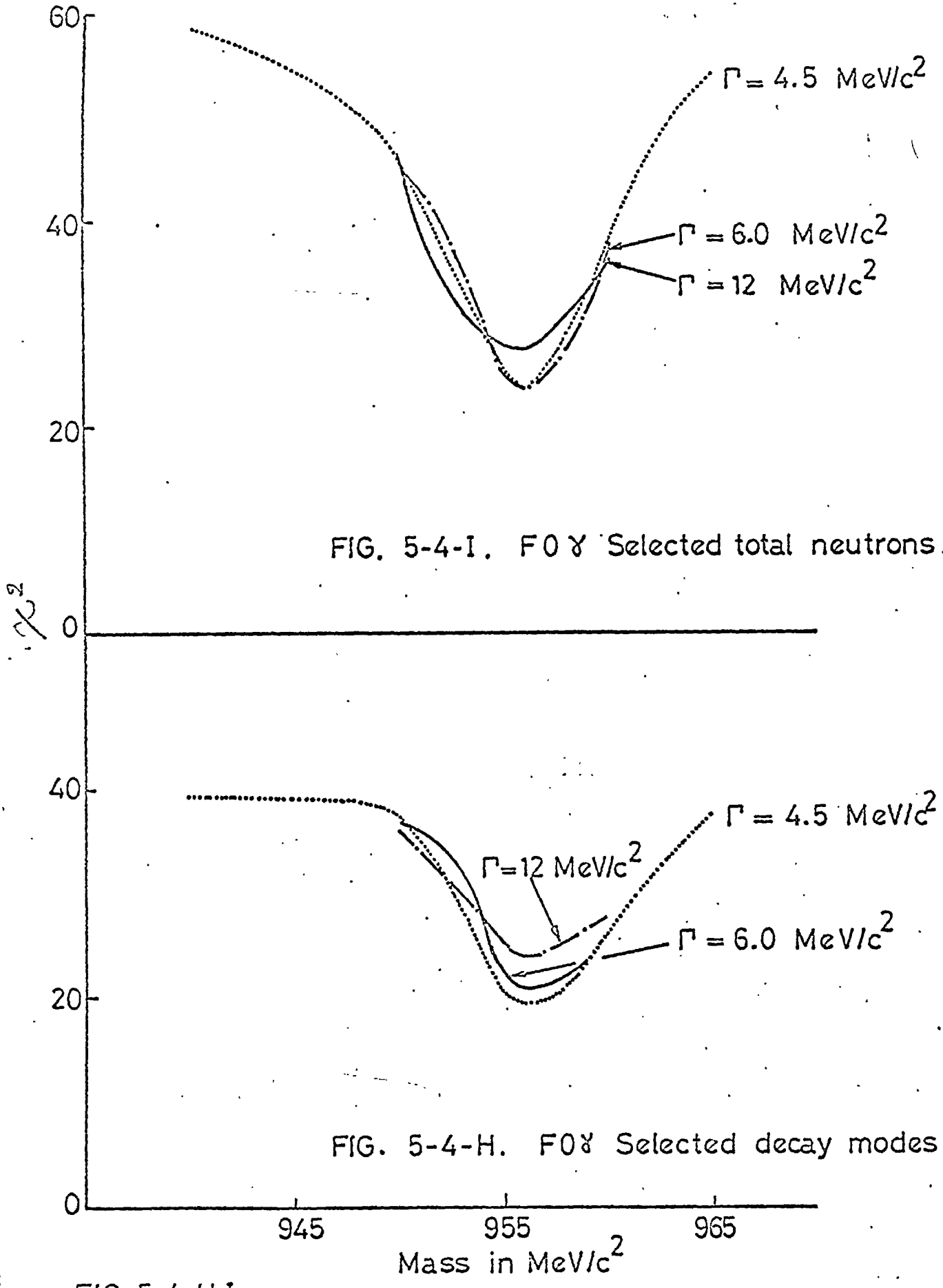

FIG. 5-4-I. F0 γ Selected total neutrons.

FIG. 5-4-H. F0 γ Selected decay modes

FIG. 5-4-H I

The values of χ^2, at a given Γ value, obtained by fitting a straight line plus th montecarlo predicted yield curve for different masses to the observed yield curve (16 degrees of freedom).

1 Duber '64 HBC

2 Kalbfleis '64 HBC

3 Badier '65 HBC

4 Trilling '65 HBC

5 Cohn '66 HBC

6 London '66 HBC

7 Mott '69 HBC

8 Ritenberg '69 HBC

9 This expt. for the selected decay mode

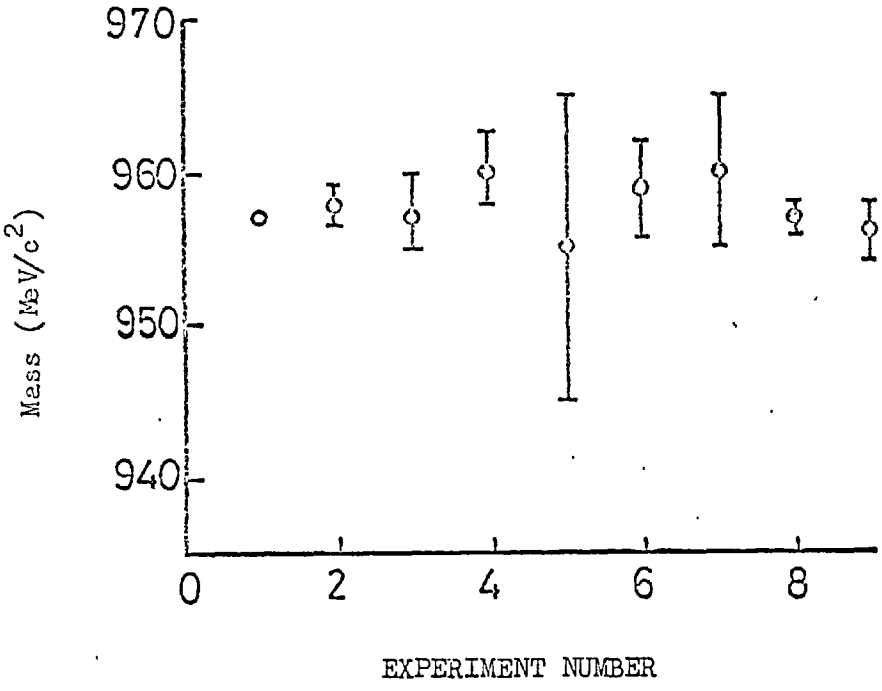

FIG 5-5-J

X^{o} Mass measurements.

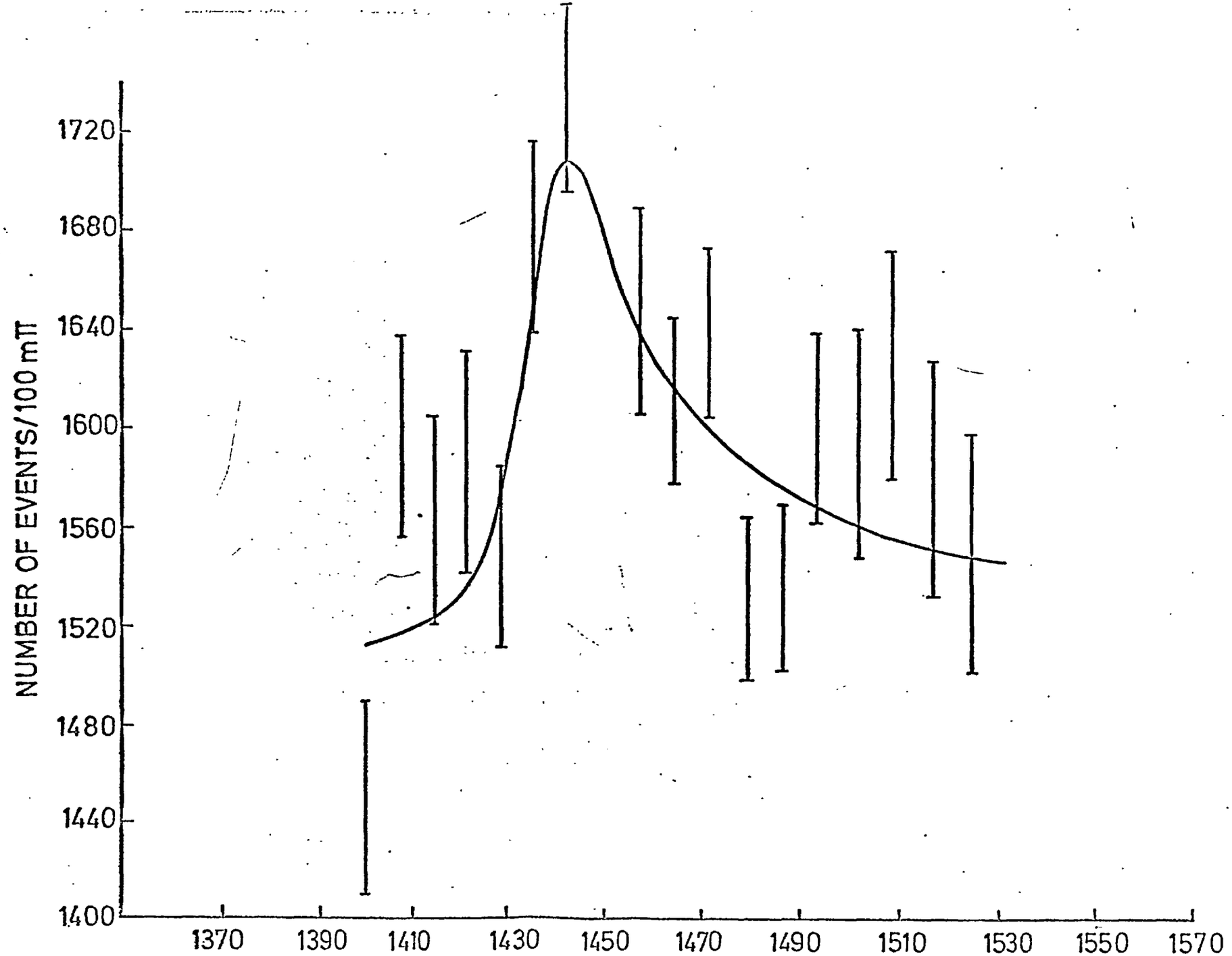

FIG. 5-5-K

The Monte Carlo predicted yield curve at mass 956 MeV/$_c$2 and Γ = 4.5 MeV/$_c$2 fitted to the observed yield curve for the selected total neutron events.

CHAPTER - 6

ANALYSIS AND THE PRELIMINARY RESULTS ON THE δ^- MESON

6.1 INTRODUCTION

To investigate the production of the δ^- meson near threshold, the data was treated in two different ways. Firstly, the total proton event rate was studied as a function of incident pion momentum but an attempt was made to achieve reproducibility in the data. For runs taken at the same momentum, the corrected proton rate in the centre-of-mass gate of PDP-8 channels 41 to 51 was found non-reproducible up to 5 standard deviation (the statistical fluctuation was $\lesssim \pm$ 0.8%).

The fact that the neutron rates were reproducible ruled out effects of dead-time or occupancy of the proton counters A1-6 or the lack of hydrogen in the target.

The true proton rate P_t in the gate was obtained by correcting the observed proton rate $P_{obs.}$ for the proton casual Pcas. measured in the casual gate and then correcting it for the occupancy of the AO counter. A non-uniform casual time-of-flight distribution would prevent a proper correction for the casuals (§ 3-4-2). Thus, the improper correction for the casuals as well as any variation from run to run in some instrumental backgrounds e.g. non-H_2 events could be blamed for this non-reproducibility. The casual rate was estimated to be between 15% and 28% of the total protons observed in the gate. OCC., the occupancy of the counter AO varied between 0.5% and 1.9%. Although the casual rate and the total proton background rate were reduced by 50% and 25% respectively by requiring a signal from the P Counter, the reproducibility was not improved. It was not possible to describe the data by the relation

$$P_{obs.} = (P_t + \alpha\, Pcas)\,(1 - \beta\, OCC)$$

where α and β were constants.

Structure in Casuals:- The non-reproducibility of the rates of two runs at P_π = 1.555 Gev/c with the same casual rates, same occupancy and the same position of the fast-peak led us to suspect this as an effect of some structure in the casual time-of-flight distribution (§ 3-4-2), which could vary from time to time viz with the variation in the beam intensity. Such a structure would have appeared by subtracting the time-of-flight distribution of one run from the other taken at the same momentum but due to statistical limitation, it was hard to find spikes either in the casual or in the other time-of-flight region. As suggested in §3-4-2,contributions of such backgrounds were reduced by discarding certain classes of events which also reduced the non hydrogen background (§ 6-2). The loss of a fraction of signal could be estimated by the montecarlo program with an assumption of an isotropic distribution of the δ^- meson decay.

Secondly, decay signatures were selected corresponding to the expected decay modes of the δ^- and the yield of such events was plotted as a function of momentum.

In plotting the yield curve besides the other gates (table 5-1-A), the c.m. gate of PDP-8 channels 42 to 53 was also considered.

6.2 Evaluation and reduction of proton backgrounds.

The major contributors to the proton background were non-hydrogen, casuals and the events associated with the ring counter, being 41%, 19% and 60% respectively of the total proton rates in the gate of PDP-8 Channels 42 to 53.

Events discarded from the total proton

(i) $1 \leq 10$ and $0 \leq 20$ (PI, IC, GA).

The non-hydrogen background was reduced by 59% by rejecting the events with these decay signatures.

(ii) $\geq$ 2N Events: 96% of these events were casuals. These were rejected to reduce the background by 5% at a negligible cost of signal.

(iii) More-than-one-proton counter events.

Due to a slight overlap of the proton counters, some events were expected to be associated with two adjacent proton counters. The pulses from these counters did not play any role in the measurement of the time-of-flight of the nucleons. These events were accepted. But, events associated with more than two proton counters were rejected at a negligible cost of signal.

With the above selections, the non-hydrogen, casuals and the ring events were observed to be 35%, 11% and 43% respectively of the hydrogen in events.

(iv) The Ring Counter events.

66% of all the casual events were associated with the ring counter. As any structure in the casual time-of-flight spectrum could not be taken into account properly, events associated with the ring counter were rejected, with an option to treat them separately, if required.

With these selections the casuals were only 6.4% of the total while the non-hydrogen events were 30% of the total (table 6-2-A).

(v) $00 \leq 3$ Events: 87% of these events were non-hydrogen.

(vi) 200 : 46% of them were non-hydrogen, and 60% of them were coplanar. The rejection of these events reduced the background by 5%

Table - 6.2A

Events		(PI,IC,GA)	Decay Channels											
	Total	001	002	00 3	102	012	112	300	301	302	312	212	210	200
H_2 in	3422	123	53	43	151	50	82	171	94	43	30	70	152	160
H_2 out	7008	123	36	32	27	25	16	9	6	4	0	6	35	73
Droop	226				8		10	24	27	10	11	14	25	37

TABLE 6.2A

Proton background per 100 m_π at P_π = 1.408 GeV/c in the gate 6.8 to 13.2 NSecS. after the fast-peak. Events associated with the ring counter were discarded. Events with decay signatures (PI, IC, GA) 0 20 and 1 10 were also discarded. A signal from the P counter was required.

With the above selections, the proton background was reduced by 77%. Besides the requirement of a pulse from the P counter, conditions (ii) and (iii) were also imposed on the decay mode analysis. These selections were incorporated into a fortran program 'BBPROTON'.

The 'total' proton yield, with the above selections at each momentum bin P πi in the centre-of-mass gate was found to be reproducible within the expected statistical fluctuation. The yield curve obtained with momentum bins combined in fives have been shown in fig 6-4-A. For discussion See §6-4.

6.3 The decay modes of the δ^- meson.

Various groups (14,16,18) have reported the δ^- meson decaying into $\eta\,\pi^-$. Neither the cross-section near its production threshold in the π^-p interaction nor the branching ratio for $\delta^- \to \eta\,\pi^-$ is known. Allowing ~100% branching ratio for this mode, $144\,\eta\pi^-$ events* per 100 m π in the peak channel was assumed, this was based on the crude estimation from the observed yield curve in the centre-of-mass gate (Fig 6-4-A). We discuss here $\delta^- \to \pi^- \eta$ ($\hookrightarrow \gamma\gamma$) (§6-3-1) and $\delta^- \to \pi^- \eta$ ($\hookrightarrow \pi^+\pi^-\pi^o$) (§6-3-2).

The number of signal in each decay mode was estimated by considering the branching ratio of the η (table 6-3-A) and the detection efficiency of the decay system. The decay mode $\delta^- \to \pi^+\pi^-\pi^-$, reported by some groups [15,43], was treated separately (§6-3-3). The events associated with the ring counter were studied without using it in definition of PI and were rejected.

TABLE 6.3.A

Decay modes	η branching ratio (46)	Decay Signatures	Number of δ^-s expected in the decay mode assuming 144 δ^- in 'total' for 100 mπ
$\delta^- \to \pi^- \eta$ ($\hookrightarrow \gamma\gamma$)	38.2	$\pi^- \gamma\gamma$	55.0
$\delta^- \to \pi^- \eta$ ($\hookrightarrow \pi^+\pi^-\pi^o$)	23.0	3π 2γ	33.2

---

*Taking into account the solid angle factor for our next set of data at 6m. this number becomes ~100 δ^-/100 mπ in the $\eta\,\pi^-$ mode.

6.3.1 $\pi^- \gamma\gamma$ mode

This mode was expected to be due to

$$\delta^- \rightarrow \pi^- \eta \rightarrow \gamma\gamma$$

The main decay channels for this mode were 102, 012, 112, 201 and 101 (See table 6-3-B). The non-hydrogen and ring events were the main background contributors in the added channels (table 6-3-B). At an expected cost of 7% signal, the rejection of ring events reduced the non hydrogen and hydrogen-in events by 50% and 40% respectively.

Considering the detection efficiency for these added channels and the 7% loss of signal, we expected 30 events for 100 $m\pi$ in this decay mode (see also table 6-3A). As the contributions of casuals, occupancy of the A0 counter and the timing shift were small, no correction was applied to the yield of these events in the gate. A possible enhancement in the yield curve (Fig 6.3.1A) was encouraging. Any possibility for the ring counter events producing such an enhancement was ruled out as no corresponding dip

RING EVENTS IGNORED					RING EVENTS REJECTED			
Decay Channels PI IC GA	Total	Ring Events	H2-out event	detection efficiency %	Total	H2-out	Casuals	'Droop' events
102	218	58	41	26.90	151	27	0	8
012	104	53	61	2.50	50	25	3	0
112	171	97	43	6.70	82	16	5	10
201	177	58	40	7.0%	119	26	1	27
101	182	58	70	15.5%	123	46	4	13
Total	852	324	255	58.60%	523	140	13	58

Table 6.3B $\pi^- \gamma\gamma$ background rate per 100 $m\pi$ in the gate of 6.8 to 13.2 n secs. Obtained from a run at $P\pi$ = 1.408 GeV/c. A signal from the P-counter was required.

was found in the yield curve of the added decay channels 101, 102, 112 and 012 associated with the ring counter (Graph 6.3.1B).

However, a reliable selection of 'η' was desirable to confirm that the enhancement was mainly due to the $\eta\,\pi^-$ mode. The backgrounds were further studied.

The other main sources of the backgrounds in the $\pi^- \gamma\gamma$ mode were $\pi^- \pi^o$ and $\pi^- \pi^o \pi^o$ decay products produced in

$$\pi^- p \rightarrow \pi^- \pi^o \rightarrow 2\gamma \qquad \text{(A)}$$

and

$$\pi^- p \rightarrow \pi^- \pi^o \pi^o p \qquad \text{(B)}$$

($\pi^o \rightarrow \gamma\gamma$, $\pi^o \rightarrow \gamma\gamma$)

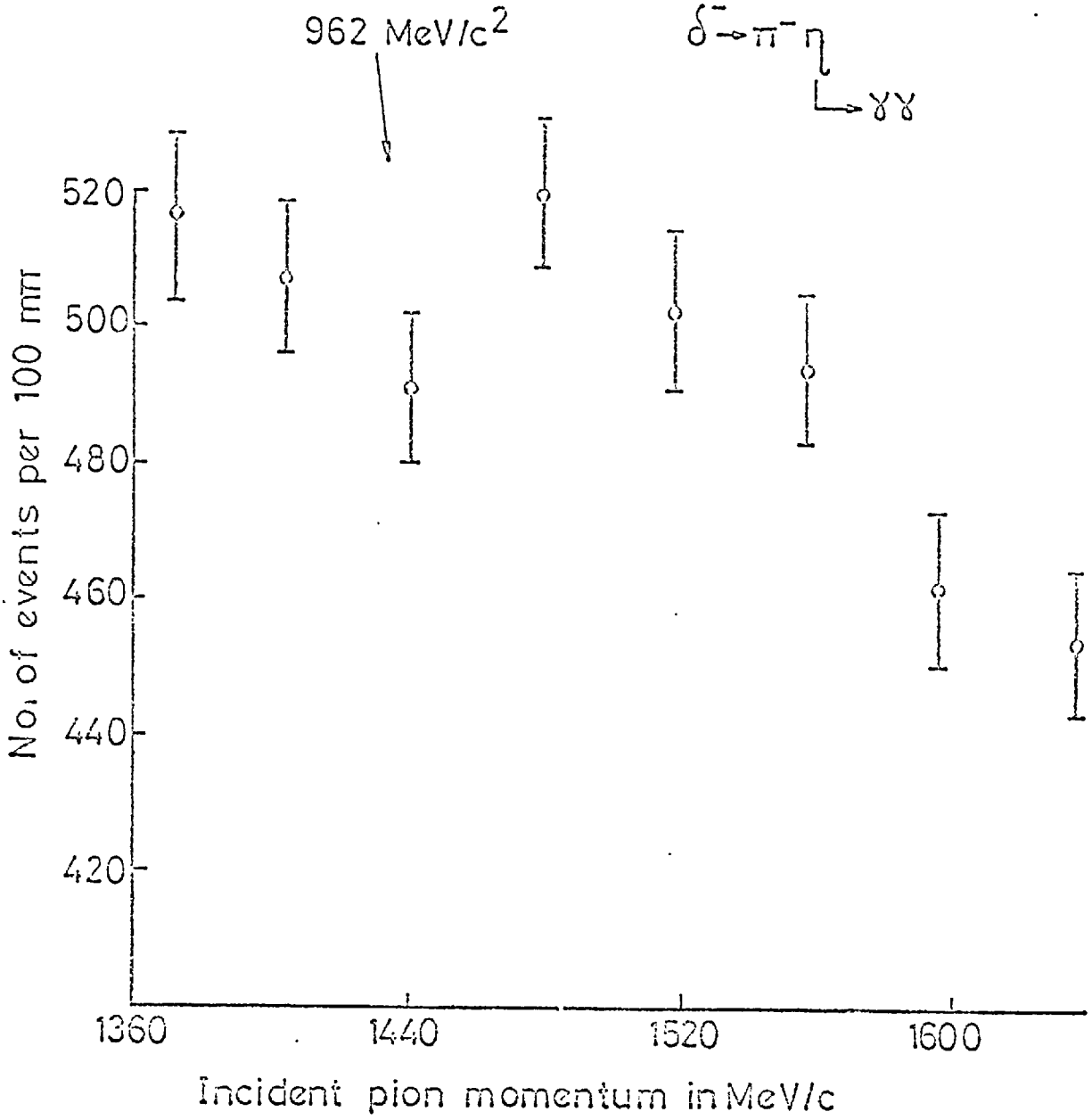

FIG.6-3-1A

Uncorrected proton yield curve. for $\delta^- \to \eta\pi^-$, $\eta \to \gamma\gamma$ with decay signatures (PI, IC, GA) 201, 101, 112, 102 and 012 added, in the gate of 6.8 to 13.2 nsecs after the fast-peak The events associated with the ring counter were rejected. A signal from the P counter was required.

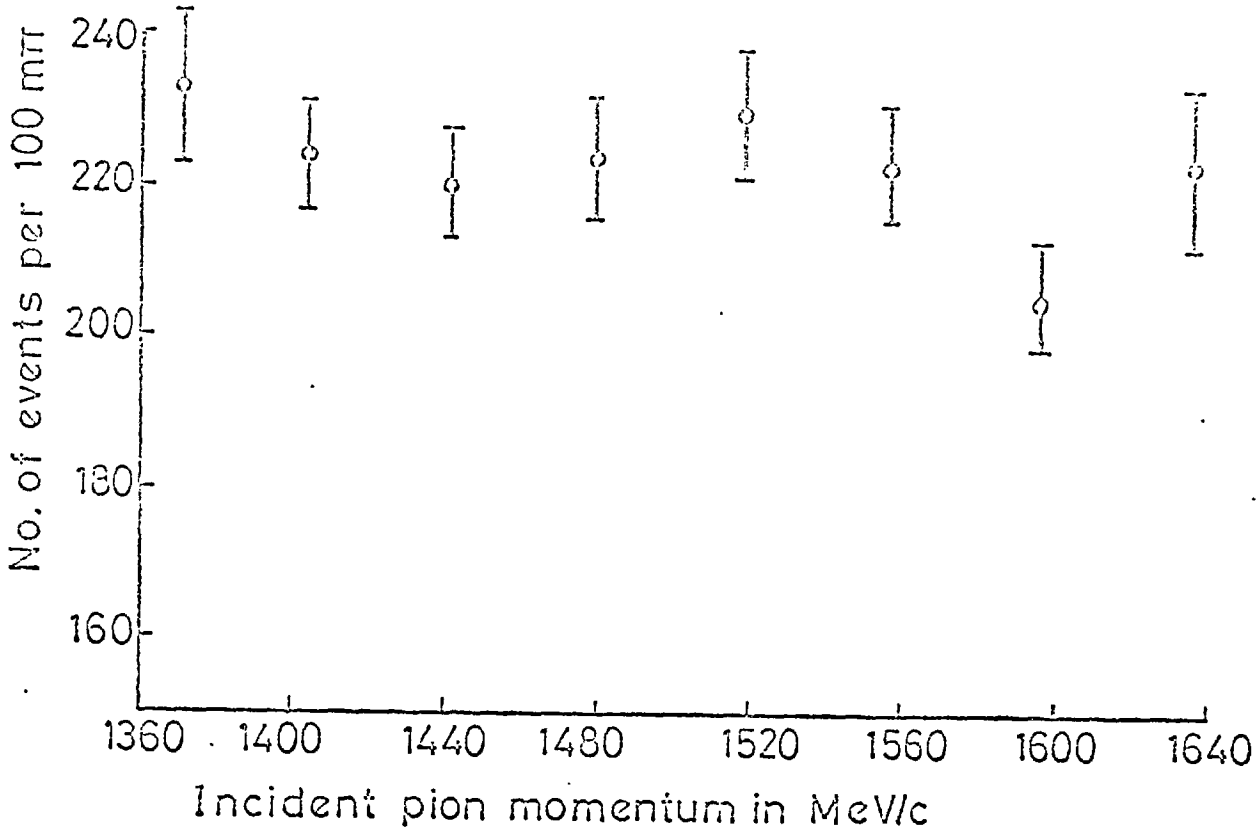

FIG. 6-3-1 B

Uncorrected proton yield curve, for $\delta^- \to \eta\pi^-$, $\eta \to \gamma\gamma$ with decay channels (PI, IC, GA) 101, 102, 112 and 012 added, in the gate of 6.8 to 13.2 nsecs after the fast-peak signals from the P counter and the ring counter were required.

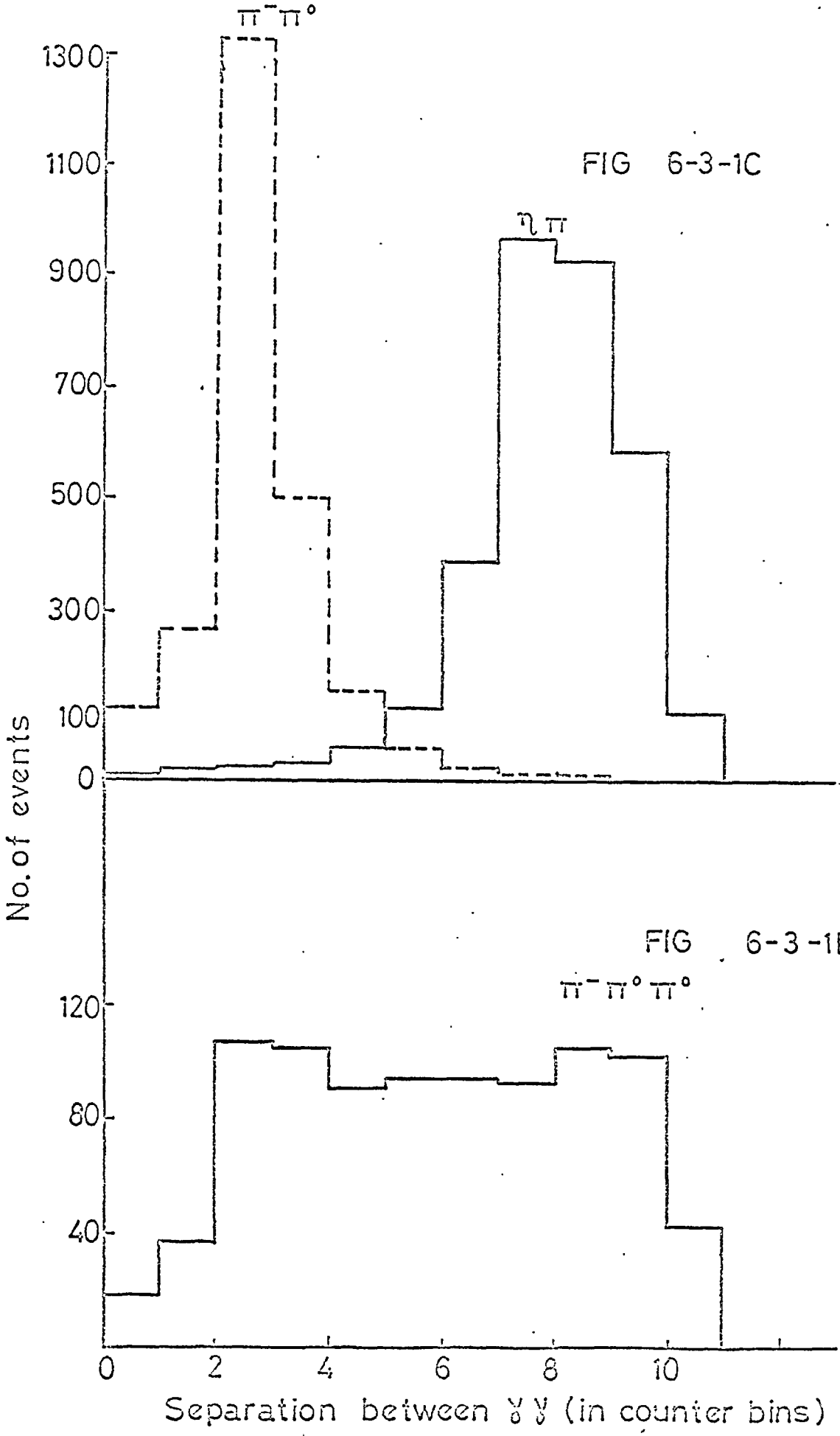

FIG 6-3-1C

FIG 6-3-1D

Montecarlo prediction for the separation between $\gamma\gamma$ in $\delta^- \to \pi_2^- \eta$, $\eta \to \gamma\gamma, \pi^-\pi^\circ$ and $\pi^-\pi^\circ\pi^\circ$ decay modes. Events produced at mass 980. Mev/c^2 and P_π = 1.480 Gev/c.

In case of two undetected gammas, the latter mode appeared as $\pi^- 2\gamma$ mode. At the cost of 3.6% of signal, we could reject 96% of $\pi^- \pi^o$ background by accepting 2γ events separated by more than four counter bins (Graph 6.3.1C). This was because the energy of each gamma coming from π^o in its centre-of-mass system would have less energy (only 69 MeV) than the energy of a gamma (275 MeV) coming from η in its centre-of-mass system. Transforming the energy in the $\pi^- p$ laboratory system, two gammas from π^o would tend to be less separated than those from η.

This constraint would also reduce 41% of $\pi^- \pi^o \pi^o$ background contributing to $\pi^- 2\gamma$ mode (graph 6.3.1D) Now, only 102, 012 and 112 could be treated together. The definitions of PI and γ were extended to detect $\pi^- \gamma\gamma$ wide; $\pi^- \gamma\gamma$ events with the bigger separation, with the high detection efficiency.

π_s = 'PI' , (a pulse from the inner charged counter and its corresponding gamma counter).

or 'Droop'

π_f = PI + an adjacent IC,

π_f = PI + an adjacent .

and $\gamma = \gamma$,

$\gamma_2 = \gamma$ + an adjacent γ .

The fortran program was modified to include these definitions of PI and γ. In the program all these PI'S were called PI and both γ and $\gamma 2$ were called γ. For discussion see §6-4.

6.3.2 3π 2γ mode.

This mode was expected from

$$\delta^- \rightarrow \pi^- \eta \hookrightarrow \pi^+ \pi^- \pi^o$$

Considering various decay channels together, the events associated with the ring counter were rejected to reduce the background at the cost of 3.6% of signal (table 6.3.2A). With the detection efficiency in two of the main decay channels (302 and 212) and the 3.6% signal loss, 8.4 per 100m π events were expected in this decay mode. An indication of a possible enhancement in the yield curve was encouraging. Any possibility for the ring counter events producing such an enhancement was ruled out as no corresponding dip was observed in the yield curve of the 302 and 212 events associated with the ring counter (Graph 6.3.2B).

The backgrounds in this mode were contributed mainly by

$\pi^- p \rightarrow \pi^- \pi^+ \pi^- \pi^o p$ (A)

and $\pi^- p \rightarrow \pi^+ \pi^- \pi^- p$ (B)

In case (B), gammas could be produced due to PI'S aberrations. The signal could not be distinguished from the background. The decay channels 303, 301, 302, 212 and 312 were included to achieve good detection efficiency and incorporated into the fortran program with the specified definitions of PI and gamma given in§6.3.1. For discussion see §6.4.

Channels PI IC GA	Detection Efficiency %	OBSERVED BACKGROUND			
		The Ring counter ignored	The events associated with the ring counter discarded		
			H2-in events	H2-out events	'Droop' H2-in
301	14.7	131	94	6	27
302	15.5	49	43	4	10
303	5.0	34	25	1	4
212	10.6	138	70	6	14
312	2.0	86	30	11	11
Total		438	219	28	66

Table 6.3.2A. The detection efficiencies and the observed background per 100 mπ in different decay channels of $\pi^+\pi^-\pi^-\gamma\gamma$ mode. For estimation of background at Pπ = 1.408 GeV/c, a signal from the P-counter was required and the gate 6.8 to 13.2 nsecs. after the fast-peak was used.

6.3.3 $\pi^+\pi^-\pi^-$ mode.

This mode has been reported [15,43] to be produced by the direct decay of the δ^- meson i.e.

$$\delta^- \rightarrow \pi^+\pi^-\pi^-$$

Only two channels with good detection efficiencies were included to study this mode (table 6.3.3A). At the cost of 9% and 7.3% of signal, the background was reduced (see table 6.3.3A) by rejecting the events associated with the ring and the droop counters respectively.

The possible sources of the backgrounds in the present mode would be

$\pi^- p \rightarrow \pi^+\pi^-\pi^- p$, non-resonant

and $\pi^- p \rightarrow \pi^+\pi^-\pi^-\pi^0 p$

$\hookrightarrow \gamma\gamma$, both gammas lost.

It was difficult to distinguish the signal from the background. The yield curve obtained is shown in figure 6.4.I. See §6.4 for discussion.

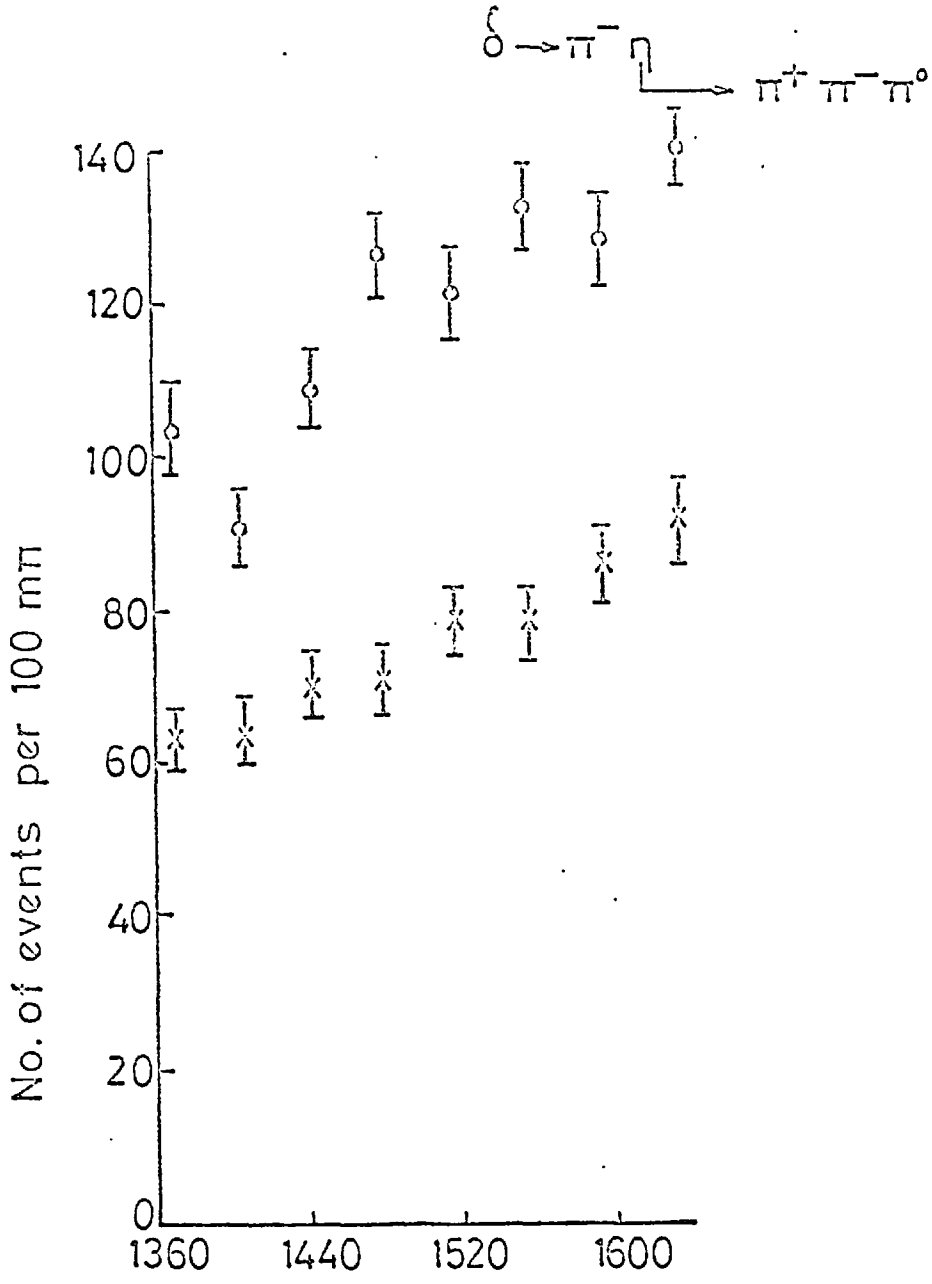

FIG. 6-3-2B

Uncorrected proton yield curve, for $\delta^- \to \eta\pi^-$, $\eta \to \pi^+\pi^-\pi^0$ with decay channels (PI, IC, GA) 302 and 212 added, in the gate of 6.8 to 13.2 nsecs after the fast-peak. A signal from the P counter was required.

o The events with the ring counter were rejected.

x A signal from the ring counter was required.

Decay Channels	Detection Efficiency %	H_2 - in events	RING EVENTS REJECTED				
			H_2 in	H_2 out	Droop + H_2 in	Casuals	Droop + H_2 out
300	38.1	248	171	9	24	2	4
210	16.6	211	152	35	25	8	13
Total	54.7	459	323	44	49	10	17

Table 6-3-3A Predicted detection efficiency and the observed proton background per 100 m π , for $\delta^- \rightarrow \pi^+ \pi^- \pi^-$ mode in the gate 6.8 to 13.2 nsecs, estimated at P π = 1.408 GeV/C. A signal from the P-counter was required.

Thus, our selectionswere

(1) General selection

(i) A signal from the P-counter was required.

(ii) The events associated with the ring counter were rejected.

(iii) Events associated with more than one neutron counter or more than two proton counters were rejected.

(iv) Gates chosen were 38-41, 42-53 and 54-63 PDP-8 channels (see table 5 - 1A).

(2) Decay particle definitions as given at the end of § 6-3-1.

(3) Decay classes considered

(i) π^- η and π^- π^0, decay channels 102, 112 and 012 were added. The separation, sep, between two gammas was constrained.

a) π^- $\gamma\gamma$ narrow with sep ≤ 4, for π^- π^0
and b) π^- $\gamma\gamma$ wide with sep ≥ 5, for π^- η

(ii) for 3 π 2 γ class, channels 302, 212, 301 and also 312 were added.

(iii) for π^+ π^- π^- mode, channels 300 and 210 were added.

(4) For total proton yield curves in three gates, events with decay signatures (PI, IC, GA) 00 ≤ 3, 1 ≤ 10, 200 and 0 ≤ 20 were discarded.

6-4 Results and discussions

The enhancement observed in the momentum region near 1.4 GeV/c to 1.6 GeV/c in the yield curve for the c.m gate 6.8 to 13.2 nsecs is considered to be genuine as

(i) No enhancement in the same momentum region is found in the yield curve of another gate (Fig 6-4-B).

(ii) No corresponding dip in the yield curve of either the rejected or the ring events is found.

These two conditions rule out an enhancement due to s-channel effect.

(iii) The yield curve at each momentum bin in the c.m gate for the enhanced region has a regular trend and each point was contributed by more than one run (Fig 6-4-H). This rules out any possibility of a few runs being accidentally high or low.

The absence of an enhancement at ~ 990 MeV/c^2 in the yield curves of the two gates (Fig 6-4-B and Fig 6-4-C) could be explained by low collection efficiency in these regions and poorer mass resolution. Especially in the case of fig 6-4-B, the worse mass resolution was $\pm$ 38 MeV/c^2 which would tend to smear the enhancement.

Indication of $\delta^- \to \eta\pi^-$ came from the enhancements observed in the yield curves of $\pi^- \gamma\gamma$ wide and $\pi^+\pi^-\pi^-\gamma\gamma$ (Figs 6-4-D and 6-4-E). As expected no enhancement was observed in the yield curve of $\pi^- \gamma\gamma$ narrow mode in the c.m region (Fig 6-4-F), and of $\pi^- \gamma\gamma$ wide mode in the gate 13.2 to 18.4 nsec after the fast peak (Fig 6-4-G). A possible enhancement in the yield curve of c.m gate (Fig 6-4-I) for $\delta^- \to \pi^+\pi^-\pi^-$ in the same incident pion momentum region requires detailed study:- a contribution to this mode coming from $\delta^- \to \pi^-\eta$, $\eta \to \pi^+\pi^-\pi^0$ can not be ignored because a fraction of $3\pi\gamma\gamma$ events will appear in the decay channels 300 and 210 (PI, IC, GA).

With an indication of enhancement in the $\eta\pi^-$ near the δ^- region, we would like to study this mode with our new set of data which is better than the present one (§ 7-3). We give an estimate of mass, width and the cross-section in the next chapter where the analysis of the new set of data is presented.

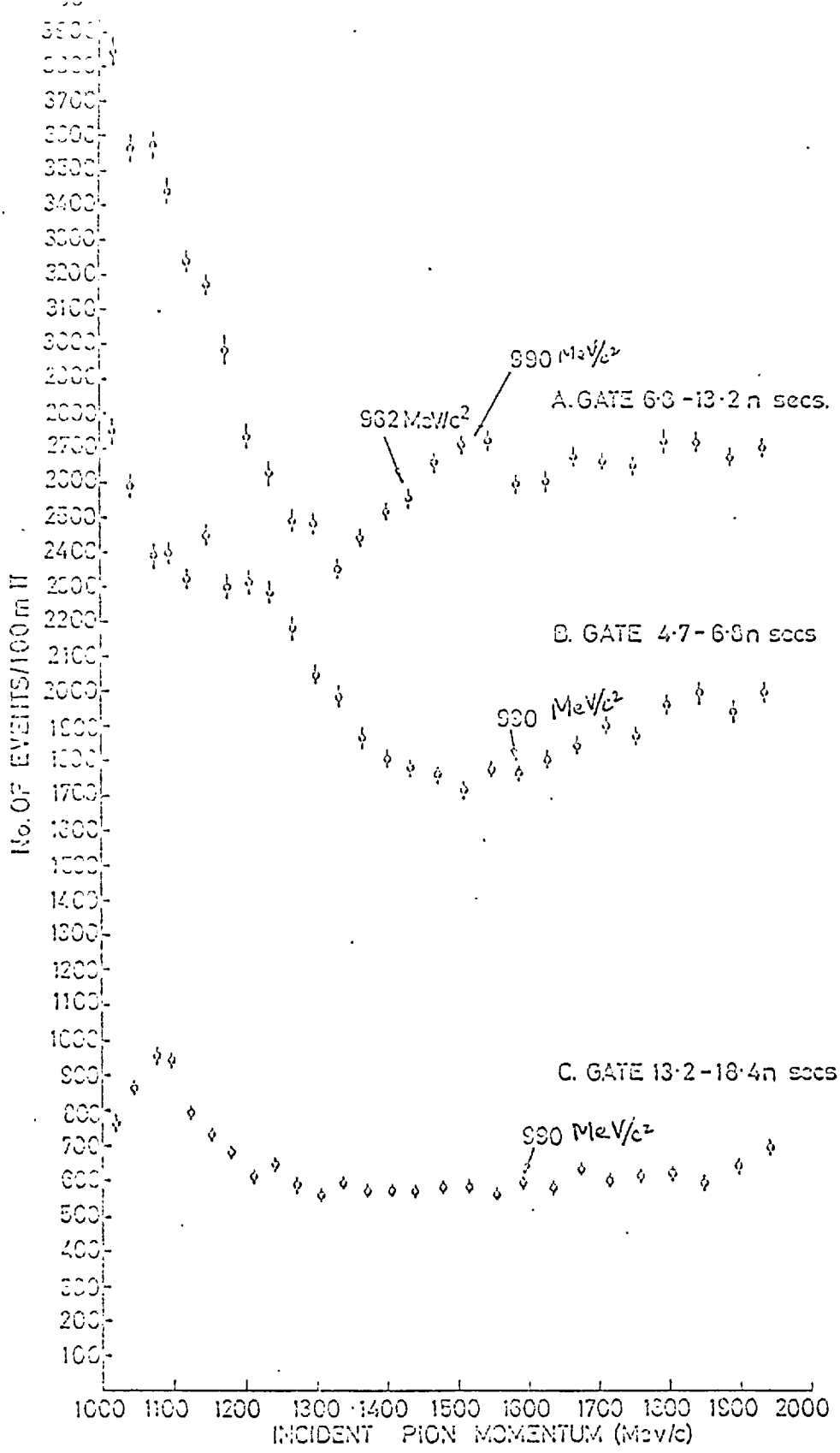

FIG 6-4 (A-C) CORRECTED PROTON YIELD CURVES IN THREE GATES. THE EVENTS WITH DECAY SIGNATURES (PI, IC, GA) 00≤3, 0≤20, 1≤10 AND 200 WERE REJECTED. THE EVENTS WITH THE RING COUNTER WERE REJECTED AND A SIGNAL FROM THE P COUNTER WAS REQUIRED.

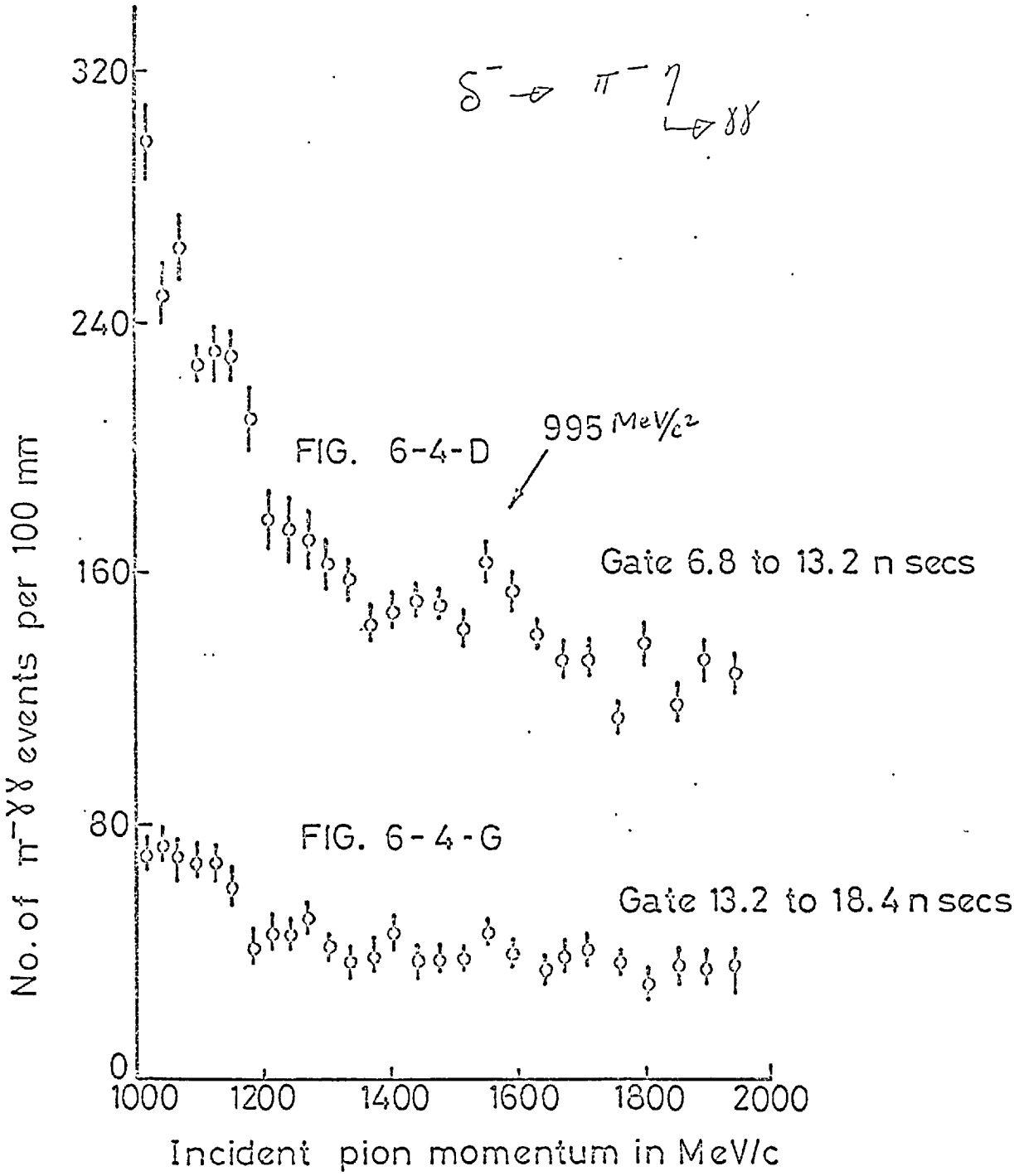

FIG. 6-4-D G

Corrected proton yield curve for $\pi^-\gamma\gamma$ wide $(\delta^- \to \pi^-\eta,\ \eta \to \gamma\gamma)$ mode with decay channels (PI, IC, GA) 102, 012 and 112, in two gates. The events associated with the ring counter were rejected and a signal from the P counter was required.

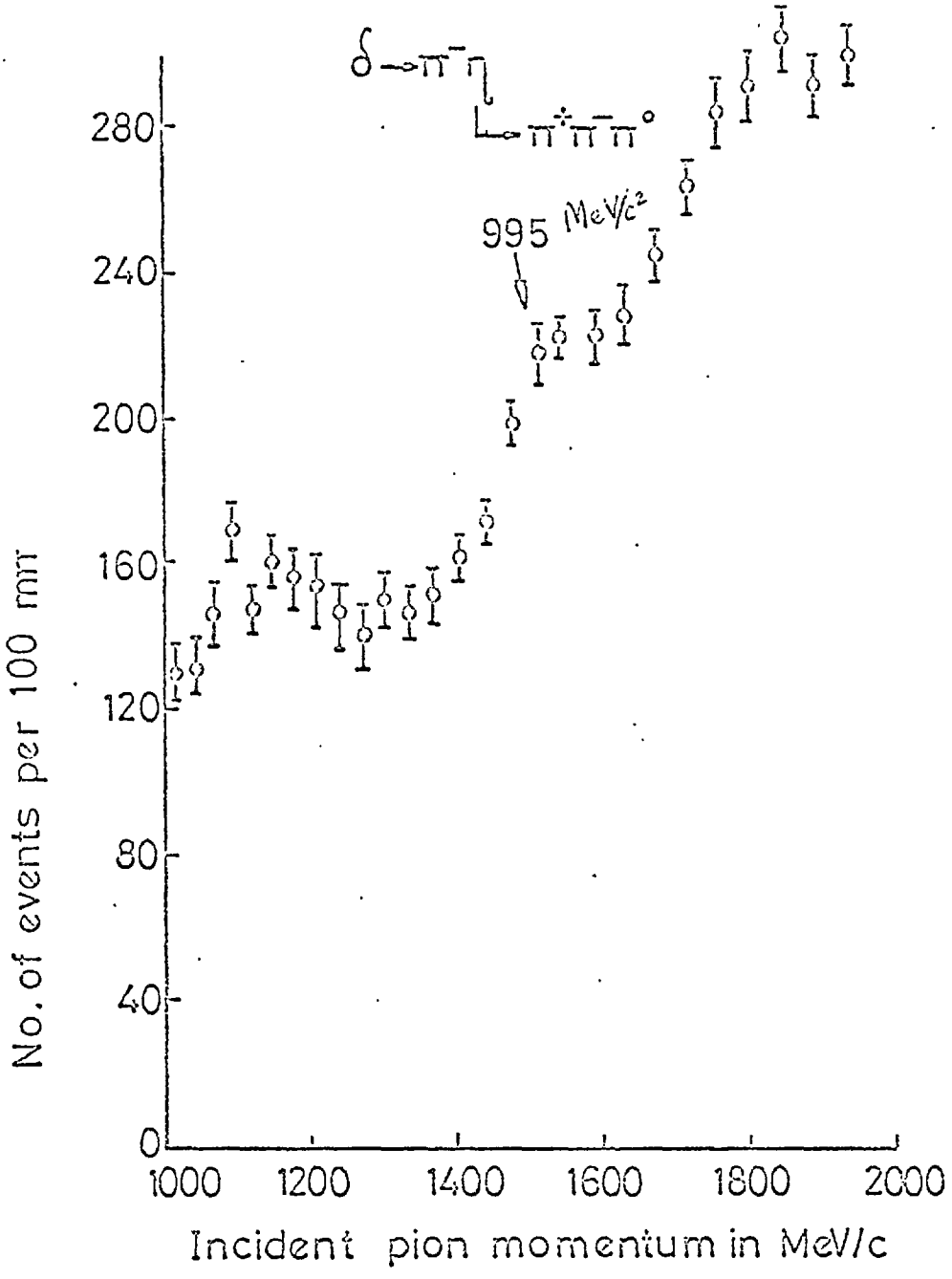

FIG. 6-4-E

Corrected proton yield curve, for $\delta^- \rightarrow \eta\pi^-$, $\eta \rightarrow \pi^+\pi^-\pi^0$ in decay channels (PI, IC, GA) 302, 301, 212 and 312, in the gate 6.8 to 13.2 nsecs after fast-peak. The events associated with the ring counter were rejected and a signal from the P counter was required.

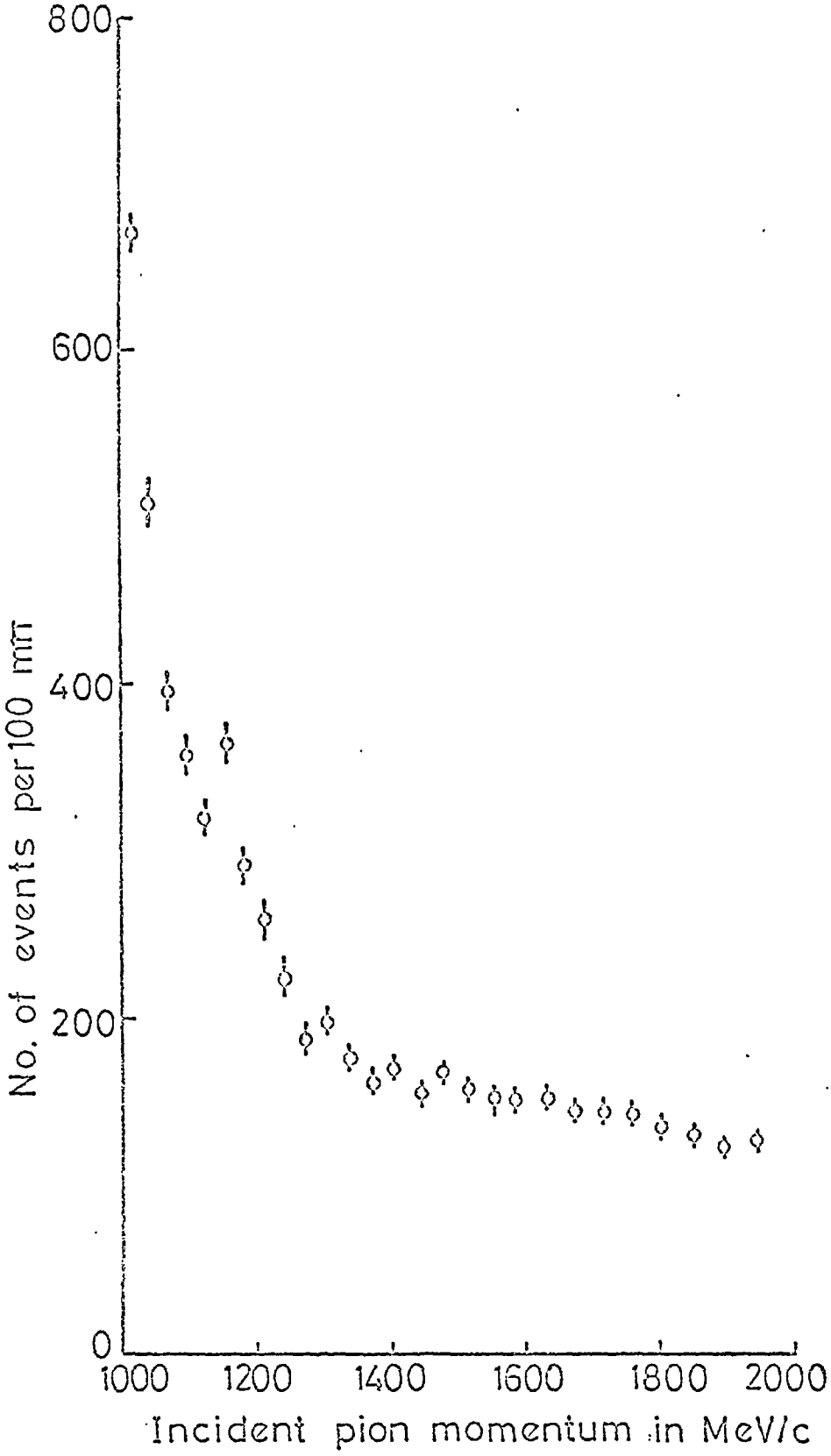

FIG. 6-4-F

Corrected proton yield curve, for $\pi^- \gamma\gamma$ narrow ($\pi - \pi^0$) mode with the decay channels (PI, IC, GA) 102, 012, and 112, in the gate 6.8 to 13.2 nsecs after the fast-peak. The events associated with the ring counter were rejected and a signal from the P counter was required.

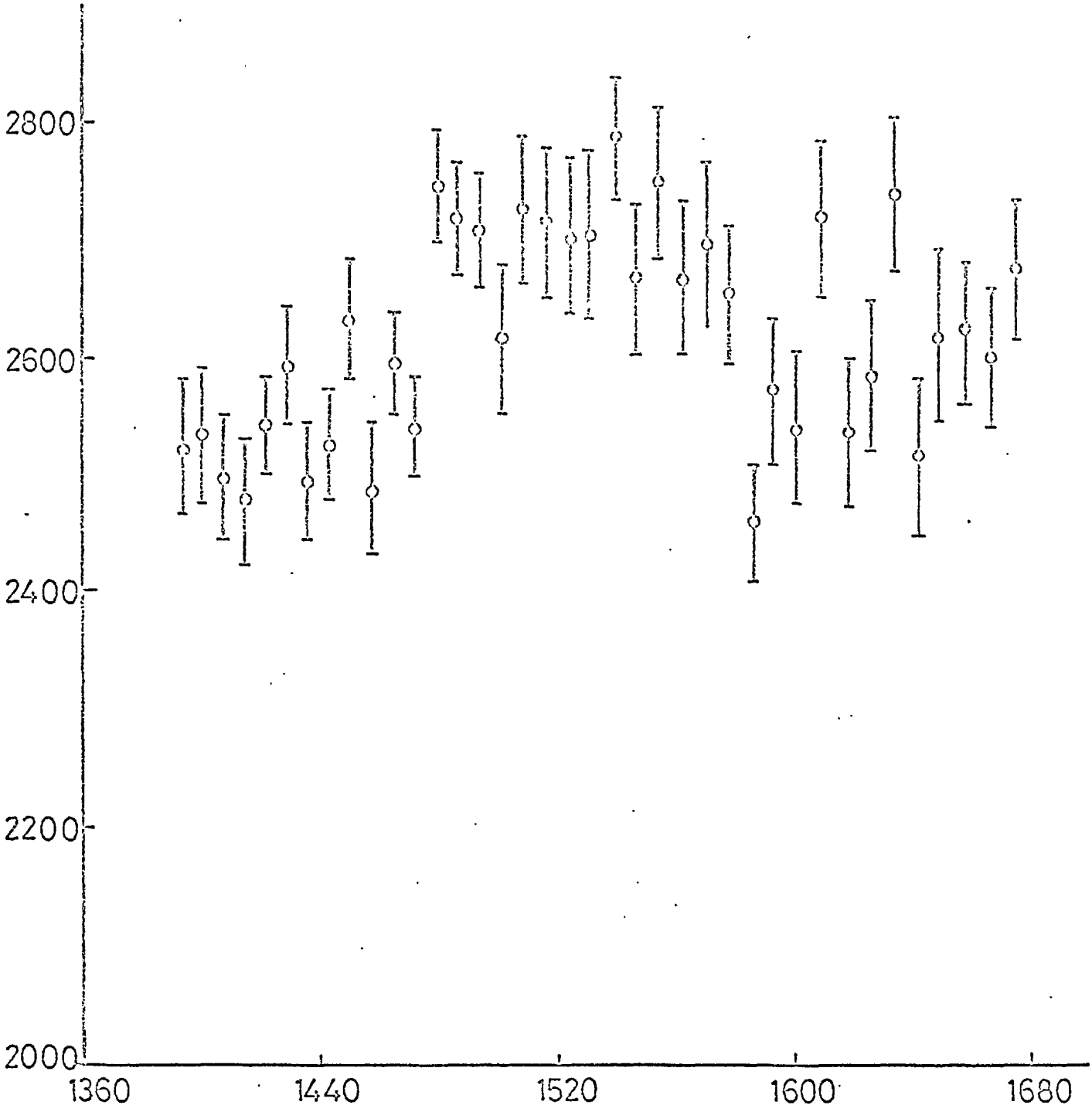

FIG. 6-4-H

The corrected proton yield curve at each momentum bin in the gate of 6.8 to 13.2 nsecs. The events associated with decay signatures (PI, IC, GA) $00 \lesssim 3$, $0 \leqslant 20$, $1 \leqslant 10$ and 200 were rejected. The events with the ring counter were rejected and a signal from the P counter was required.

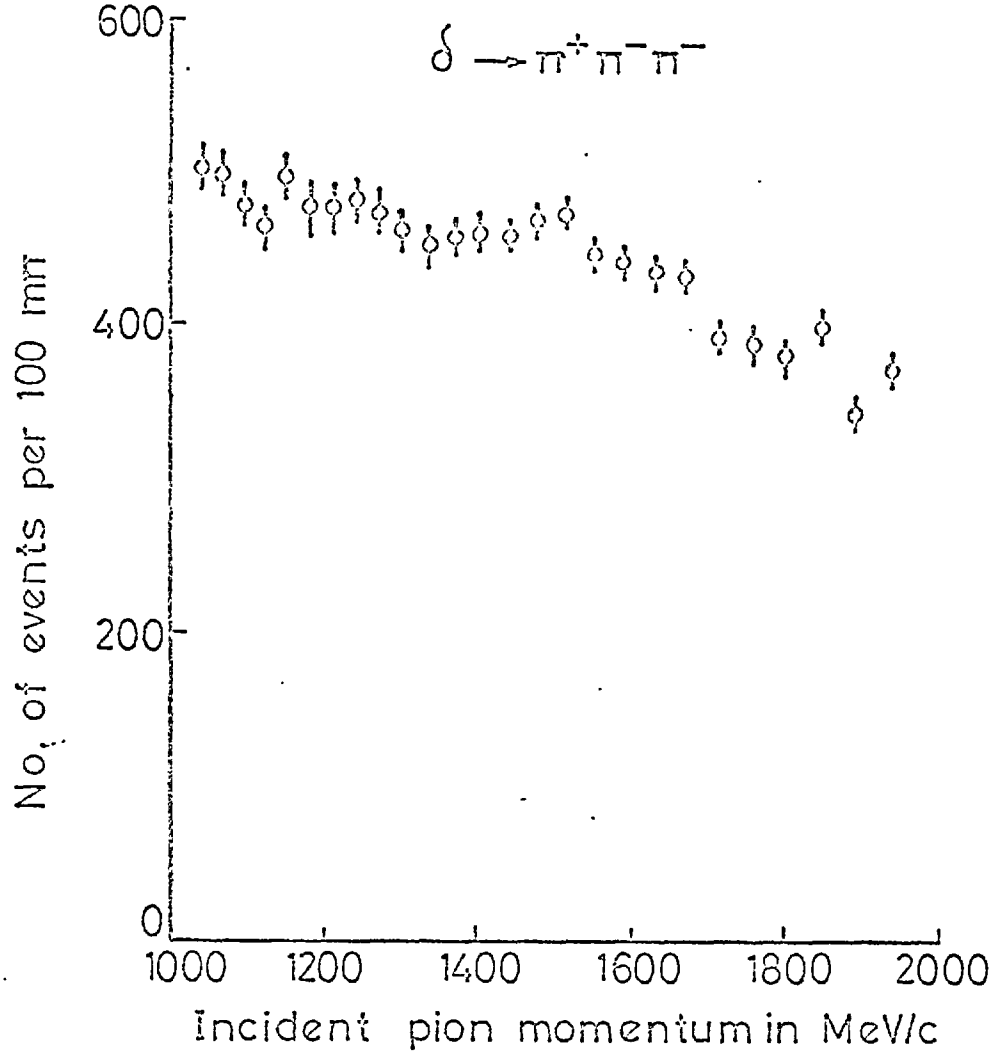

FIG. 6-4-I

The corrected proton yield curve, for $\delta^- \rightarrow \pi^+\pi^-\pi^-$ with decay signatures 300 and 210, in the gate 6.8 to 13.2 nsecs. The events associated with the ring counter as well as the droop counters were rejected. A signal from the P counter was required.

CHAPTER - 7

MODIFICATIONS, DATA ACQUISITION AND ANALYSIS

7.1 Modifications

The apparatus was modified to reduce the background and also to get more information on forward going decay particles. We will discuss now these modifications.

a) The A13 Counter

The analysis of the previous set of data revealed that a large fraction of total events were non hydrogen and casual backgrounds. Some classes of these backgrounds were reduced by rejecting the beam particle associated with a rectangular counter A13, containing a hole in it, installed upstream of the hydrogen target (Fig 2-3-G). See page 13.

b) The Ring Counters R1 and R2

The previous ring counter was replaced by two semi-annular counters R1 and R2 Fig 2-3-G.

c) The Polar Angle Counters L1 and L2

Each of these two semi-annular counters was installed to cover a portion of ten Lidgamma Counters and provided better information on decay particle going forward through the Lidgamma Counters (Fig 2-3-G).

d) The Target Counters

A set of six ring shaped counters called the 'target counters' was mounted around the hydrogen target for a better estimate of the interaction point to be determined with the knowledge of which target counters were fired by the charged decay particles. A reduction in the non hydrogen background was anticipated with the use of these counters (Fig 2-3-G).

e) The A0 and A01 Counters

Failure of the A0 veto circuit forming ST3 ($\Sigma P_{\pi L} \overline{A0}$) could result in the formation of a trigger, even with a non-interacting beam particle. The structure observed in the time-of-flight distribution of the proton events associated with the counters A0 and A01 vanished with an increase in the resolving time of the A0 veto circuit. The structure was not entirely due to the failure of the IR as the resolving time had to be increased more than just to cover the s-counter dead-time effect on the IR.

7.2 Data Acquisition

The aim of this set of the data-taking runs was to study, in detail, the resonances in the mass region from 0.5 GeV/c^2 to 2.0 GeV/c^2 with our improved apparatus with high statistical accuracy.

The distance from the target to the neutron counter was chosen to be six meters to improve the mass resolution so as to observe the A2 split, if any, above the production threshold.

One 7-track tape with about 500 to 600 million incident pions was written at each momentum bin to achieve $\lesssim \pm$ 1% statistical fluctuation on the neutron rate. 43 runs in the δ^- region covering the incident pion momentum range from 1.386 GeV/c to 1.684 GeV/c were taken in two-cycles; scanning first from higher to lower momenta taking three bins out of 5 grouped momentum channels and then from lower to higher momenta completing the rest of the bins.

7.3 Comparison between the 5M and the 6M Data

Except for the disadvantage of less geometrical collection efficiency of the neutron counters, the advantages of the new set of data over the last set were the following.

i) The instrumental backgrounds were considerably reduced with the modifications (§7-1).

ii) The better estimation of the beam interaction point, provided by the target counter, enabled a) a more accurate determination of the nucleon time-of-flight and b) a better correction in proton time-of-flight for its energy loss in the target.

This, in turn, gave better mass resolution.

iii) More polar information on the forward going decay particles was provided by the polar angle and the ring counters.

iv) The timing reference peak was monitored during each run while in the previous set of data the peak position was only measured before and after each run.

v) The occupancy of the P Counter was also measured.

vi) The performance of the apparatus, eg the time digitizer calibration, was checked quite often.

vii) Appreciable variation in the beam rate was not allowed.

Although there was a slight change in the nucleon angle in the laboratory detected by the neutron counter, there was no change in the value of momentum transfer, 't'.

7.4 Analysis

7.4.1 Selection of Runs

Out of 43 runs (§ 7-2) in the δ^- region, two runs at incident pion momenta 1.443 GeV/c and 1.458 GeV/c were omitted due to electronic trouble in trigger; while one run at 1.684 GeV/c was rejected due to wrong magnet current setting.

7.4.2 The Neutron Counter Inefficiency

The third neutron counter N3 became inefficient during runs (1751) to (1772) (1.339 GeV/c to 1.563 GeV/c) due to the failure of an 'AND Gate' Card. The inefficiency for each run was calculated by

comparing the ratio R, $(\frac{N3}{\text{all Ni} - N3})$ with its averaged value $\bar{R}$ obtained for other runs. To take this into account a correction factor worked out for each run was applied to the number of incident pions 'N3COR' in the analysis programs.

7.4.3 'The Krunch Program'

Data summary tapes were written by analysing all of our tapes using a fortran program called 'Krunch'. In this program, the ring counter was allowed only once to define a PI ($\overline{\pi}$s) in the presence of a free IC. A spare IC was called the 'δ_2' . Other classes of PI's and gammas were the same as listed at the end of section 6-3-1.

7.4.4 Reproducibility of Runs

The number of events in decay modes $\pi^- \pi^o$ and three charged pions in a sliding cm. gate was found reproducible within the statistical fluctuation of $< \pm 2\%$.

7.4.5 Selection of the Decay Modes

The $\pi^- \gamma\gamma$ wide (§ 6-3-1) decay mode was found to be the best mode to study the $\delta^- \to \eta\pi^-$ (Table 6-3A) for the following reasons.

i) Most of the $\pi^- \pi^o$ background was removed by constraining the separation of $\gamma\gamma$ (§ 6-3-1) in $\pi^- \gamma\gamma$ mode.

ii) The signal to background ratio was estimated to be at least twice as good for $\pi^- \gamma\gamma$ wide as for two other modes ie $3\pi\, 2\gamma$ and π^- neutrals ($\to 4\gamma$).

7.5 Study of $\pi^- \gamma\gamma$ wide Mode

Assuming 100 δ^-/100 mπ (§ 6-3) detected in $\eta\pi^-$ mode, the number of δ^- events expected in $\pi^- \gamma\gamma$ and $\pi^- \gamma\gamma$ wide modes were 38/100 mπ (table 6-3A) and 36.6/100 mπ (§ 6-3-1) respectively.

The possibilities for including different channels for $\pi^- \gamma\gamma$ wide mode were found by studying the expected number of the detected events predicted by the montecarlo program and the background (in a c m gate, 8 to 16 nsecs after the fast-peak) obtained from a run at P_π = 1.436 GeV/c taken below the δ^- production threshold.

The observed number of events with γ_2 was almost the same as the number predicted by the montecarlo program as γ aberration (table 7-5-A). Therefore, γ_2 was included in the gamma definition. Approximately 34% of the signal was included by selecting channels 100020 and 100011 (table 7-5-A).

For further selection, we studied the background and a channel would only be added if the ratio of signal to noise became better after the addition.

The non-hydrogen events were the main contributor to the background. The requirement of the target counter with each event could reduce

a) The non-hydrogen background by 87%, and

b) the hydrogen-in background by 42%, at the cost of those events in

which the pions went backward or forward and were not detected by the target counter.

The fraction of the signal f lost by such constraint would depend upon the spin of the δ^- meson. An appreciable fraction of non-zero spin particles would tend to go backward or forward, missing the target counters but could be detected by either the droop counters or the ring counters.

Secondly, demanding a target counter would improve S/B and S/n ratios (table 7-5-A, these have been calculated on the assumption of f = 10%). This assumption was based on the fractions of $\pi^-\gamma\gamma$ wide events passing through the droop and the ring counters predicted by the montecarlo program with an isotropic decay distribution of the δ^- meson. However, these ratios could be worse for the 'spinning' δ^- meson.

Therefore, the events associated with and without the target counter should be treated separately.

On the basis of table 7-4-B, the selection 'a' was a good selection as ratios S/B and S/n would not be improved by including other decay channels. The detection efficiency for this selection was considerably higher than that for any selection. So, we decided to consider only selection 'a' ie 100020 and 100011.

At the cost of 3.3% signal, a further subtraction of 14.4% of $\pi^-\pi^0\pi^0$ background was achieved by accepting 6 or more counter bins separation between π^- and the bisecor of two gammas of $\pi^-\eta$ and $\pi^-\pi^0\pi^0$ modes (graph 7-5-C). Thus to study the $\pi^-\gamma\gamma$ decay mode of the δ^- meson, the requirements on the proton events were

i) a pulse from the P-counter

ii) $\not>$ 2N->2A rejected

iii) the separation between $\gamma\gamma \not> 5$

iv) the separation between the bisector of $\gamma\gamma$ and $\pi^- \not> 6$

v) 100020 and 100011 channels considered

vi) events with and without the target counter, could be studied separately.

The analysed events on the data summary tape fulfilled all the requirements except a) the events associated with the droop counters were rejected and b) the target counter was not required for the event.

However, a correction in the time-of-flight was applied by estimating the interaction point depending upon which target counter fired. In the absence of the target counter the interaction point was assumed to be in the downstream end of the target.

With these known conditions, it was decided to use the results stored on the data summary tape; because (i) $\pi^-2\gamma$ wide events associated with the droop counters were only 4.7% estimated by the montecarlo program assuming an isotropic distribution, and (ii) the uncertainty in the mass introduced by the uncertainly in the estimate of the interaction point could be predicted by a montecarlo program simulating the same conditions as used in the analysis program. Alternatively, should there be an indication of an

MONTECARLO PREDICTION
SEPARATION BETWEEN π^- AND THE BISECTORS
OF 2δ FROM $\pi^-\eta$ AND $\pi^-\pi^0\pi^0$

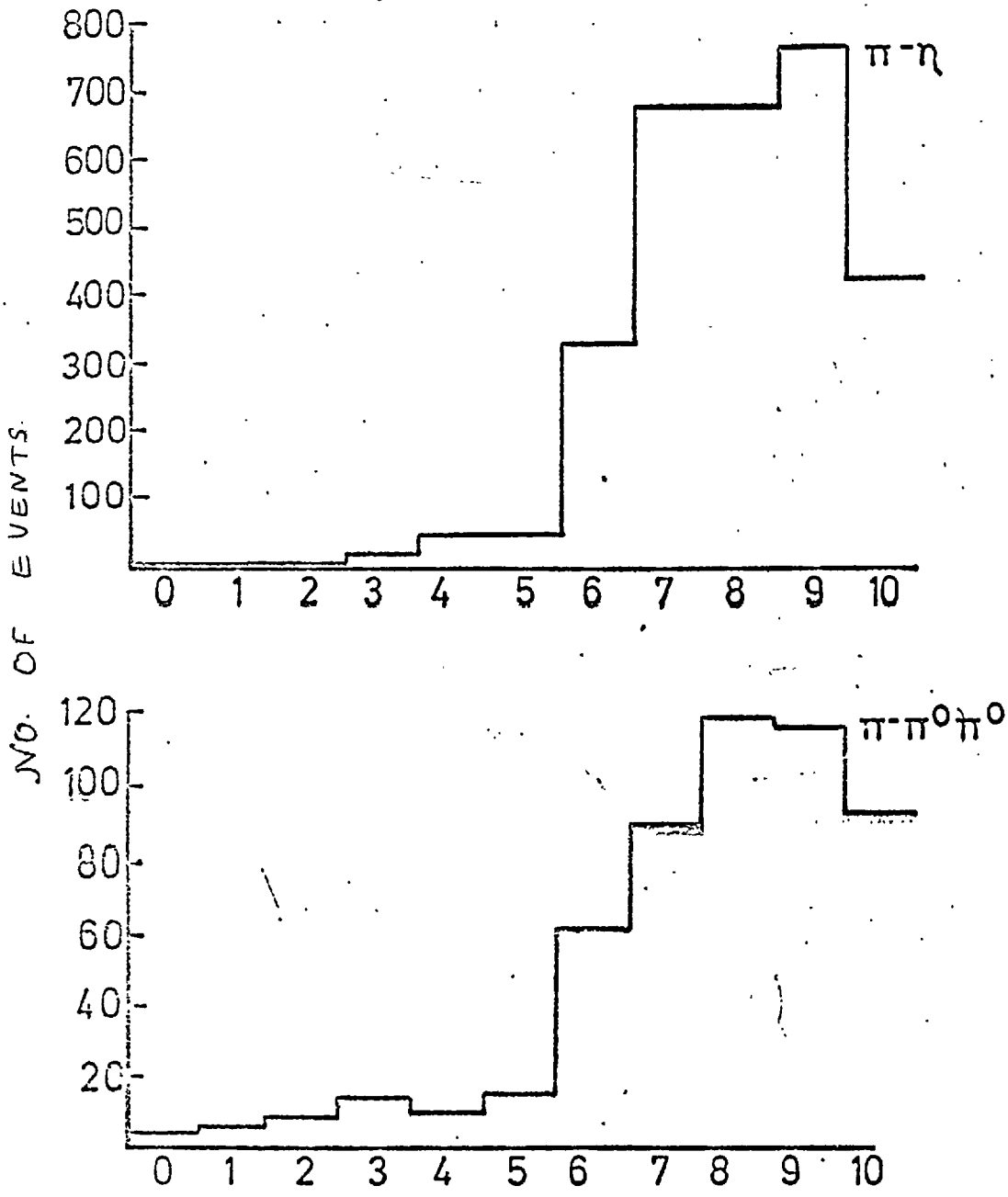

SEPARATION BETWEEN π^- AND THE BISECTOR
OF $\delta\delta$ (IN COUNTER BINS)

FIG. 7-5-C

enhancement in any one of the yield curves of the longer time of flight gates, all the data could be reanalysed requiring the target counter for each event.

	Decay Channels	Signal		Background/557.6 mπ				
				H2 in			H2 out	
		Detection Efficiency %	Number expected per 100 mπ assuming 36.6 produced	H2 in	Target Counter Demanded	Ring Demanded	H2 out	Target Counter Demanded
	$\pi_3\pi_\gamma\pi_\delta$ Sp $\delta\delta_2$							
a)	100020	26.0%	12.77	250	158	43	60	3
	100011	8.90		100	63	14	3	3
b)	000120	2.50	1.24	125	40	6	63	9
	000111	0.89		34	10	0	27	3
c)	010020	1.60	.77	44	22	2	3	0
	010011	0.50		11	10	0	3	3
d)	001020	1.40	.63	21	13	4	12	0
	001011	0.33		5	2	0	3	0
e)	100120	5.30	2.64	115	84	22	27	3
	100111	1.90		33	20	2	12	3
f)	010120	0.23	0.10	20	14	3	0	0
	010111	0.04		9	6	0	0	0
g)	001120	0.13	0.06	22	15	5	3	0
	001111	0.03		6	5	0	0	0
Total		49.75		795	462	100	213	27

TABLE 7-5-A. Expectation of Signal and Evaluation of H2 in and non-hydrogen backgrounds with and without demanding the target counter in different decay channels of $\pi^-\delta\delta$ wide mode. Gate 8-16 nsec.

Signature	Target Counter Ignored				Assume 10% Loss of Signal Target Counter Demanded			
	S Signal 100 mπ	b Background for 557 mπ	S/b	S/n	S per 100 mπ	b for 557 mπ	S/b	S/n
a	12.77	350 ± 18.6	$\frac{1}{4.9 \pm .3}$	3.7	11.49	221 ± 14.8	$\frac{1}{3.4 \pm .2}$	4.3
b + a	14.01	509 ± 22.6	$\frac{1}{6.5}$	3.5	12.61	271 ± 16.5	$\frac{1}{3.8}$	4.2
c + a	13.54	405 ± 20.2	$\frac{1}{5.3}$		12.19	253 ± 15.9	$\frac{1}{3.7}$	
d + a	13.54	376 ± 19.3	$\frac{1}{5.0}$	3.8	12.06	236 ± 15.4	$\frac{1}{3.5}$	
e + a	15.41	498 ± 22.3	$\frac{1}{5.6 \pm .3}$		13.87	325 ± 18.0	$\frac{1}{4.2 \pm .2}$	
f + a	12.87	379 ± 19.5	$\frac{1}{5.3}$		11.58	241 ± 15.5	$\frac{1}{3.7}$	
g + a	12.83	378 ± 19.4	$\frac{1}{5.3}$		11.55	241 ± 15.5	$\frac{1}{3.7}$	

TABLE 7-5-B. Calculation of Signal to Background, S/B and Signal to Noise ratio, S/n for different decay channels of $\pi^- \gamma\gamma$ wide mode, with and without demanding a target counter.

7-6 SELECTION OF GATES

As it was desired to observe the narrow $\delta^-(962)$, a series of narrow gates ($\sim$ 4 nsecs wide) of small mass acceptances were selected (Table 7-6-B). Good mass resolution was expected around the C.M. gate of 11-14 nsecs. after the fast peak (Fig 7-6-A). A bin of two Pπi channels was chosen to improve the statistical significance.

7-7 RESULTS, DISCUSSIONS AND CONCLUSIONS

Figs 7-7-A and 7-7-B show the corrected yield curves in the four selected gates for $\pi^-\gamma\gamma$ wide mode selection. Except in the yield curve corresponding to the gate 11-14 nsecs, no significant enhancement was observed. It was unlikely that the enhancement observed in the corrected yield curve in this gate was due to a few runs being accidentally high; since each point had contributions from several runs and also points seem to follow a definite trend. A straight line to the points of the yield curve was a poor fit with C.L. of $P(\chi^2) = 0.8\%$. However, a straight line fit through the points of non-resonance regions (suggested by the MonteCarlo program of mass 990 MeV/c^2 and $\Gamma = 40$ MeV/c^2) ranging from $P\pi = 1373 - 1419$ MeV/c and $1614 - 1663$ MeV/c was a reasonable fit with confidence level of $P(\chi^2) = 68.8\%$. Thus, the background shape was consistent with the straight line.

The yield curve for $\pi^-\gamma\gamma_{\text{narrow}}$ ($\pi^-\pi^0$) mode (Fig 7-7-C) in the 11-14 nsecs gate did not show such an enhancement and its shape was consistent with a straight line with C.L. of $P(\chi^2) = 77.6\%$.

$\delta^-(962)$: No significant enhancement in the $\delta^-(962)$ region was observed in the yield curves of either the C.M. gates or of the longer time-of-flight gates (Figs 7-7-A and 7-7-B). For an upper limit on the production cross-section of the $\delta^-(962)$ in relation $\sigma^- = A\,P^*$, the value of A will be quoted assuming that the cross-section changes slowly with increasing $|t|$. The bin of mass 962 MeV/c^2 of the yield curves of the four gates were aligned together (by shifting the bins) to add their contributions. The observed curve and the MonteCarlo predicted curve (obtained similarly) are shown in Fig 7-7-D.

From the MonteCarlo prediction we expected to see an enhancement in three bins (1 bin = 7 MeV/c^2).

If the branching ratios for $\delta^-\to\eta\pi^-$ and $\eta\to\gamma\gamma$ are assumed to be 100% and 38% respectively we expect 11.8 events in $\pi^-\gamma\gamma_{\text{wide}}$ selection (assuming a cross-section giving 100 δ^- per 100 mπ). Assuming A = 1 in relation $\sigma^- = A\,\mu b/(\text{MeV/c})$, we expected 475 δ per 100 mπ to be seen in the plot p^* of fig 7-7-D (1). The upper limit of the value of A, $\leq (-0.016 \pm 0.007)\,\mu b/(\text{MeV/c})$ with C.L. of 68% was obtained by fitting a straight line through the observed points between mass 949 to 978 MeV/c^2 excluding the three points in the $\delta^-(962)$ region.

The absence of enhancement in the $\delta^-(962)$ region for $\delta^-\to\pi^-\eta_{\to\gamma\gamma}$ in $|t|$ range 0.12 to 0.29 $(\text{GeV/c})^2$ signifies that either the production cross-section or the $\delta^-\to\eta\pi^-$ branching ratio was very small. Alternatively no $\delta^-(962)$ is produced in this $|t|$ region.

There is some indication of a possible enhancement in the mass region ~995 MeV/c^2. An attempt was made to measure the mass, the width and the cross-section of the enhancement observed in the gate 11-14 nsecs. So, the MonteCarlo predicted yield curves for various masses and widths with straight line background were fitted to the observed yield curve in the gate 11-14 nsecs and the value of χ^2 was minimised to find the best value of the quantity under consideration. At the value of mass 995 MeV/c^2 (Fig 7-7-E), the best value of the width of the enhancement was found to be Γ = 40 MeV/c^2 with an error of $\pm^{40}_{36}$ MeV/c^2. Holding this value of width constant, the minimum χ^2 occurred at m = 996 with an error of ± 12 MeV/c^2. For comparison with the results of the other experiments. See Fig 7-7-F

The total number of events in the observed yield curve above the fitted background (Fig 7-7-B) was (29.3± 5.6) events per 100mπ , which corresponded to A = (0.16 ±0.03) μb/(MeV/c). (We expected 185.8 events per 100 mπ in this selection for A = 1).

The statistical significance of the enhancement, given by

$$\frac{\text{S', the total number of events above the fitted background}}{\text{Error on S'}}$$

is 5.2 standard deviation.

The ratio S/B , signal to background is 10%

Thus, in the $|t|$ region 0.22 to 0.29 (GeV/c)^2, the 5.2 standard deviation enhancement of mass 996±12 MeV/c^2 with Γ = 40^{+40}_{-36} MeV/c^2 is significant; the probability for this sample being consistent with a straight line is 0.8%. The strong decay in $\eta\pi^-$ mode implies $I^G = 1^-$ and J^P in series 0^+, 1^-, 2^+ etc.

Some more work is required to confirm this enhancement as a meson state. As the effect was only seen in one gate it was not possible to rule out the possibility that the effect may be due to a narrow N* appearing in this decay mode. (Mass would be ~1940MeV/c^2, but no such N* has been reported). The data is available to search for the neutral state.

CONCLUSION

No enhancement in the /t/ region 0.12 to .29 (GeV/c)^2 was observed for $\bar{\delta}$ (962) in $\eta\,\pi^-$ mode, $\eta \to \gamma\gamma$. A 5.2 standard deviation enhancement at mass 996±12 MeV/c^2 with = $^{40}_{36}$ MeV/c^2 in $\eta\pi^-$ mode, $\eta \to \gamma\gamma$ was observed in the /t/ region 0.22 to 0.29 (Gev/c)^2. Its $\eta\,\pi^-$ decay mode signifies that if this were a meson state then $I^G = 1^-$ and $J^P = 0^+$, 1^-, 2^+ etc. However we cannot rule out the possibility that this may be N* of mass ~1940 MeV/c^2.

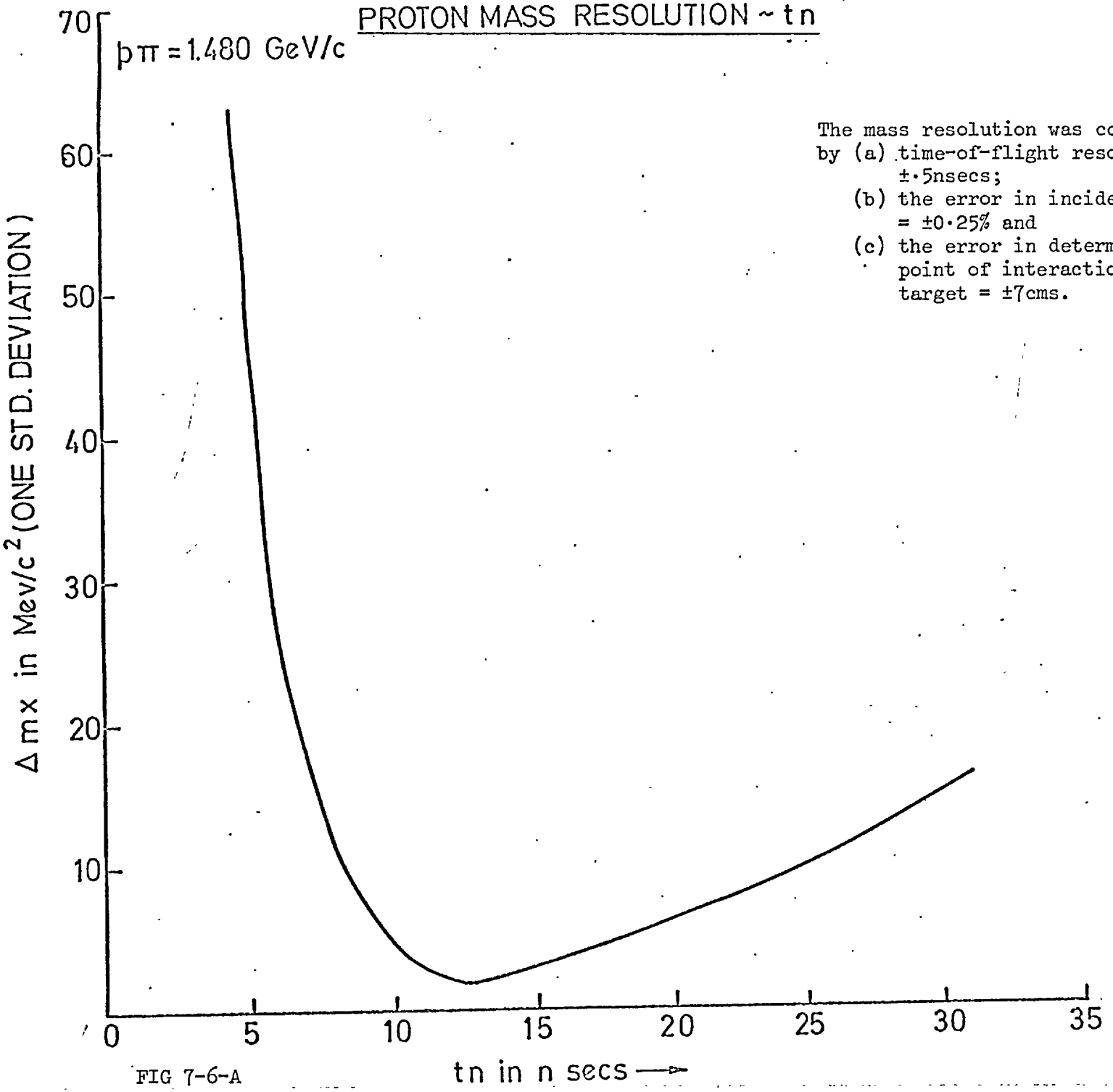

The mass resolution was contributed by (a) time-of-flight resolution of ±·5nsecs;
(b) the error in incident pion momentum = ±0·25% and
(c) the error in determining the point of interaction in the H_2 target = ±7cms.

FIG 7-6-A

Gate in nsecs after the fast-peak	$\|t\|$ in $(\text{GeV/c})^2$	Peak positions for Mass Mx_j (in mev/c)	
		$Mx = 995$ MeV/c^2	$Mx = 962$ MeV/c^2
		$\Gamma = 40$ MeV/c^2	$\Gamma = 5$ MeV/c^2
11-14	0.29 - 0.22	1521	1446.5
14-17	0.22 - 0.18	1536	1461.3
17-20	0.18 - 0.15	1551	1476.3
20-23	0.15 - 0.12	1583	1521.0

Table 7-6-B. Selected gates. The MonteCarlo predicted peak positions in the yield curve obtained by grouping incident pion momentum bins in twos are given.

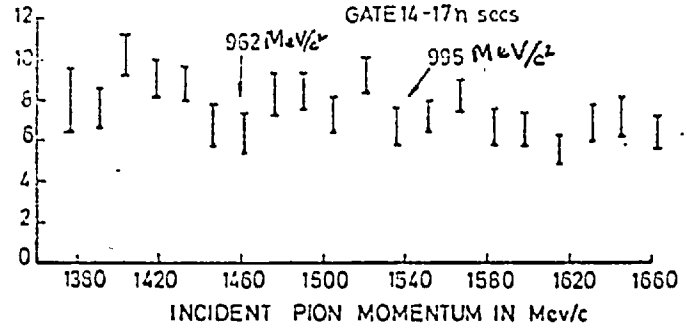

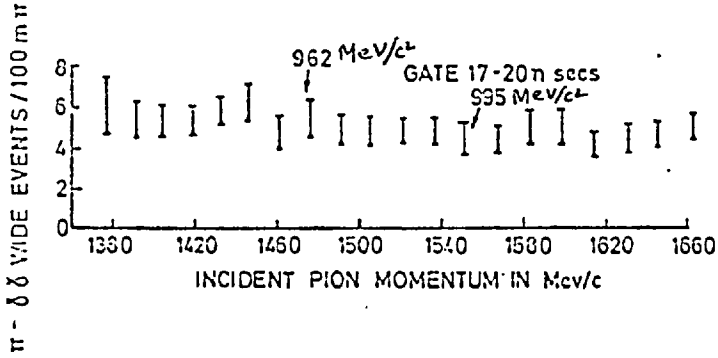

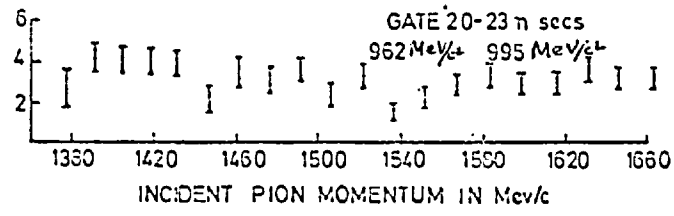

FIG. 7-7-A THE CORRECTED YIELD CURVES IN DIFFERENT GATES FOR THE $\pi^- \eta$ DECAY MODE WITH $\pi^- \gamma\gamma$ WIDE DECAY SIGNATURE.

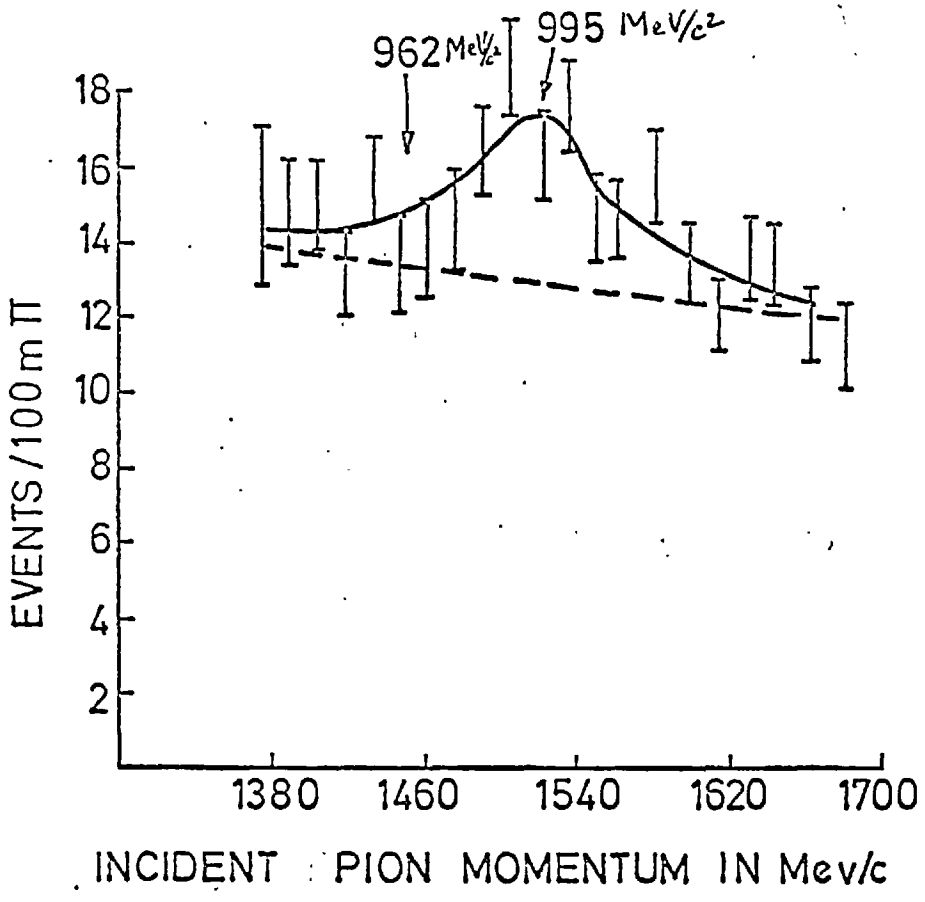

FIG. 7-7-B

The corrected yield curve for the $\pi^- \eta$ decay mode with $\pi^- \gamma\gamma$ wide decay signature in the gate 11-14 nsecs. The dotted line is the fitted background. The fitted curve predicted by the Monte Carlo program for mass 996 MeV/$_c$2 at Γ = 40 MeV/$_c$2 is shown by the solid line.

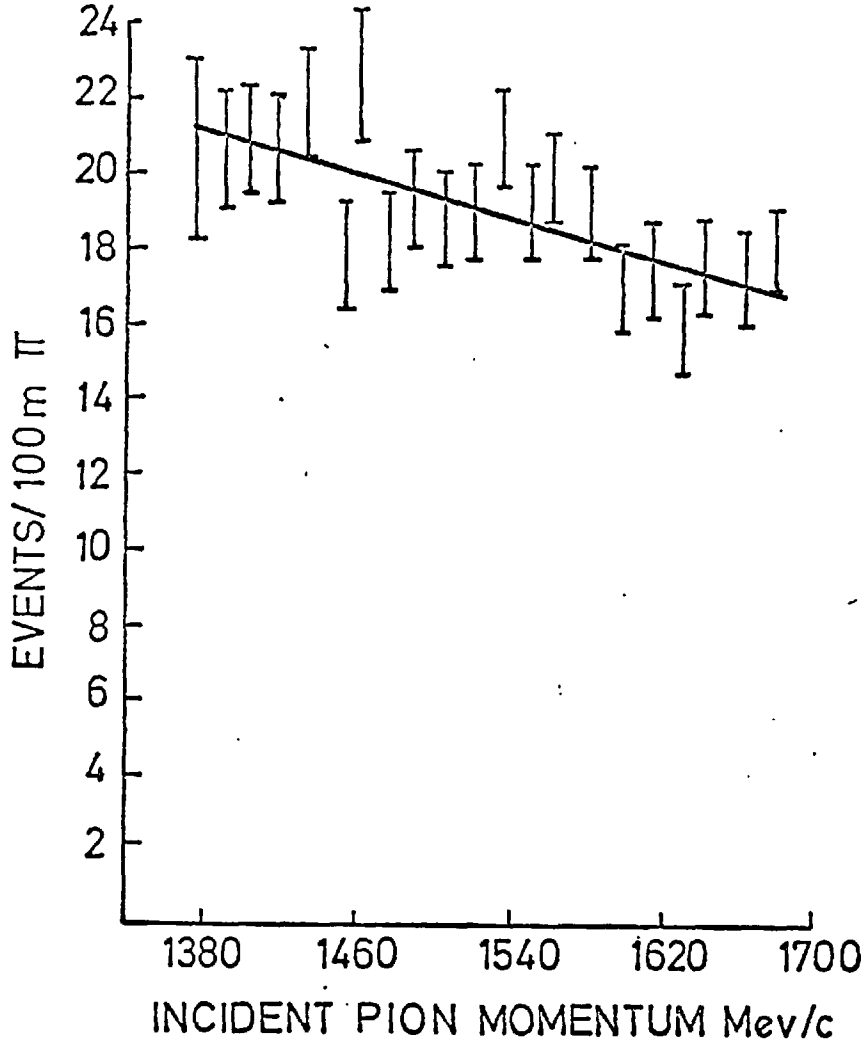

FIG.7-7-C

A straight line fit through the points of the yield curve of $\pi^{-}\gamma\gamma$ narrow ($\pi^{-}\pi^{o}$) mode in the gate 11-14 Nsecs.

(2) The observed mass plot

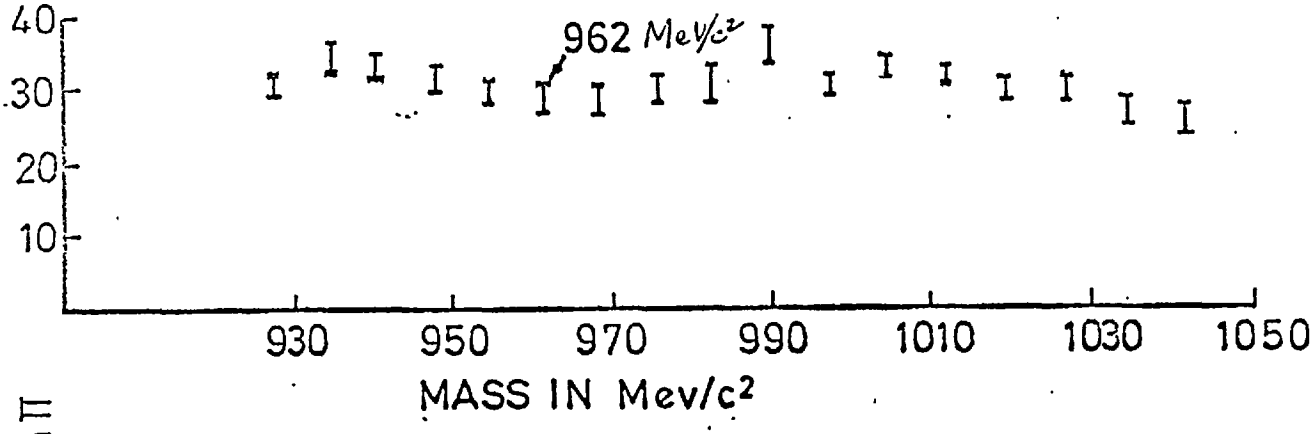

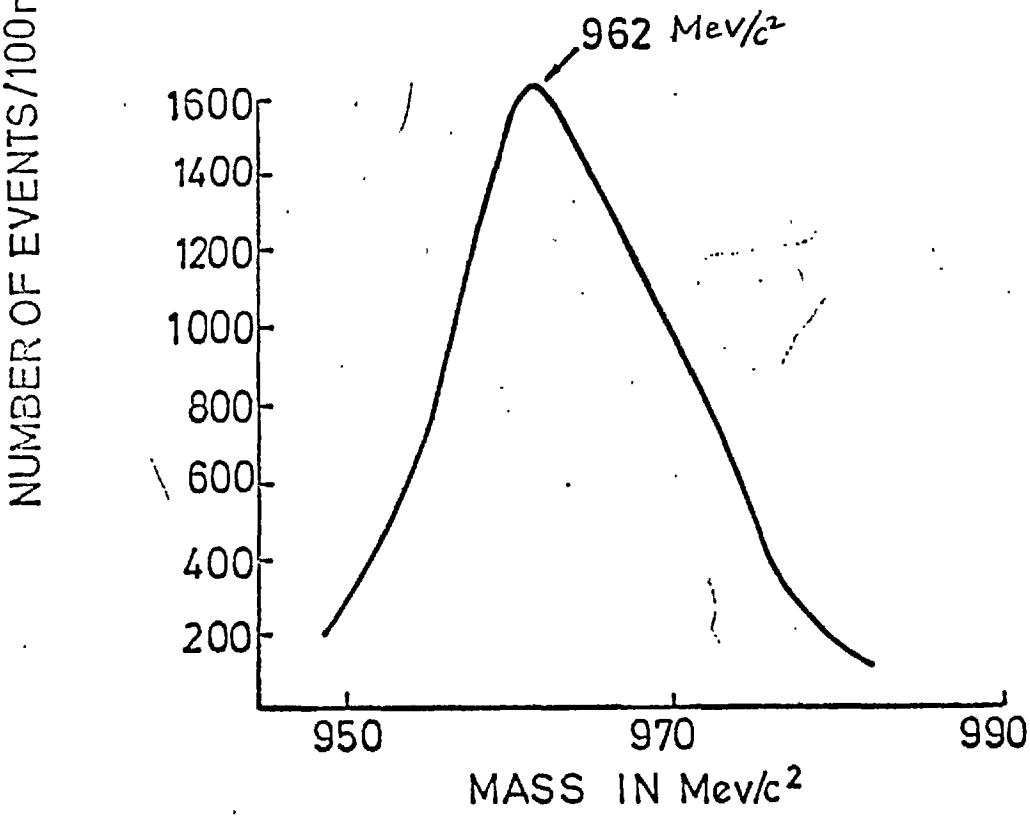

(1) MONTECARLO PREDICTION

FIG.7-7-D

The observed and the montecarlo predicted mass plot obtained by combining the contributions of the four gates (table 7-6-B) for Mass 962 MeV/c^2 and Γ = 5 MeV/c^2. (Each bin = 7 MeV/c^2).

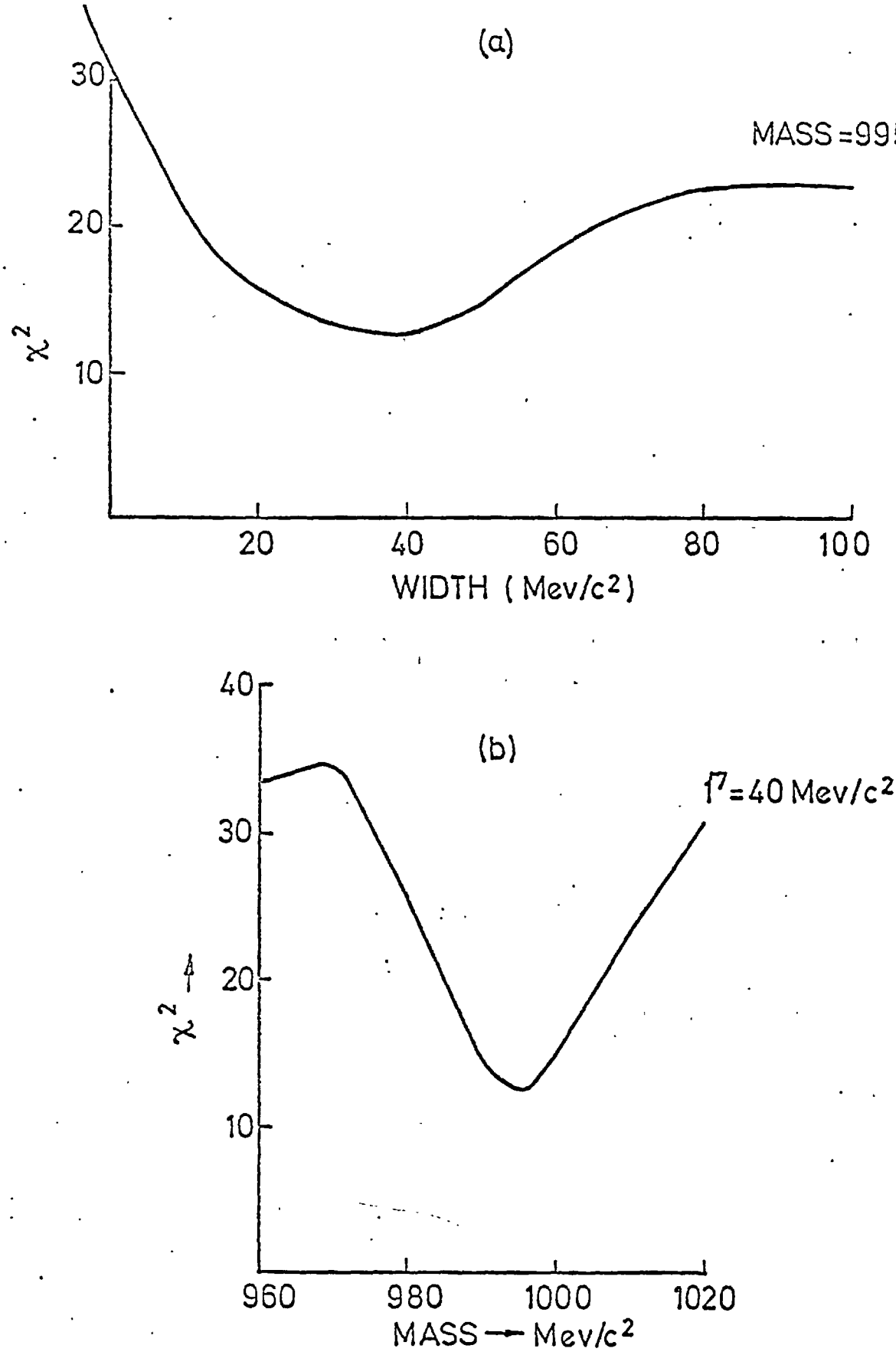

FIG. 7-7- E

The values of χ^2 was obtained (a) at a constant mass value 995 MeV/c^2 by changing the width and (b) at width = 40 MeV/c^2 by changing the mass. Straight line plus MonteCarlo predicted curve was fitted to the yield curve in the gate 11-14 nsecs (17 degrees of freedom).

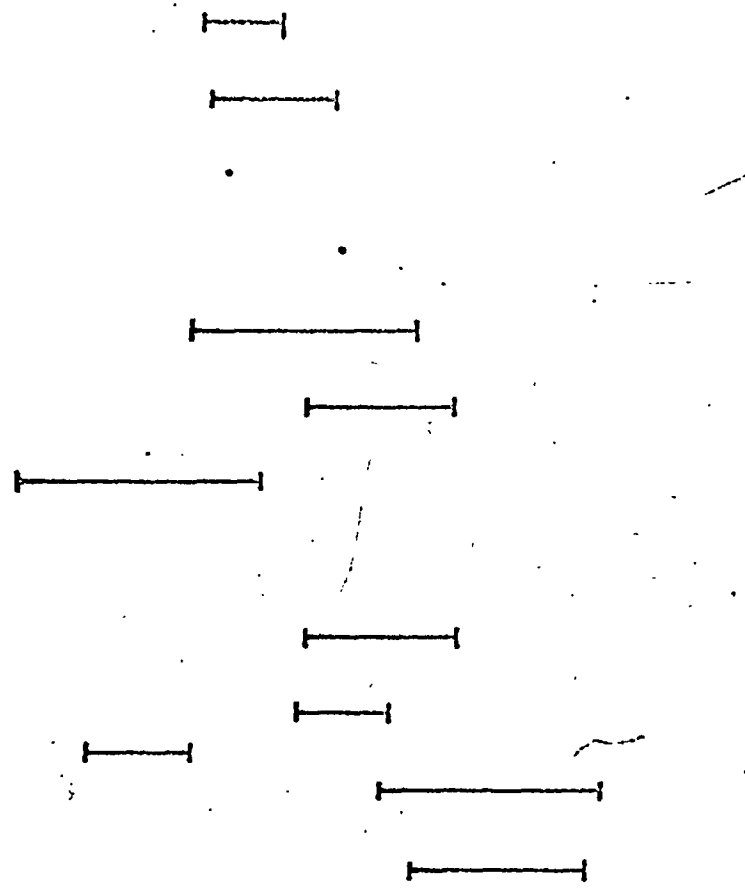

1	962 ± 5 Mev/c²	KIENZLE	65 MMS
2	966 ± 8	OOSTENS	66 MMS
3	960	CHUNG	68 HBC
4	975	DEFOIX	68 HBC
5	970 ± 15	BARNES	69 HBC
6	980 ± 10	MILLER	69 HBC
7	948 ± 16	OTWINOSK	69 HBC
8	980 ± 10	AMMA R	70 HBC
9	975 ± 6·0	ABOLINS	70 MMS
10	948 ± 7·0	OTWINOSK	70 HBC
11	995 ± 15	OXFORD UCLA	70 HBC
12	996 ± 12	THIS EXPERIMENT	

FIG 7-7-F MASS MEASUREMENTS

ACKNOWLEDGEMENTS

I wish to thank Professors C C Butler and P T Mathews for the opportunity of carrying out research as a member of the High Energy Physics Group at Imperial College.

It has been a great pleasure to have worked under the guidance of Dr D M Binnie. His invaluable instruction and encouragement is most gratefully acknowledged.

My sincere thanks are expressed to my colleagues at Imperial College and Southampton University who collaborated in this experiment. I am especially indebted to Dr D A Garbutt, Mr A Duane, Dr W G Jones, Dr R F George and Dr J G McEwen for their useful discussions and suggestions.

Thanks are also due to Mr R F Hobbs and Mr D J Scholes for their careful construction of much of the apparatus and also to Mr D Miller and Mr R J Gray for their continued assistance. I would also like to thank the Staff of the Rutherford Laboratory for their indispensable help.

I am extremely grateful to my mother for her inspiration and generous financial support. Acknowledgement is made of the financial support of the Science Research Council during the period from July 1969 to date.

A great debt is to my wife, Pramila, for her sacrifice and encouragement which enabled me to complete this work.

The assistance of Mr S P Majumdar in preparation of this thesis is also acknowledged.

REFERENCES

1. KIENZLE et al PL 19, 438, 1965
2. BANNER et al PL 25B, 300, 1967
3. FOCCACCI et al PRL Vol 17 890, 1966
4. CHUNG et al PR Vol 165, 1491, 1968
5. ALLEN et al PL Vol 22, 543, 1966
6. OTWINOWSKI et al PL Vol 29B, 529, 1969
7. OOSTENS et al PL 22, 708, 1966
8. BANNER et al PL 25B, 569, 1967
9. DEFOIX et al PL 28B, 353, 1968
10. ASTIER et al PL 25B, 294, 1967
11. CAMPBELL et al PRL 22, 1204, 1969
12. A BARBARO-GALTIERI et al PRL 20, 349, 1968
13. 'REVIEW OF PARTICLE PROPERTIES' PL 33B, August 1970
14. MILLER et al PL 29B, 255, 1969
15. JUHALA et al PL 27B, 257, 1968
16. BARNES et al PRL 23, 610, 1969
17. CRENELL et al PRL 22, 1398, 1969
18. AMMER et al PRL 21, 1832, 1968
19. KRUSE et al PR Vol 177, 1963, 1969
20. 'MESONIC RESONANCE STATES' R H DALITZ (1968). Paper presented at the topical conference on meson spectroscopy at the University of Philadelphia
21. ANDERSON et al PRL Vol 26, 108, 1971
22. J W GARDENS and D WHITESIDE

    (a) NIRL/M/21, 1961 and (b) NIRL/M/44
23. N M KING and P W SIMPSON,RHEL/R/103
24. J G WILSON, Ph.D Thesis, 1970, London University
25. D M BINNIE and A DUANE Nucl. Inst. Method 77(1970) 329-330

26. D M BINNIE et al PL 18, 348, 1965

27. W G JONES et al PL 23, 597, 1966

28. D C MASON, Ph. D Thesis, 1968 London University

29. W G JONES, Ph. D Thesis, 1967, London University

30. N HORWITZ, Rutherford Laboratory note

31. D G CRABB et al Nucl. Inst. and Methods, 48, 87 (1967)

32. M E KAY, Experimental test of scintillation counters designed to detect γ-rays, Internal Paper (IC)

33. M E KAY, Resonant Decay Simulation Program, Imperial College, Internal Group Paper

34. J V CRESSWELL et al HEP Electronics Group, Rutherford Laboratory 'THE TUNNEL SYSTEM': A new approach to the instrumentation of counter experiments.

35. MILBORROW, HEP Electronics Group, RHEL, 'MLS'.

36. PDP-8 Computer Manual Handbook

37. 'STACKER' by M J MITCHELL RHEL/M/C2

38. DUFEY et al PL Vol 26B, 1968

39. WEST et al Phy Rev 149, 1089, 1966

40. JACOBS UCRL 16877

41. CLEAR et al Nuovo Cimento 49A, 399, 1967

42. ABOLINS et al Phy Rev Lett 25, 469, 1970

43. ALLISON et al PL 25B, 619, 1967

44. I BUTTERWORTH (Unpublished)

45. MILLER et al (Kiev Conference, 1970)

46. Particle Properties January 1970.